NASA-CR-174701
PWA-5594-248

ENERGY EFFICIENT ENGINE FLIGHT PROPULSION SYSTEM

PRELIMINARY ANALYSIS AND DESIGN REPORT - FINAL UPDATE

by

J. W. Bisset and D. C. Howe

UNITED TECHNOLOGIES CORPORATION
Pratt & Whitney
Engineering Division - Connecticut Operation

Prepared for

NATIONAL AERONAUTICS AND SPACE ADMINISTRATION
Lewis Research Center
Cleveland, Ohio 44135

FOREWORD

The Energy Efficient Engine Component Development and Integration Program is being conducted under parallel National Aeronautics and Space Administration (NASA) contracts by Pratt & Whitney, Engineering Division, and the General Electric Company. The overall project is under the direction of Mr. Carl C. Ciepluch. The Pratt & Whitney effort is being conducted under Contract NAS3-20646, and Mr. Frank Berkopec is the NASA Project Engineer responsible for the portion of the contract described in this report. Mr. David E. Gray is the Manager of the Energy Efficient Engine Project at Pratt & Whitney. This report was prepared by Mr. John W. Bisset and Mr. David C. Howe.

TABLE OF CONTENTS

Table of Contents (Continued)

LIST OF ILLUSTRATIONS

LIST OF ILLUSTRATIONS (continued)

LIST OF ILLUSTRATIONS (continued)

LIST OF ILLUSTRATIONS (continued)

LIST OF ILLUSTRATIONS (continued)

LIST OF TABLES

LIST OF TABLES (continued)

LIST OF TABLES (continued)

LIST OF TABLES (continued)

SECTION 1.0
SUMMARY

The NASA-sponsored Energy Efficient Engine program is being conducted by Pratt & Whitney to develop and demonstrate an advanced technology base for a new generation of fuel-efficient engines designed for use in future commercial transport aircraft.

This report details results evolving from the final analysis and design of the flight propulsion system, as conducted under Task 1 of the Energy Efficient Engine program. This effort was undertaken to evaluate and confirm flight propulsion system design criteria and define performance potential compared to the following NASA-established design goals relative to the JT9D-7A reference engine.

- 12 percent minimum reduction in cruise thrust specific fuel consumption
- 5 percent minimum reduction in direct operating cost
- 50 percent less performance deterioration
- meet Federal Aviation Regulation Part 36 (1978) noise rules and EPA-proposed 1981 exhaust emissions standards

Successful completion of this Task 1 effort included detailed design analyses (supported by component technology programs) of test hardware required for the integrated core/low spool, the test vehicle used to simulate the aero-thermal-mechanical characteristics of the flight propulsion system. Results from the completed evaluation indicate that the flight propulsion system, as designed, is capable of meeting all design goals with one exception: the EPA-proposed 1981 emissions standard for oxides of nitrogen. Cruise thrust specific fuel consumption is estimated to be 15 percent lower than that of the JT9D-7A reference engine, which surpasses the NASA design goal of 12 percent. Economic analyses, which have been updated for fuel price and 1980 year-dollars, show a current direct operating cost reduction of 11.3 percent. This far exceeds the NASA design goal of a 5 percent reduction. Program detailed design and test efforts have reinforced an estimated performance deterioration rate one-half that of the JT9D-7A, which meets the NASA goal. An updated noise calculation for a fully treated nacelle indicates the potential of surpassing the 1978 noise rules in future domestic and international aircraft. Reassessment of exhaust emissions indicates Environmental Protection Agency Parameter estimates fall below proposed 1981 carbon monoxide and unburned hydrocarbon level design goals. However, program experience continues to confirm estimates that nitrogen oxide emissions will exceed the 1981 regulations by over 40 percent. The Society of Automotive Engineers smoke level estimate of 4 surpasses the design goal level of 20.

This report also presents information detailing the salient results from a study conducted under Task 1 of the Energy Efficient Engine program to define a turbofan propulsion system, known as the maximum efficiency engine, which incorporates a reoptimization of the fuel saving technologies for improved fuel economy and direct operating costs relative to the flight propulsion system. This engine will be used as a basis for determining the full performance potential of the Energy Efficient Engine technology. With the dominant influence of fuel costs affecting current airline operating economics, this engine was defined to provide an estimated improvement of five percent in cruise thrust specific fuel consumption (TSFC) compared to the flight propulsion system. Performance improvement changes for the maximum efficiency engine, as compared to the flight propulsion system, include a three-inch larger fan, two additional turbine stages, a more tightly gapped compressor and a simpler, one-stage combustor. This propulsion system is aimed at providing excellent fuel efficiency and operating economics while meeting currently projected environmental regulations.

SECTION 2.0
INTRODUCTION

The National Aeronautics and Space Administration (NASA) has the objective of improving the energy efficiency of future United States commercial aircraft so that substantial savings in fuel can be realized. One of the elements of the overall technology plan devised to attain this objective is the Energy Efficient Engine. Through the evolutionary extension of the current technology base, the Energy Efficient Engine program is designed to develop and demonstrate the technology for achieving higher thermodynamic and propulsive efficiencies in future environmentally acceptable turbofan engines. It is estimated that these improvements in turbofan engines will initially result in a ten to fifteen percent lower specific fuel consumption as compared to the current JT9D-7A commercial engine.

The Energy Efficient Engine Component Development and Integration Program, which is based on the results of the Energy Efficient Engine Preliminary Design and Integration Studies (NASA contract NAS3-20628), will develop the component technology to achieve the National Aeronautics and Space Administration goals of at least a 12 percent reduction in cruise thrust specific fuel consumption, a 5 percent reduction in direct operating cost and 50 percent less performance deterioration. In addition, FAR Part 36 (1978) noise rules and EPA-proposed 1981 exhaust emissions standards must be met.

The Energy Efficient Engine program consists of the following two tasks designed to meet these program objectives.

Task 1 - Flight Propulsion System Analysis, Design, and Integration
Task 2 - Component Analysis, Design, and Development

Under Task 1, final design of the conceptual study engine, known as the flight propulsion system, was defined based on results of the Energy Efficient Engine Preliminary Design and Integration studies (NAS3-20628). Component analysis and design work was conducted under Task 2.

The flight propulsion system reflects a dual spool, direct drive, mixed exhaust configuration. A short, stiff high rotor and a single-stage high-pressure turbine are among the major features in providing both performance retention and major reductions in maintenance and direct operating costs. Improved active clearance control in the high-pressure compressor and high-pressure turbine along with incorporation of advanced single crystal turbine blades and vanes are among the major features contributing to performance improvement. In addition to design definition, an analytical evaluation was performed under Task 1, with assistance from airframe company subcontractors to provide flight and economic performance characteristics of future commercial aircraft using Energy Efficient Engine propulsion systems.

This report details results that evolved from the final analysis and design update of the flight propulsion system, as conducted under Task 1 of the Energy Efficient Engine program. The design effort included a final definition of the engine, major components, internal subsystems, and nacelle. Various analytical representations and results from component technology programs were used to verify aerodynamic and structural design concepts and to predict performance. Also presented in this report is information detailing salient results from a separate study conducted under Task 1 to define a turbofan propulsion system known as the maximum efficiency engine. The study intent was to optimize the fuel savings technology developed in the Energy Efficient Engine program for improved fuel economy and direct operating costs relative to the flight propulsion system. Technology developed under both efforts is projected for the 1988 time period.

An overall description of the flight propulsion system along with a detailed discussion concerning final analysis and design of individual engine components and subsystems are provided in Sections 3.0 and 4.0. Section 4.0 also presents performance design goals and operating economic data based on installation of the updated flight propulsion system into future commercial aircraft. Section 5.0 provides a detailed discussion concerning preliminary analysis and design of individual components for the maximum efficiency engine designed to represent full performance potential with Energy Efficient Engine technology.

SECTION 3.0
OVERVIEW OF DESIGN

Task 1 of the Energy Efficient Engine Component Development and Integration Program was devoted to the preliminary design, evaluation and update of an Energy Efficient Engine flight propulsion system. A flight engine preliminary design is necessary to 1) identify the areas of new technology required to establish the technology base, 2) evaluate the configuration's operating economics, and 3) serve as a benchmark by which component and overall system performance may be measured and tracked throughout the program.

As other tasks in the Energy Efficient Engine program progressed, overall flight propulsion system performance was tracked under Task 1 to reflect results from these completed program elements with periodic flight propulsion system status updates. The final update detailed in this report incorporates all of the program analytical and test results into an updated flight propulsion system design.

Performance and design of the flight propulsion system are consistent with standard commercial aircraft engine practice and with applicable Federal Aviation Administration and Environmental Protection Agency regulations.

There is no intention on the part of NASA to carry the flight propulsion system preliminary design through into prototype, development, or production programs. The intent of Task 1 was solely to provide a focus for the technology needed by the engine manufacturer to initiate design and development of an energy efficient commercial engine with only the usual and normal business risk.

The following presents a brief explanation of the flight propulsion system by describing the systems's basic design features, overall cycle definition and performance status relative to program goals.

3.1 Flight Propulsion System Description

The flight propulsion system, shown in Figure 1, is configured for a balance of fuel efficiency, lower operating economics and environmental acceptability using advances in aerodynamics, materials/cooling techniques and structure-mechanics. Inlet air is channeled to conventional solid, shrouded fan blades by the inlet duct and spinner. Eighty-seven percent of the fan discharge air is ducted around the outside of the close-coupled flow splitter. The remaining air is further supercharged when it enters a four-stage low-pressure compressor which forces the air inward within a curved flowpath. The smaller diameter, 10-stage high-pressure compressor increases the pressure to provide a design overall pressure ratio of 38.6:1. Compressor exit flow is turned radially outward through the exit guide vanes and curved wall pre-diffuser to direct air into the combustion zones. The outwardly canted combustor, which has two independent fuel supply manifold systems and combustion zones for low emissions, feeds hot gases directly into a one-stage, air-cooled high-pressure turbine which drives the high-pressure compressor.

The discharge gases are decelerated and turned slightly outward to be further expanded through a four-stage low-pressure turbine which drives the fan and low-pressure compressor. The core exhaust and the fan duct air are mixed by means of lobed chutes positioned around a large diameter central tailplug.

The nacelle was designed to share flight loads, serve as an aerodynamic shell around the engine, provide access to the engine, absorb noise, and provide thrust reverse.

A full authority digital electronic control system is used to promote efficient engine operation and reduce the effects of deterioration. The digital system was designed to manage fuel for the flight propulsion system's two-stage combustor and provide control of variable high-pressure compressor vanes, start bleeds, intercompressor surge bleeds, and air valves for active clearance control. The control system regulates hydraulic pressure for stator vanes and bleed actuators with minimum fuel temperature rise and at minimum system cost and weight.

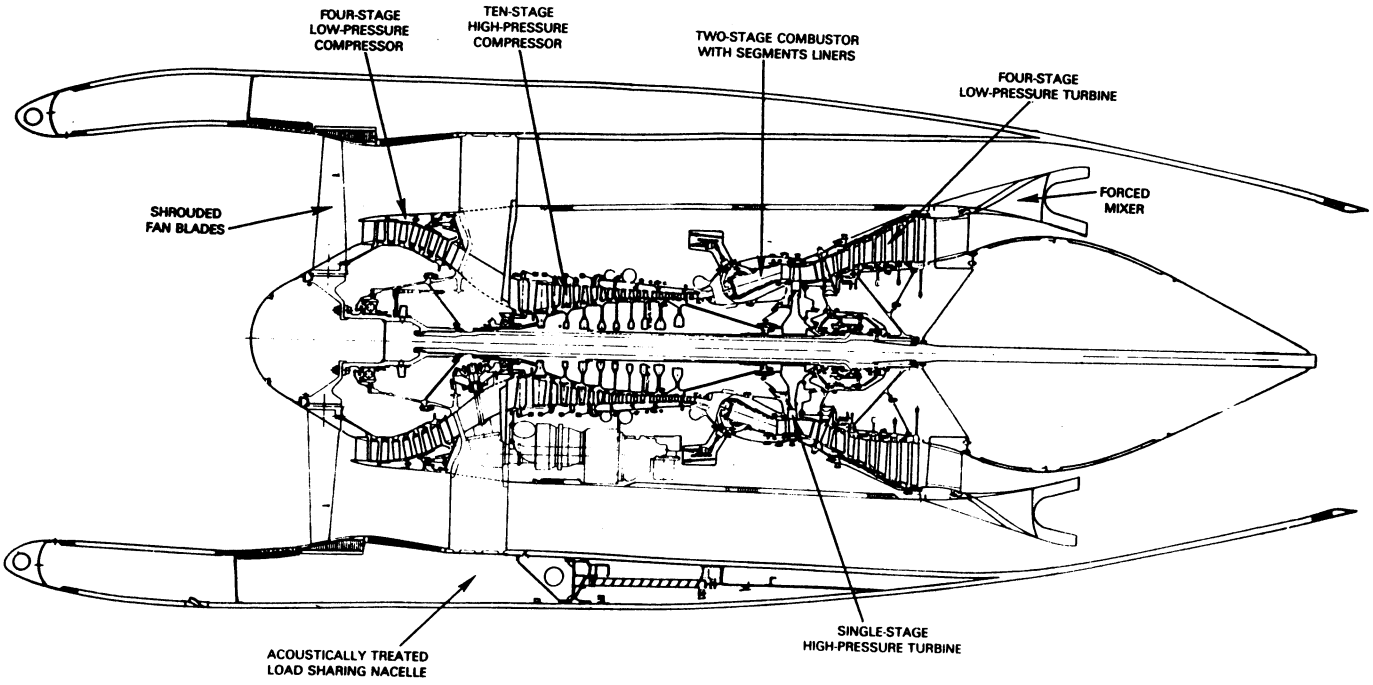

Figure 1 Energy Efficient Engine Flight Propulsion System

The flight propulsion system is a five bearing design with two main support frames and two main bearing compartments. The fan design features a single aft-positioned shroud and tip trenches to provide efficiency improvement. Controlled endwall loss and reduced airfoil loss concepts are utilized to raise efficiency levels in the lowand high-pressure compressors. In addition, the high-pressure compressor (1) operates at higher rotor speeds relative to the JT9D-7A high rotor for reduced weight and cost and (2) incorporates an active clearance control system for improved efficiency. A two-stage combustor is utilized for low emissions. The high-pressure turbine features a single stage design to provide a significant reduction in initial cost and engine maintenance cost. Single crystal alloys are used in the turbine airfoils to reduce cooling airflow requirements. In addition, the high-pressure turbine incorporates active clearance control to improve component efficiency. The low-pressure turbine counterrotates relative to the high-pressure turbine. This component also incorporates active clearance control to increase efficiency. The exhaust mixer is a scalloped eighteen lobe design which provides for reduced pressure loss, increased efficiency, and lighter weight. Key nacelle features include (1) an integrated engine-nacelle structure which improves engine performance retention by reducing engine deflections caused by thrust and cowl duct loadings, (2) composite and honeycomb materials used in nacelle construction to reduce weight, and (3) incorporation of internal and external contouring improvements and advanced sealing techniques for reduced losses.

Two major changes made from the initial design described in Ref. (1) were (1) the incorporation of a shrouded blade in place of the shroudless, hollow blade for the fan component, and (2) downsizing the entire flight propulsion system approximately twelve percent in order to obtain the maximum technology benefit for the smaller thrust engines expected to be required in the mid-to-late 1980's. A comparison of the initial and current flight propulsion system design cross sections is shown in Figure 2.

3.2 Overall Cycle

The flight propulsion system's basic cycle has been maintained throughout the design process. Aerodynamic design point cycle parameters kept constant are: a 6.5 fan bypass ratio, a 1.74 duct portion fan pressure ratio, and a 38.6 overall pressure ratio. Performance updating was accomplished using a 'rubber engine' approach in which the turbine and exhaust nozzle control areas were varied to hold the design cycle, fan total airflow, and compression system operating lines. Combustor exit temperature was adjusted to keep the pressure ratio constant at the exhaust mixing plane resulting in a turbine rotor inlet temperature of 1223°C (2235°F). Resulting differences between design parameters affecting hardware size for the current flight propulsion system and the initial design are summarized in Table 1. A comparison of the principal component performance levels at the aerodynamic design point is shown in Table 2. Table 3 summarizes current performance parameters at the significant engine operating conditions.

TABLE 1

FLIGHT PROPULSION SYSTEM HARDWARE SIZING PARAMETER COMPARISON
(Aerodynamic Design Point: 10675 m (35,000 ft), 0.8 Mach Number, Standard Day)

	Initial Design*	Current Design
Fan	Shroudless	Shrouded
Low Pressure Compressor	Base	Base
High Pressure Compressor	Base	Base
High Pressure Turbine		
% ΔInlet Flow Parameter ($W\sqrt{T}/P$)	Base	-0.7
% ΔInlet Speed Parameter ($N_2/\sqrt{T}$)	Base	-0.1
Low Pressure Turbine		
% ΔInlet Flow Parameter ($W\sqrt{T}/P$)	Base	-2.5
% ΔInlet Speed Parameter ($N_1/\sqrt{T}$)	Base	Base
Mixer		
% Δ Core Area	Base	-0.3
% Δ Duct Area	Base	-0.1
Exhaust		
% Δ Mixed Area	Base	-0.1

* Thrust size of initial engine design was downsized 12 percent.

Differences between the initial and current design component performances are small, except for (1) the fan efficiency (duct section) deficit associated with the change to the shrouded fan, (2) the high-pressure turbine efficiency improvement determined by subsequent testing, and (3) the lower turbine transition duct pressure loss, also determined by subsequent testing.

3.3 Thrust Size

Shortly after the initial design was completed, the flight propulsion system was downsized 12 percent in airflow to obtain the maximum technology benefit for the smaller thrust engines expected to be required in the 133,446 to 222,410 N (30,000-50,000 lb) thrust class in the 1980's. The fan was resized from a corrected airflow of 707 to 622 kg/sec (1560 to 1373 lb/sec) at the aerodynamic design point in the process.

TABLE 2

COMPARISON OF FLIGHT PROPULSION SYSTEM COMPONENT PERFORMANCE LEVELS
(Aerodynamic Design Point: 10675 m (35,000 ft), 0.8 Mach Number, Standard Day)

	Initial Design	Current Design
Fan		
Pressure Ratio, Duct	1.74	1.74
Pressure Ratio, Core	1.56	1.56
Duct Efficiency (%)	87.3	86.5
Core Efficiency (%)	90.2	90.2
Low Pressure Compressor		
Pressure Ratio	1.77	1.77
Efficiency	89.9	90.0
High Pressure Compressor		
Pressure Ratio	14.0	14.0
Efficiency (%)	88.2	88.3
Combustor		
Efficiency (%)	99.95	99.95
Pressure Loss (%)	5.5	5.5
High Pressure Turbine		
Pressure Ratio	4.03	3.99
Efficiency (%)	88.2	89.1
Low Pressure Turbine		
Transition Pressure Loss (%)	1.5	0.7
Pressure Ratio	5.60	5.72
Efficiency (%)	91.5	91.6
Exit Vane Pressure Loss (%)	0.9	0.9
Fan Duct		
Pressure Loss (%)	0.6	0.6
Exhaust Mixer		
Efficiency (%)	85.0	85.0
Duct Pressure Loss (%)	0.18	0.18
Core Pressure Loss (%)	0.24	0.24
Exhaust Nozzle		
Pressure Loss (%)	0.34	0.34
Velocity Coefficient (%)	99.6	99.6
Secondary System		
Cooling/Leakage Airflow (%)	16.45	17.2

TABLE 3

CURRENT FLIGHT PROPULSION SYSTEM PERFORMANCE PARAMETERS

	Engine Operating Condition			
	Aero. Des. Point	Maximum Cruise	Maximum Climb	Takeoff
Altitude m (ft)	10668 (35000)	10668 (35000)	10668 (35000)	0
Mach Number	0.8	0.8	0.8	0
Ambient Temperature °C (°F)	-54 (-66)	-54 (-66)	-44 (-48)	28 (+84)
Net Thrust (Uninstalled) Kg (lb)	41612 (9355)	39744 (8935)	44304 (9960)	164,694 (37025)
TSFC Kg/hr/Kg (lb/hr/lb)				
(Uninstalled)	0.550	0.548	0.570	0.327
(Installed)	0.576	0.575	0.596	0.330
Overall Pressure Ratio	38.55	37.35	40.25	31.05
Bypass Ratio	6.51	6.60	6.39	6.83
Fan Pressure Ratio (Duct Section)	1.74	1.71	1.78	1.58
HPT Rotor Inlet Temperature °C (°F)	1223 (2235)	1201 (2195)	1321 (2410)	1362 (2485)

An uninstalled sea level static takeoff thrust of 164,694 N (37,025 lb) is predicted for the current flight propulsion system versus 160,935 N (36,180 lb) (downsized) for the initial design. Base engine thrust flexibility in the class is considered to be equivalent to the initial base size. Table 4 presents the overall installation dimensions for both the initial and current flight propulsion systems. Length increases have resulted from several component flowpath revisions, with the high-pressure compressor being the largest contributor along with exhaust mixer and tailplug changes.

3.4 Ratings

Ratings for the flight propulsion system were initially established using thrust ratios selected to improve maximum climb and maximum cruise thrust relative to takeoff thrust as compared to the JT9D-7A reference engine (see Reference 2). For subsequent status updates, the initial levels of rated combustor exit temperatures were kept constant for the maximum cruise and takeoff ratings. The maximum climb rating definition has continued to be based on a maximum climb-to-maximum cruise thrust ratio of 1.115. As a result, status rated thrusts have varied with updates in component performance. Table 5 presents a comparison of combustor exit temperatures and thrusts at various ratings for both the initial and current flight propulsion systems. The only significant change is a 2.3 percent increase in takeoff thrust relative to the initial design. This increase in takeoff thrust is a result of matching changes associated primarily with map revisions made as part of the detailed design of the fan for the integrated core/low spool.

TABLE 4

FLIGHT PROPULSION SYSTEM INSTALLATION DIMENSIONS COMPARISON

	Initial Design*	Current Design
Nacelle Maximum Diameter - cm (in)	268.7 (105.8)	268.7 (105.8)
Fan Tip Diameter - cm (in)	206.5 (81.3)	206.5 (81.3)
Exhaust Nozzle Diameter - cm (in)	154.6 (60.9)	154.6 (60.9)
Overall Nacelle Length - cm (in)	628.1 (247.3)	676.9 (266.5)
Fan Leading Edge-to-Turbine Exit Flange Length - cm (in)	302.2 (119.0)	322.8 (127.1)

* Values shown are after thrust size of initial engine design was downsized 12 percent.

TABLE 5

FLIGHT PROPULSION SYSTEM PERFORMANCE AT RATINGS COMPARISON

Ratings	Initial Design*	Current Design
Takeoff (0 ft, 0 Mn, Std + 13.9°C (25°F) Day)		
Combustor Exit Temperature - °C (°F)	1435 (2615)	1435 (2615)
Uninstalled Thrust - N (lb)	160935 (36180)	164694 (37025)
Maximum Climb (10675 m (35,000 ft), 0.8 Mn, Std. + 10°C (18°F) Day)		
Combustor Exit Temperature - °C (°F)	1387 (2530)	1393 (2540)
Uninstalled Thrust - N (lb)	44570 (10020)	44304 (9960)
Maximum Cruise (10675 m (35,000 ft), 0.8 Mn, Std. Day)		
Combustor Exit Temperature - °C (°F)	1268 (2315)	1268 (2315)
Uninstalled Thrust - N (lb)	39967 (8985)	39744 (8935)

* Values shown are after thrust size of initial engine design was downsized 12 percent.

3.5 System Performance Status Relative To Goals

The evolution of the flight propulsion system design was based on meeting or exceeding the program goals established by NASA. The degree to which this is achieved in the final design update is shown in Table 6. Economic years, fuel prices and flight propulsion system sizes are indicated and represent the basis for the parameter values shown. The comparison shows that, with the exception of emissions of nitrogen oxides, program goals have been met or exceeded. The engine is slightly heavier and more costly than the reference JT9D-7A engine but does have a maintenance cost advantage due primarily to a reduction in the number of parts.

TABLE 6

FLIGHT PROPULSION SYSTEM STATUS RELATIVE TO GOALS

	Program Goal	Current Design Evaluation
TSFC Reduction* - %	12.0	15.0
DOC Reduction** - %		
Domestic Average	5.0	10.2
International Average	5.0	13.1
Noise - EPNdB	FAR 36 (1978)	FAR 36(1978) -3 to -5
Emissions - EPAP		
Total Hydrocarbons	0.4	0.32
Carbon Monoxide	3.0	1.8
Nitrogen Oxides	3.0	4.3
TSFC Deterioration* -%	50	***
Engine Weight* -%	-	+1.9
Engine Cost* -%	-	+4.7
Engine Maintenance Cost* -%	-	-4.6
Remarks:	Full Size, 1977$ $.40-.45/3.78 liters	88% Size, 1980$ $1.50/3.78 liters

Note: 3.78 liters = 1.0 US Gallon
* Relative to JT9D-7A reference engine scaled to flight propulsion system airflow size
** Relative to JT9D-7A engine installed in same airplane
*** Not estimated

SECTION 4.0
FLIGHT PROPULSION SYSTEM COMPONENT DESIGN UPDATE

This section of the report describes the major components of the flight propulsion system in more detail, discusses the predicted performance of each and identifies changes relative to the initial flight propulsion system design of Reference 1.

4.1 Fan

The flight propulsion system fan component, as designed, is a high performance, single-stage system featuring a fan rotor with integral disk/hub geometry for reduced component weight and recessed rub strips in the fan containment case for reduced blade tip leakage. This configuration has a predicted efficiency of 86.5 percent which translates into approximately 20 percent of the total 15 percent reduction in cruise thrust specific fuel consumption for the flight propulsion system as compared to the JT9D-7A reference engine. In addition, the fan component is predicted to meet or surpass goals established for surge margin, structural integrity and durability.

A shroudless, hollow blade fan component was initially designed for the flight propulsion system. However, results from supporting technology work conducted under Task 2 of the Energy Efficient Engine program indicated cost effective fabrication technology readiness extended beyond the time period established for final design of the flight propulsion system. As a result, the fan program effort proceeded with design of a more conventional solid fan blade having a single, aft-positioned shroud. Figure 3 compares cross sections of the initial and current designs of the fan component. As shown in this figure, the fan rotor is supported by two main bearings housed in a common bearing support attached to the compressor intermediate case. The fan overhangs its support in a cantilevered configuration. The major design parameters for both the initial and current designs are presented in Table 7. As shown in the table, there is much similarity between the two designs except for changes to the blade type, number of blades and the number of duct exit vanes and struts.

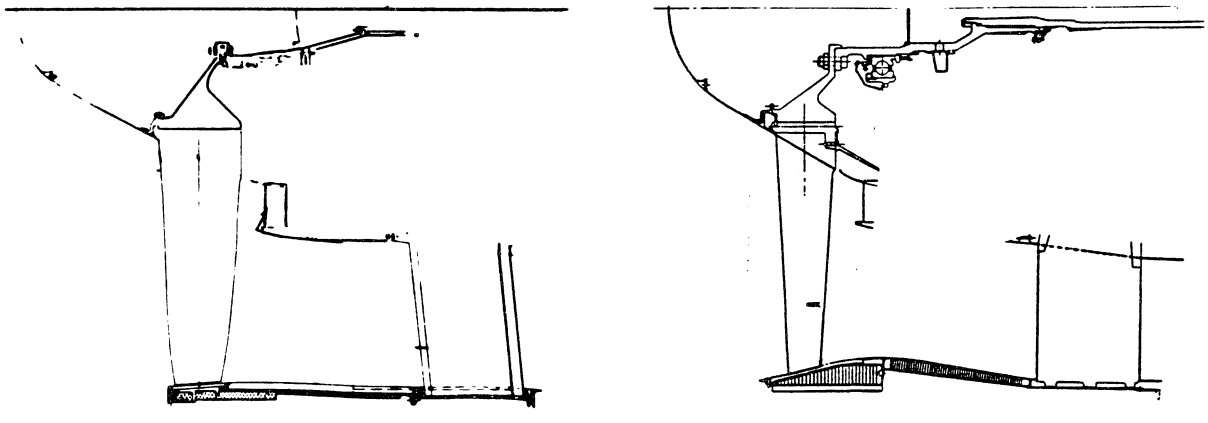

Figure 3 Flight Propulsion System Initial and Current Fan Section Comparison

TABLE 7

FLIGHT PROPULSION SYSTEM FAN SECTION DESIGN COMPARISON
(Aerodynamic Design Point: 10675 m (35,000 ft), 0.8 Mn, Standard Day)

	Initial Design*	Current Design
Number of stages	1	1
Pressure ratio (duct)	1.74	1.74
Corrected airflow, kg/sec (lb/sec)	622 (1373)	622 (1373)
Bypass ratio	6.51	6.51
Surge Margin (percent)	15	15
Corrected tip speed, m/sec (ft/sec)	457 (1500)	455 (1496)
Inlet specific airflow, lb/sec/sq ft	43	43
Inlet hub/tip radius ratio	0.34	0.34
Blade aspect ratio (avg length/root chord)	2.5	4.0
Number of shrouds per blade	0	1
Number of blades	24	36
Number of duct exit vanes and struts	33	29

* Values shown are after thrust size of initial engine design was downsized 12 percent.

The initial fan component was redesigned with minimal modification so that the shorter chord shrouded fan blade for the flight propulsion system is located at the desired distance upstream of the low-pressure compressor inlet vane. The shrouded fan blade flowpath diagram is presented in Figure 4.

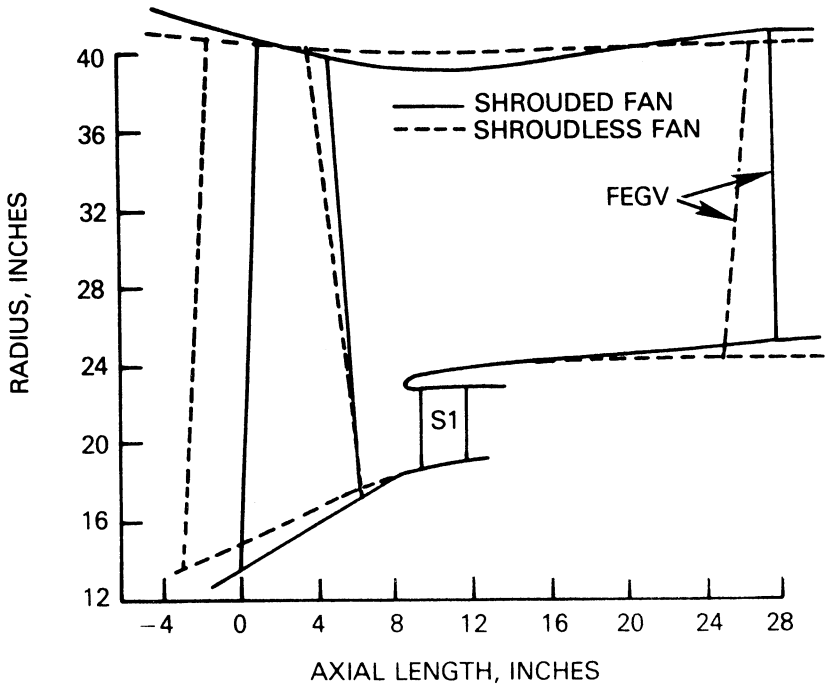

Figure 4 Flight Propulsion System Flowpath For Shrouded Blade Fan Component

The shrouded fan blade design is similar to current high bypass ratio blade designs (Reference 3). The shrouded fan blade rotor consists of 36 titanium fan blades with each blade having an aft part span shroud to provide the necessary stability and durability requirements. The radial pressure ratio distribution was modified from that of the shroudless-bladed fan to compensate for the additional aerodynamic loss caused by the part span shroud. Design contoured airfoil sections were incorporated in the duct portion of the blade span while the core portion of the blade span contains conventional multiple circular arc airfoil sections. The blade root slope was increased to blend into the existing low-pressure compressor configuration. Optimization of the blending required a minor recontouring of the compressor inlet guide vane. In addition, the number of duct exit guide vanes was reduced to maintain compatibility with the first stage of the high-pressure compressor during component redesign to a lower hub/tip radius ratio. The aft part-span shroud on the fan blade was designed in accordance with conventional shroud design criteria. Based on test results with this type of shroud, a 65 degree shroud angle was incorporated. Subsequent vibration analysis showed blade resonant and flutter design criteria were met in all areas.

Because of the greater flowpath convergence at the tip of the shrouded blade to accomplish the desired area ratio and loading level, the fan containment design incorporates a honeycomb ring between the fan case and the Kevlar® to provide a cylindrical surface for the Kevlar® wrap. Case thickness was set by containment criteria. Blade passing resonance was not a factor in the case design for the shrouded fan.

The fan stubshaft, hub, and nose cone for the flight propulsion system were redesigned for the shrouded fan. Stubshaft thickness was established by the design requirements of the rotor for the shrouded fan blade, with blade loss setting flange thickness. The hub and the nose cone assembly, including the blade retention feature, were redesigned using flight propulsion system criteria.

Predicted Performance

An assessment was conducted to establish performance estimates for the shrouded fan component. The adiabatic efficiency prediction for the duct section is shown in Table 8. Current efficiency exceeds the 86.3 percent goal level established for the shrouded fan, which includes a 1.0 percent penalty for the addition of the shroud. The efficiency predicted for the fan with the current state-of-the-art design system is 85.2 percent. A 1.1 percent improvement in predicted efficiency was made possible by incorporation of several advanced technology features, including quasi three-dimensional design and design-contoured blades, controlled diffusion vanes, and rotor tip trenching. Mechanical design results showed a capability to achieve a 0.139 cm (0.055 in) rotor tip clearance for the flight propulsion system fan compared to a goal clearance of 0.205 cm (0.081 in). This 0.066 cm (0.026 in) tip clearance improvement was estimated to increase duct section efficiency an additional 0.2 percent.

TABLE 8

CURRENT FLIGHT PROPULSION SYSTEM FAN (DUCT) ADIABATIC EFFICIENCY PREDICTION
(Aerodynamic Design Point: 10,675 m (35,000 ft), 0.8 Mn, Standard Day)

	Percent
State-of-Art Design System (Goal Clearance)	85.2
Rotor Tip Trench	+0.2
Specially Contoured Blades	+0.7
Specially Contoured Exit Vanes	+0.2
Reduced Tip Clearance	+0.2
Predicted Efficiency (Status Clearance)	86.5
Goal Efficiency (Goal Clearance)	86.3

On a preliminary basis, the assessment indicated no difference in the predicted efficiency (90.2 percent) of the core section of the fan relative to the shroudless configuration. Fan rotor and duct exit vane/strut performance maps were updated at the completion of the detailed aerodynamic design.

Current fan aerodynamic design parameters and maps were incorporated into the flight propulsion system performance simulation. Updated performance was defined at the aerodynamic design point and at key off-design operating points. A comparison is presented in Table 9 of the updated performance results for the fan section to performance predicted for the initial shroudless fan design. Current and initial design fan performance is similar except for fan duct section efficiency which is different because of shroudless versus shrouded blade configuration effects.

4.2 Low-Pressure Compressor

The flight propulsion system low-pressure compressor component, as designed, is an efficient four-stage system featuring fixed inlet guide vanes, a drum rotor assembly supported directly to the fan disk rim, controlled diffusion airfoils for low loss incidence, abradable rub-stripped trenches for reduced tip leakage, mini-cavities to reduce endwall losses, and a full-annular modulated bleed system designed to avoid compressor surge. This configuration exceeds the design goal with a predicted adiabatic efficiency of 90.0 percent. The low-pressure compressor component is predicted to meet or surpass goals established for structural integrity and durability.

Figure 5 compares cross sections of the initial and current designs for the flight propulsion system low-pressure compressor component. As shown in this figure, the current design reflects little change from the initial design except in the rotor hub configuration where the single-hub rotor support configuration was deleted in favor of attaching the rotor directly to the fan disk rim. The major parameters governing the aerodynamic design of the low-pressure compressor component for both the initial and current designs are presented in Table 10.

TABLE 9

FLIGHT PROPULSION SYSTEM FAN PERFORMANCE PARAMETER COMPARISON

	AERO DESIGN POINT(1)		MAXIMUM CRUISE(2)		MAXIMUM CLIMB(3)		TAKEOFF(4)	
	Initial Design*	Current Design	Initial Design*	Current Design	Initial Design*	Current Design	Initial Design*	Current Design
Pressure Ratio								
Duct Section	1.74	1.74	1.71	1.71	1.79	1.78	1.57	1.58
Core Section	1.56	1.56	1.55	1.54	1.59	1.58	1.44	1.45
Bypass Ratio	6.51	6.51	6.59	6.60	6.38	6.39	7.02	6.83
Efficiency - %								
Duct Section - Adiabatic	87.3	86.5	87.3	86.7	87.1	85.9	88.2	86.9
- Polytropic	88.1	87.3	88.1	87.5	88.0	86.8	88.8	87.5
Core Section - Adiabatic	90.2	90.2	90.4	90.4	90.1	90.1	91.4	91.4
- Polytropic	90.7	90.7	90.9	90.9	90.6	90.6	91.7	91.7
Corrected Airflow - kg/sec								
Total	622	622	615	615	633	632	544	550
Duct Section	539	539	534	533	547	546	476	480
Core Section	82.9	82.9	81	80.8	85.8	85.5	67.9	70
Inlet Specific Airflow - kg(lb)/sec/.093 sq.m	19.5 (43.0)	19.5 (43.0)	19.2 (42.5)	19.2 (42.5)	19.8 (43.8)	19.8 (43.7)	17.0 (37.6)	17.2 (38.0)
Corrected Tip Speed - m/sec (ft/sec)	139 (457)	138 (455)	137 (451)	136 (449)	145 (477)	144 (474)	137 (452)	138 (456)
Rotor Speed - rev/min	3902	3902	3852	3846	4073	4065	3865	3905
Exit Temperature - °C								
Duct Section	22	22	20	21	38	38	75	77
Core Section	11	11	10	10	25	25	65	66

Design and Off-Design Operating Conditions:

(1) Aerodynamic Design Point - 10675 m (35,000 ft), 0.8 Mn, Standard Day
(2) Maximum Cruise - 10675 m (35,000 ft), 0.8 Mn, Standard Day
(3) Maximum Climb - 10675 m (35,000 ft), 0.8 Mn, Standard Day + 10°C (18°F)
(4) Takeoff - SLTO, 0 Mn, Standard Day + 13.9°C (25°F)

* Values shown are after thrust size of initial engine design was downsized 12 percent.

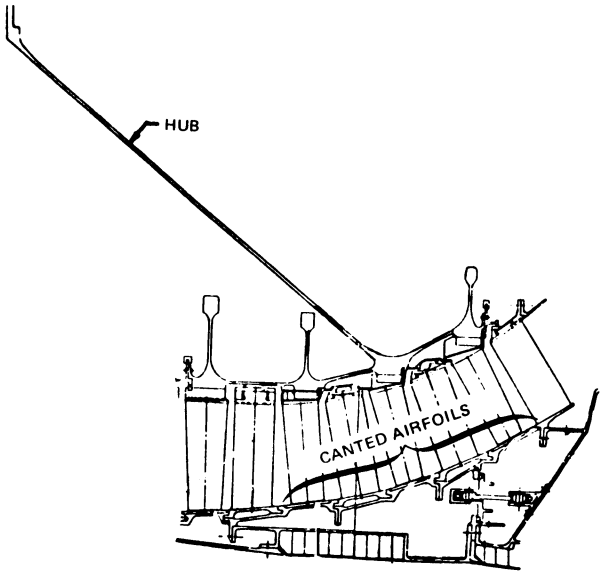

INITIAL

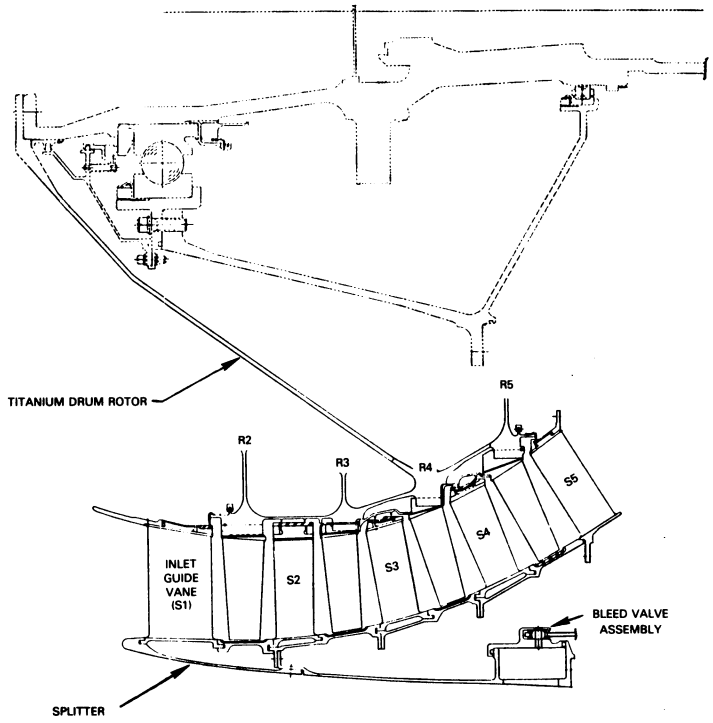

CURRENT

Figure 5 Flight Propulsion System Low-Pressure Compressor Section Comparison

TABLE 10

FLIGHT PROPULSION SYSTEM LOW-PRESSURE COMPRESSOR SECTION DESIGN COMPARISON
(Aerodynamic Design Point: 10675 m (35,000 ft), 0.8 Mn, Standard Day)

	Initial Design*	Current Design
Number of Stages	4	4
Pressure Ratio	1.77	1.77
Corrected Inlet Airflow - kg(lb)/sec	56.9 (125.6)	56.9 (125.6)
Surge Margin - %	20	18
Corrected Inlet Tip Speed - m(ft)/sec	242 (797)	242 (797)
Inlet Specific Airflow - kg(lb)/sec/.093 sq.m	16.1 (35.6)	16.1 (35.6)
Hub/Tip Radius Ratio		
Inlet	0.82	0.83
Exit	0.84	0.81
Average Airfoil Aspect Ratio	2.40	2.24
Average Gap/Chord Ratio	0.9	0.84
Average Axial Velocity-to-Wheel Speed Ratio	0.7	0.72
Number of Airfoils	779	820

* Values shown are after thrust size of initial engine design was downsized 12 percent.

The Energy Efficient Engine low-pressure compressor design for the flight propulsion system is based largely on the technology inherent in current Pratt & Whitney commercial engines. Aerodynamic design for the flight propulsion system component evolved from the detail design effort undertaken for the integrated core/low spool low-pressure compressor (see Reference 4). The mechanical design features of the flight propulsion system low-pressure compressor were retained in the integrated core/low spool but its compressor was not optimized for flight weight.

Low-pressure compressor flowpath dimensions were based on final detail design specifications for the flight propulsion system fan component and compressor intermediate case. Area distribution was established to give a smooth axial loading distribution and flowpath. Final airfoil aspect ratio and solidity (gap/chord ratio) distributions through the low-pressure compressor were set to minimize two-dimensional losses while balancing the loading and achieving the desired surge margin. The critical surge margin requirement was determined to be at part speed. Consequently, loadings were balanced accordingly and resulted in a surge margin of 18 percent at the aerodynamic design point. Controlled diffusion airfoils are used throughout to minimize losses.

The titanium drum rotor assembly concept of the initial design was retained. However, the single hub connecting the rotor assembly to the rotor shaft at the joint forward of the No. 1 bearing in the initial design and the integrated core/low spool design was eliminated in favor of tying the drum directly to the rim of the fan disk. The drum rotor was sized based on preliminary analyses of stress levels and deflections. Resulting stresses and lives met flight propulsion system design requirements. Subsequent structural analysis indicated that critical speed met the design criteria.

A flight-weight case for the flight propulsion system was defined that very closely resembled the initial design. Stresses in the case were found to be acceptable.

The low-pressure compressor exit surge bleed was moved from its initial design location aft of the fifth stator to forward of the fifth stator in the current design in order to improve performance of the bleed system. The bleed annulus at the outer wall of the core flowpath is specially contoured to minimize capture and turning losses. In the current design, turning vanes are used to direct the bleed discharge into the fan duct at the proper incidence angle for the exit guide vanes.

Predicted Performance

An assessment was conducted to define performance predictions for the current design of the low-pressure compressor. As shown in Table 11, the efficiency predicted for the current state-of-the-art low-pressure compressor design base is 89.7 percent. With incorporation of advanced technology applications, the adiabatic efficiency prediction exceeds the 89.9 percent goal level established for the low-pressure compressor at completion of the initial design.

TABLE 11

CURRENT FLIGHT PROPULSION SYSTEM LOW-PRESSURE COMPRESSOR
ADIABATIC EFFICIENCY PREDICTION
(Aerodynamic Design Point: 10675 m (35000 ft), 0.8 MN, Standard Day)

	Percent
State-of-the Art Design Base (Goal Clearance)	89.7
Rotor Tip Trenches	+0.2
Reduced Tip Clearance	+0.1
Predicted Efficiency (Status Clearance)	90.0
Goal Efficiency (Goal Clearance)	89.9

Benefits derived from specially contoured airfoil leading edges and improved cavity design are included in the current system estimate. An additional 0.2 percent increase is attributed to rotor tip trenching. Mechanical design results showed the capability to achieve a 0.0495 cm (0.0195 in) average rotor tip clearance for the low-pressure compressor of the flight propulsion system compared to a goal clearance of 0.0533 cm (0.0210 in). This 0.0038 cm (0.0015 in) tip clearance improvement was estimated to increase efficiency an additional 0.1 percent. The low-pressure compressor map was reviewed and updated at the completion of the detailed aerodynamic design.

The current low-pressure compressor aerodynamic design parameters and map were incorporated into the flight propulsion system performance simulation. Updated performance was defined at the aerodynamic design point and at key off-design operating points. Table 12 compares these results to the performance for the initial design. Current and initial design low-pressure compressor performance is generally similar at each operating point. Differences in airflow, speed, and efficiency (especially at the takeoff point) are attributable to map and off-design matching revisions made since the initial design. However, pressure ratio and exit temperature are unaffected by these differences.

TABLE 12

LOW-PRESSURE COMPRESSOR PERFORMANCE PARAMETER COMPARISON

	AERO DESIGN POINT(1)		MAXIMUM CRUISE(2)		MAXIMUM CLIMB(3)		TAKEOFF(4)	
	Initial Design*	Current Design	Initial Design*	Current Design	Initial Design*	Current Design	Initial Design*	Current Design
Pressure Ratio	1.77	1.77	1.75	1.75	1.80	1.79	1.64	1.64
Efficiency - %								
Adiabatic	89.9	90.0	90.0	90.4	89.5	89.3	90.7	92.2
Polytrophic	90.6	90.7	90.7	91.1	90.3	90.1	91.3	92.6
Corrected Inlet Airflow - (kg/sec)	56.9	56.9	56.1	56	58.1	58	49.8	51
Inlet Specific Airflow - (kg(lb)/sec/.093 sq.m)	16.1 (35.6)	16.1 (35.6)	15.9 (35.1)	15.8 (35.0)	16.5 (36.4)	16.4 (36.3)	14.1 (31.1)	14.5 (32.0)
Corrected Inlet Tip Speed - (m/sec.)	242	242	239	239	253	246	240	222
Exit Temperature - °C	66	66	64	63	86	85	121	121

Design and Off-Design Operating Conditions:

(1) Aerodynamic Design Point - 10675 m (35,000 ft), 0.8 Mn, Standard Day
(2) Maximum Cruise - 10675 m (35,000 ft), 0.8 Mn, Standard Day
(3) Maximum Climb - 10675 m (35,000 ft), 0.8 Mn, Standard Day + 10°C (18°F)
(4) Takeoff - SLTO, 0 Mn, Standard Day + 13.9°C (25°F)

* Values shown are after thrust size of initial engine design was downsized 12 percent.

4.3 Compressor Intermediate Case

The compressor intermediate case supports the fan case along with the low and high-pressure spool rotors, forms the flowpath from the low-pressure compressor to the high-pressure compressor inlet, and transfers engine loads to the mount system ring attached to the backside of the struts. In addition, the intermediate case contains the provisions and plumbing for the rotors and accessory drive shafts and gears.

The basic aerodynamic requirements of the compressor intermediate case are to remove exit swirl from the fan rotor and to duct air from the low-pressure compressor to the high-pressure compressor inlet without separation and with minimum loss. The case includes an inner ring which forms the outer diameter wall of the front bearing compartment and the inner diameter flowpath transition wall between the low-pressure and high-pressure compressors. Ten main structural core struts extend radially outward to the outer fan case to form the fan exit struts. Nineteen additional nonstructural fan exit guide vanes are bolted between the inner and outer fan walls. A center casing, which forms the outer diameter core flowpath wall and fan inner diameter wall is welded to the struts. This casing transfers engine loads to the mount system ring attached to the backside of the struts. The accessory drive system includes a drive gear which transfers power from the high-pressure compressor rotor to the accessory towershaft drive within the bottom strut. This shaft then transfers the power to an angled gearbox used to drive the main gearbox.

Figure 6 compares cross sections of the initial and current compressor intermediate case designs. These designs are quite similar with the current configuration representing the case designed in detail for the integrated core/low spool.

The current compressor intermediate case design is the same in concept as the initial design. However, two changes did occur during the detailed design of the case and the detailed design of the high-pressure compressor for testing in the integrated core/low spool. The number of struts was reduced from eleven to ten and acoustic treatment was removed from the intermediate case ring walls in the fan duct.

Matching of the exit vane array in the fan duct to minimize back pressure distortion on the fan rotor (caused by the thick upper pylon strut) resulted in the optimized array of the current design shown in Figure 6. Optimization included the removal of the vane adjacent to the suction side of the pylon to reduce distortion and avoid the extreme vane uncamber needed to achieve a reasonable passage area distribution.

INITIAL COMPRESSOR INTERMEDIATE CASE CROSS SECTION

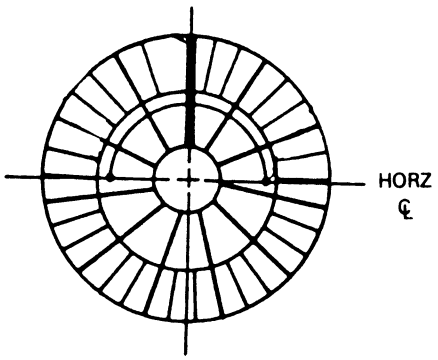

CURRENT COMPRESSOR INTERMEDIATE CASE CROSS SECTION

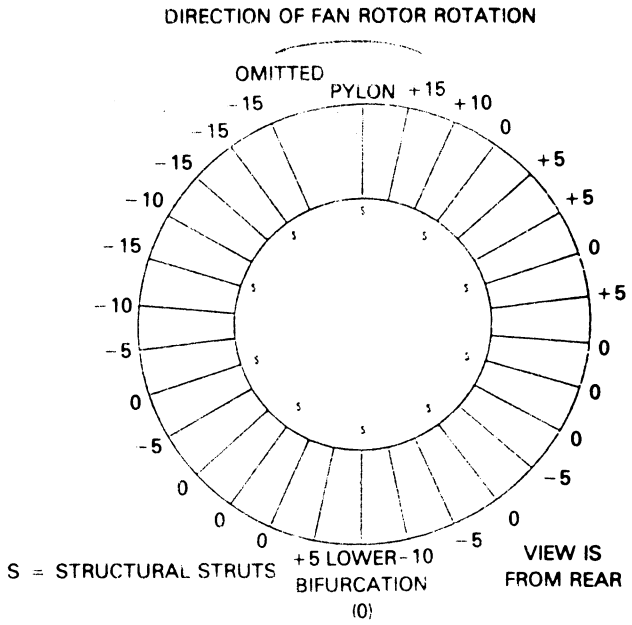

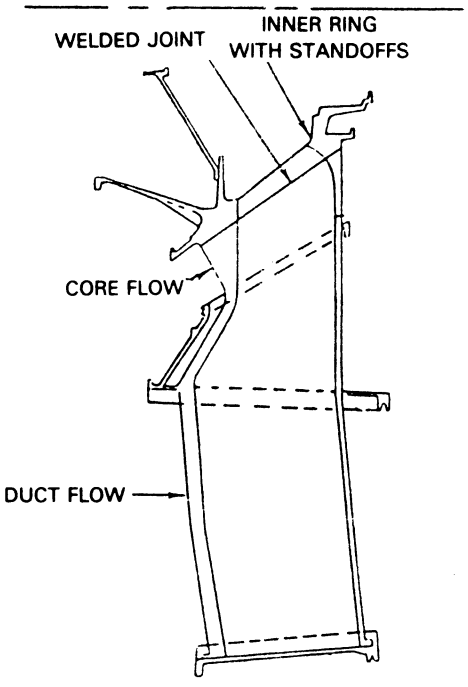

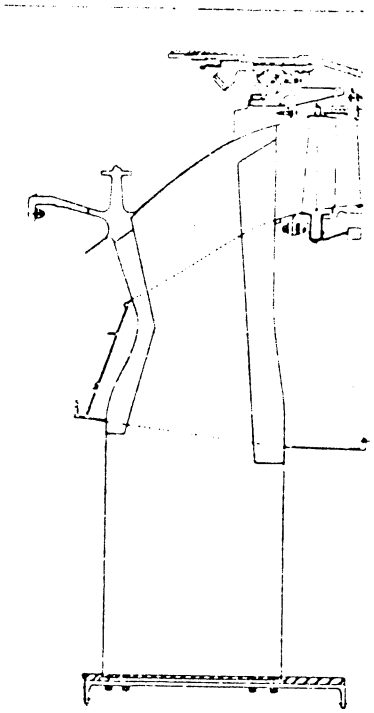

Figure 6 Flight Propulsion System Compressor Intermediate Case Section Comparison

The core portion of the structural struts is nonturning, with the last stator of the low-pressure compressor and the inlet guide vane to the high-pressure compressor aerodynamically accommodating the counterrotation of the low and high pressure spools. Flowpath design controls the wall static pressure gradients and avoids the risk of wall boundary layer separation, while making the radial transition between the compressors. A combination airfoil section (i.e., 65 series circular arc between the leading edge and maximum thickness point and 400 series to the trailing edge) was used to minimize leading edge blockage while providing increased thickness in the trailing edge region for improved resistance to foreign object damage.

The current design of the compressor intermediate case was analyzed in terms of the different types of loading effects on deflections and stresses. Thrust and gust loads, shown schematically in Figure 7, resulted in only a slight increase in maximum inner case radial ovalization. Distortion of the high-pressure compressor front case was found to have only a small impact on blade tip clearance under maximum thrust conditions. Flange and wall connections were thickened at the No. 1 and No. 2 bearing support interface and at the high-pressure compressor front case interface to achieve acceptable stress margins. The impact of strut gas load-induced deflections of the center casing, shown in Figure 8, was determined to cause no problem in outer case rotation for the flight propulsion system with its core case-mounted gearbox and accessories. Inner case twisting caused by strut-induced axial moments was found to be negligible. No local distortions were predicted and stresses in the structural struts were low. Nonstructural strut stresses were of no consequence because these vanes carry only their own tangential loads, and vane flutter stability was assessed as adequate.

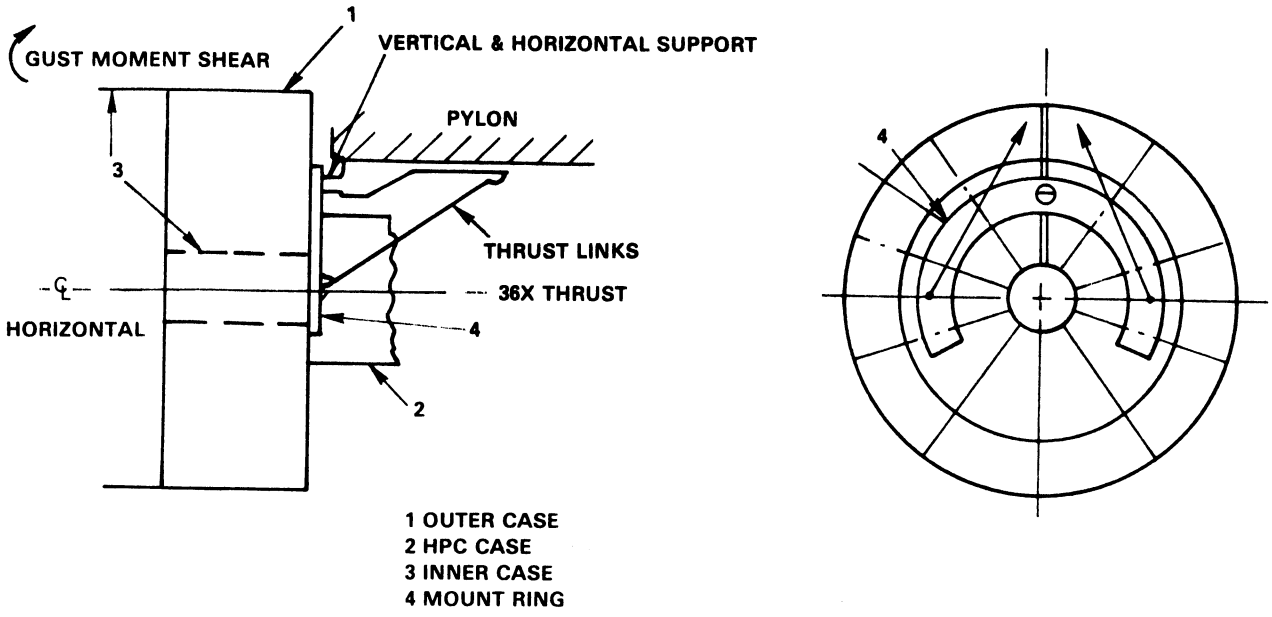

Figure 7 Current Compressor Intermediate Case Gust and Thrust Loads

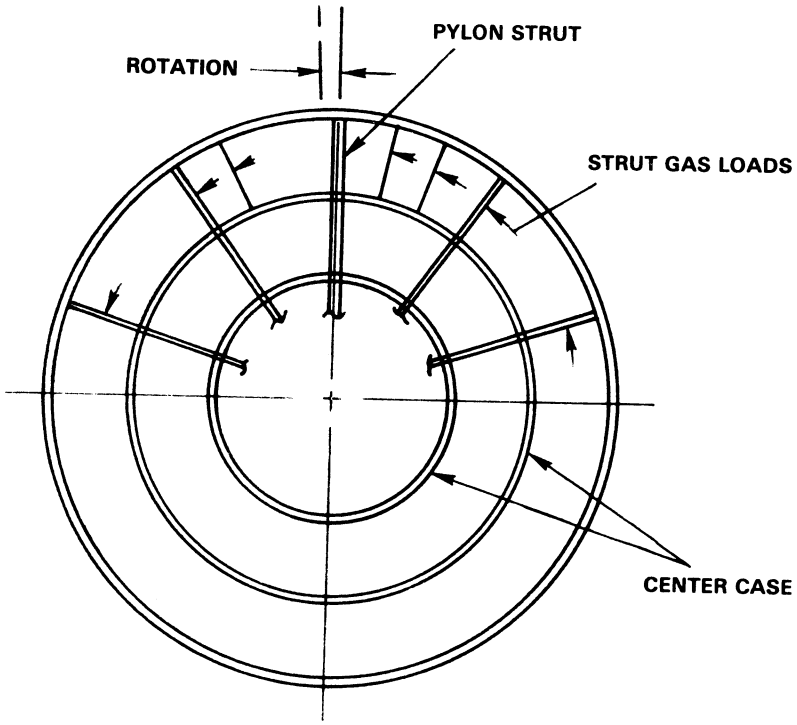

Figure 8 Current Compressor Intermediate Case Strut Gas Loading

4.4 High-Pressure Compressor

The flight propulsion system high-pressure compressor is an efficient ten-stage configuration designed to produce a 14:1 pressure ratio and achieve an adiabatic efficiency of 88.3 percent at the aerodynamic design point. Major aeromechanical features include a drum rotor, reduced interstage cavities, abradable blade tip trenches for improved internal aerodynamic efficiency, an axially-split front outer case containing variable geometry vanes in the first four stages, and a single-piece rear case accommodating the remaining stages of fixed stators. An additional feature which enables the design goals and durability estimates to be met is low loss, highly-loaded airfoils.

Figure 9 compares cross sections of the initial and current designs of the high-pressure compressor. A design summary is presented in Table 13. The most significant changes include a reduction in inlet hub/tip radius ratio from 0.63 to 0.56, an average reaction reduction from 0.58 to 0.52, endwall camber modifications, an average gap/chord ratio reduction from 0.93 to 0.89, and use of controlled diffusion airfoils in the majority of the airfoil rows. Other changes include relocation of the inner diameter bleed tube and several revisions to the rear case. Otherwise, aerodynamic designs for the initial and current high-pressure compressors are similar. The mechanical designs differ only in detail. The aerodynamic design and, for the most part, the mechanical design of the high-pressure compressor for the flight propulsion system were done in detail for the integrated core/low spool portion of the program.

TABLE 13

FLIGHT PROPULSION SYSTEM HIGH-PRESSURE COMPRESSOR SECTION DESIGN COMPAPISON
(Aerodynamic Design Point: 10675 m (35,000 ft), 0.8 Mn, Standard Day)

	Initial Design*	Current Design
Number of Stages	10	10
Pressure Ratio	14.0	14.0
Corrected Inlet Airflow, kg (lb)/sec	35.2 (77.5)	35.2 (77.5)
Surge margin - %	25	20
Corrected Inlet Tip Speed-m(ft)/sec	403 (1323)	379 (1245)
Inlet Specific Airflow, kg(lb)/sec/.093 sq.m	17.2 (38.0)	17.2 (38.0)
Hub/Tip Radius Ratio		
Inlet	0.63	0.56
Exit	0.922	0.924
Exit Mach Number (no blockage)	0.28	0.28
Average Aspect Ratio	1.56	1.52
Average Gap/Chord Ratio	0.93	0.89
Average Axial Velocity-to-Wheel Speed Ratio	0.55	0.559
Number of Airfoils (with inlet vane)	1352	1298
Number of Variable Stator Rows	4	4

* Values shown are after thrust size of initial engine design was downsized 12 percent.

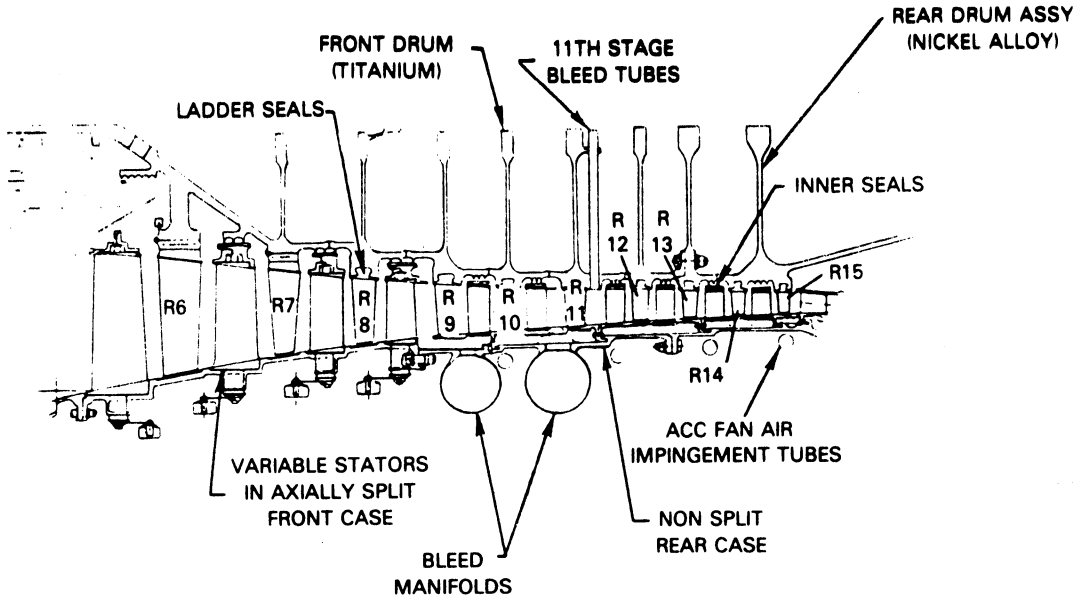

INITIAL HIGH PRESSURE COMPRESSOR CROSS SECTION

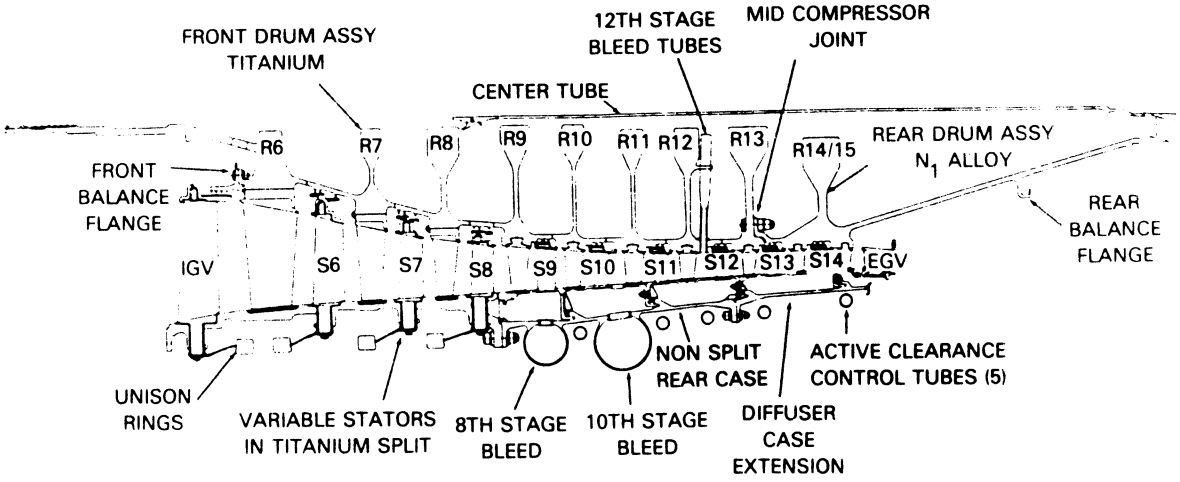

CURRENT HIGH PRESSURE COMPRESSOR CROSS SECTION

Figure 9 Flight Propulsion System High-Pressure Compressor Section Comparison

The newly defined flowpath is shown in Figure 10. The inlet hub/tip ratio of 0.56 represents the lowest obtainable ratio with the mechanical constraints imposed by the No. 3 bearing compartment. The annulus area distribution was set for the inlet specific flow using essentially a linear axial velocity decrease to the no-blockage exit Mach number. The flowpath approximates a constant mean diameter with some local variation to achieve the design surge margin (20 percent). The exit stage flowpath was canted about 5 degrees outward from the centerline to improve the aerodynamic match with the combustor diffuser section. Controlled diffusion airfoils were used throughout, with the exception of the first two blade rows (rotors 6 and 7) which were bladed with multiple circular arc airfoils. A 50 percent reaction level through the rear stages resulted in a turning requirement of 52 degrees in the last stator row to achieve axial discharge. A single row exit guide vane configuration was selected to do this because it permits shorter length, fewer airfoils, and lower weight as opposed to a two-row vane configuration. A 400 series airfoil was selected for the high-pressure compressor inlet guide vane because of its inherent large incidence range and choke margin capabilities.

Structural analyses resulted in a change from the eleven strut compressor intermediate case initially designed to a ten-strut configuration. All high-pressure compressor airfoil rows have adequate resonance and flutter margins.

Axial gaps were set to preclude rotor-to-stator contact during engine operation. Initial gapping of the high-pressure compressor included the incorporation of flow guides in stages nine through fifteen. Further analysis did not substantiate the anticipated performance benefits so these flow guides were removed from the current design.

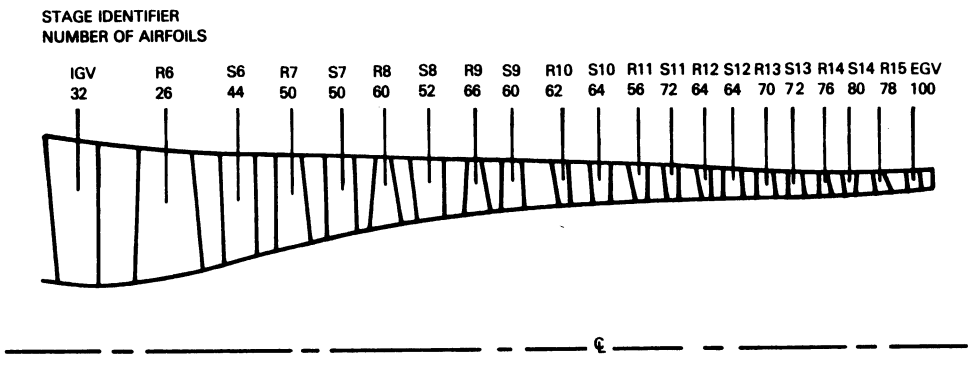

Figure 10 Flight Propulsion System High-Pressure Compressor Revised Flowpath

Several mechanical revisions were made to the high-pressure compressor compared to the initial design. These revisions include:

- o moving the inner diameter bleed tube from the eleventh to the twelveth stage;
- o reducing inner seal cavity sizes;
- o revising the center tube configuration;
- o increasing the disk bore diameters in stages eleven through fourteen to provide necessary clearance for the revised center tube;
- o and the removal of heat shielding and insulation from between the inner and outer walls of the rear case.

An oval entrance for the bleed tube through the compressor rotor drum, as shown in Figure 11, was used to reduce stress concentration.

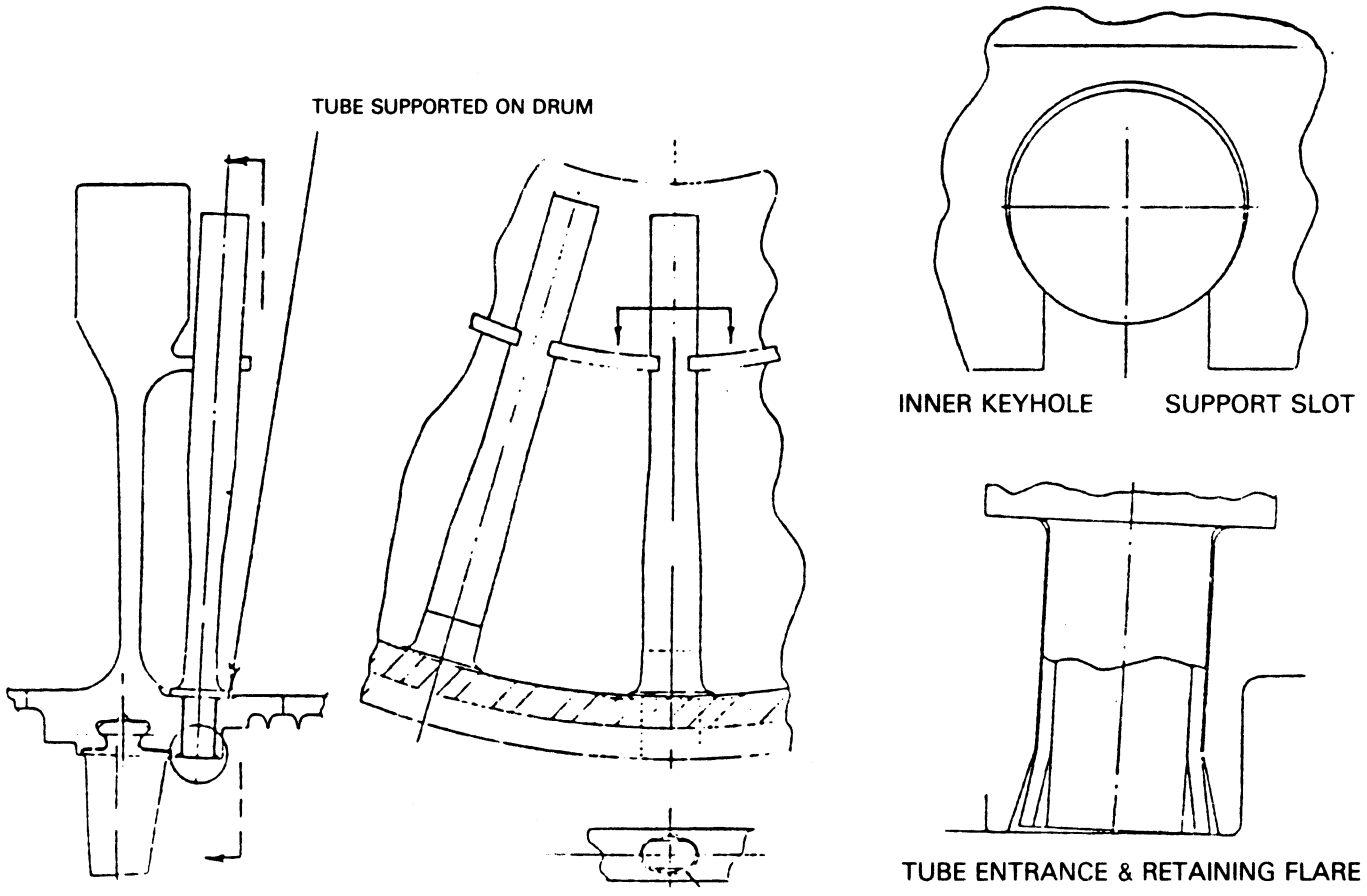

Figure 11 Current Solid Body Bleed Tube Configuration

Interstage cavity sizes were minimized, relative to the initial design, to reduce recirculation losses and the elimination of flow guides from the rear stages contributed to further loss reduction.

Current disk and rotor drum sizing was based on stress and life requirements for the flight propulsion system. Analyses showed most of the goals established for the flight propulsion system were met. Some perturbations were required in part thicknesses, weld locations, fillet radii, etc. for all areas to meet flight propulsion system goals. Areas requiring further analyses include the ninth, tenth, and thirteenth stage tangential attachments where disk lug stresses are too high, and the thirteenth stage rim which did not achieve the creep life goal.

Fully developed seals incorporated into the flight propulsion system prevent any passage of oil. Stages nine through fifteen are sufficiently sealed by the center tube to prevent oil from entering. In addition, the solid body bleed tubes act as a centrifugal separator for the drum bleed air.

Analysis of the initial center tube configuration indicated that local damping was required to provide adequate vibration margins. To accomplish this requirement, a stiffened design was developed and found acceptable. An increase in the bore diameters of the eleventh through the fourteenth stage disks was required for proper clearance. For ease of fabrication and assembly, it was also necessary to change from a one-piece to a two-piece center tube design.

The configuration of the initial front high-pressure compressor case was simply refined while some modifications were made to the rear case, including the redesign of stator vane retention hooks. In addition, thermal analysis indicated that heatshields and insulation between the inner and outer cases could be removed without affecting accurate temperature control of the case hooks, which are an integral part of the active clearance control system.

Predicted Performance

An assessment was conducted to define performance predictions for the current high-pressure compressor. The adiabatic efficiency estimate is shown in Table 14.

TABLE 14

CURRENT FLIGHT PROPULSION SYSTEM HIGH-PRESSURE COMPRESSOR
ADIABATIC EFFICIENCY PREDICTION
(Aerodynamic Design Point: 10675 m (35,000 ft), 0.8 Mn, Standard Day)

	Percent
State-of-Art Design System (Goal Clearances)	87.0
Rotor Tip Trenches	+0.8
Controlled Diffusion Airfoils	+0.4
Reduced Tip Clearance	+0.1
Predicted Efficiency (Status Clearance)	88.3
Goal Efficiency (Goal Clearance)	88.2

The current efficiency prediction of 88.3 percent exceeds the 88.2 percent goal level established for the high-pressure compressor at the completion of the initial design. The efficiency predicted for the high-pressure compressor with the current state-of-the art design system is 87.0 percent. Benefits derived from multiple circular arc airfoils, 20AA airfoil surface finish, stator clearances for good cavity design, and the compressor intermediate case pressure loss are included in the state-of-the-art design system estimate. An additional 1.2 percent benefit increase is attributed to the incorporation of rotor tip trenching and controlled diffusion airfoils. Mechanical design results showed the capability to achieve a 0.030 cm (0.012 in) average rotor tip clearance for the high-pressure compressor of the flight propulsion system compared to the goal clearance of 0.033 cm (0.013 in). This 0.003 cm (0.001 in) tip clearance improvement was estimated to increase efficiency an additional 0.1 percent. The high-pressure compressor map was essentially unchanged with only the flight propulsion system operating lines and points having varied from the initial design.

Current high-pressure compressor aerodynamic design parameters and the compressor map were incorporated into the flight propulsion system performance simulation. Updated performance was defined at the aerodynamic design point and at key off-design operating points. Table 15 compares these results to the performance for the initial design. Performance for the current and initial design high-pressure compressor is generally similar at each operating point except for reduced corrected inlet tip speeds caused by the lower inlet hub/tip radius ratio configuration for the current design. Some differences in parameter values do exist at take off because of off-design matching evolution, including the effects of high-pressure compressor tip clearance improvement compared to the initial design.

TABLE 15

FLIGHT PROPULSION SYSTEM HIGH-PRESSURE COMPRESSOR PERFORMANCE COMPARISON

	AERO DESIGN POINT(1)		MAXIMUM CRUISE(2)		MAXIMUM CLIMB(3)		TAKEOFF(4)	
	Initial Design*	Current Design	Initial Design*	Current Design	Initial Design*	Current Design	Initial Design*	Current Design
Pressure Ratio	14.0	14.0	13.8	13.8	14.2	14.2	12.8	13.0
Efficiency-%								
Adiabatic	88.2	88.3	88.3	88.4	88.0	88.1	88.9	89.4
Polytrophic	91.6	91.7	91.7	91.7	91.5	91.6	92.0	92.4
Corrected Inlet Airflow - (kg/sec)	35.1	35.2	34.9	34	35.4	35.5	32.7	33.6
Inlet Specific Airflow - (kg(lb)/sec/.093 sq.m)	17.2 (38.0)	17.2 (38.0)	17.1 (37.8)	17.1 (37.7)	17.3 (38.3)	17.4 (38.4)	16.0 (35.4)	16.4 (36.3)
Corrected Inlet Tip Speed - m/sec (ft/sec)	122 (403)	115 (379)	122 (402)	115 (378)	123 (404)	115 (380)	119 (393)	113 (373)
Rotor Speed - rev/min	13178	13177	13104	13092	13586	13586	13866	13969
Exit Temperature - °C	481	481	474	472	525	524	568	570

Design and Off-Design Operating Conditions:

(1) Aerodynamic Design Point - 10675 m (35,000 ft), 0.8 Mn, Standard Day
(2) Maximum Cruise - 10675 m (35,000 ft), 0.8 Mn, Standard Day
(3) Maximum Climb - 10675 m (35,000 ft), 0.8 Mn, Standard Day + 10°C (18°F)
(4) Takeoff - SLTO, 0 Mn, Standard Day + 13.9°C (25°F)

* Values shown are after thrust size of initial engine design was downsized 12 percent.

4.5 Combustor

The flight propulsion system combustor component design features an annular, two-stage configuration that combines advances in aerodynamic, thermodynamic and structure-mechanics technology to provide a compact system capable of low emissions and high performance. This configuration has a predicted efficiency of 99.95 percent at design and off-design operating conditions and meets all performance, structural and emissions goals established for the program with the exception of oxides of nitrogen. Major design features include a short curved-wall, dump diffuser; pilot and main zone combustion; and advanced segmented liners with enhanced cooling capabilities and improved durability.

The combustor design also includes a curved-wall prediffuser which turns the airflow outward to more nearly align the airflow with the combustor centerline and reduce pressure losses associated with flow turning around the front end of the combustor. An outward flowpath cant of five degrees in the high-pressure compressor exit guide vanes initiates the turning. The prediffuser has an overall area ratio of 1.5, with a length-to-inlet height ratio of 3.5 and accomplishes, in itself, nine degrees of turning relative to the engine centerline. Twenty-four diffuser case struts are located downstream of the prediffuser dump plane to transfer inner case loads to the outer case. The combustor includes pilot and main burning zones patterned after the Experimental Clean Combustor Program two-stage design to improve control of emissions. The pilot zone is designed to minimize emissions of carbon monoxide and unburned hydrocarbons at low power flight conditions. At higher powers, the majority of fuel is injected into the main zone, which is designed to minimize oxides of nitrogen and smoke emissions. The two-stages are designed to provide a maximum temperature rise of 865°C (1589°F) within a 24.1 cm (9.5 in) overall combustion chamber length. A total of 120 counter parallel FINWALL® (CPFW) segments is used to line the combustion chamber. This liner design approach enables a component low cycle fatigue life of 11700 hours (7200 missions). External to the diffuser case, fuel supply tubes and manifolds are completely shrouded to contain fuel leaks. The diffuser case centerbody includes integrally cast struts and bosses for installing fuel nozzle mount pins and ignitors.

Figure 12 compares cross sections of the initial and current designs of the combustor. As shown in this figure, the current combustor design is relatively unchanged from the initial design. The combustor for the flight propulsion system was designed in detail for use in the integrated core/low spool. Design details are reported in Reference 5.

The major aerodynamic and thermo-mechanical design parameters for both the initial and current designs of the combustor are presented in Table 16. As shown in the table, there is much similarity.

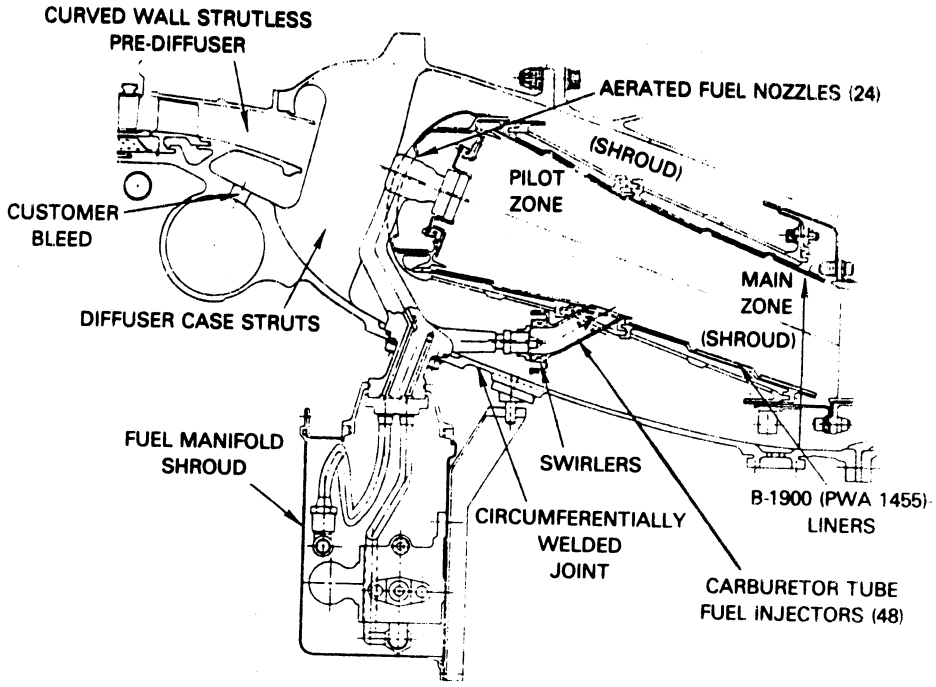

INITIAL COMBUSTOR CROSS SECTION

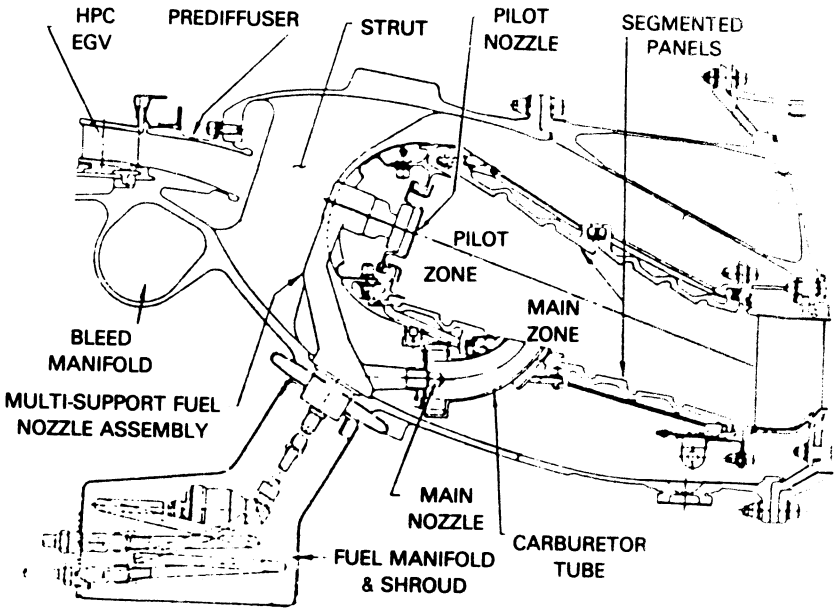

CURRENT COMBUSTOR CROSS SECTION

Figure 12 Flight Propulsion System Combustor Section Comparison

TABLE 16

FLIGHT PROPULSION SYSTEM COMBUSTOR SECTION DESIGN COMPARISON
(Aerodynamic Design Point: 10675 m (35,000 ft), 0.8 Mn, Standard Day)

	Initial Design*	Current Design
Corrected inlet airflow, kg/sec (lb/sec)	3.15 (6.96)	3.12 (6.90)
Inlet pressure, MPa (psia)	1.40 (203)	1.40 (203)
Inlet temperature, °C (°F)	481 (899)	481 (898)
Section pressure loss (percent)	5.50	5.50
Fuel/air ratio	0.0240	0.0242
Combustor exit temperature, °C (°F)	1287 (2348)	1293 (2359)
Efficiency (percent)	99.95	99.95
Prediffuser		
Area Ratio	1.5	1.5
Length-to-Inlet Height Ratio	3.5	3.5
Number of Struts	24	24
Overall Combustion Chamber Length - cm (in.)	24.1 (9.5)	24.1 (9.5)
Number of Nozzles		
Pilot Zone	24	24
Main Zone	48	48

* Values shown are after thrust size of initial engine design was downsized 12 percent.

The structural configuration contains the following features: Turbine vane torque loads are taken at the vane outer attachment to avoid transmitting them to the inner combustor case. The inner attachments of the turbine vanes are designed to allow radial growth of the vanes to prevent the high radial loads imposed on the inner combustor case assembly from causing deflection and rubbing of the high-pressure compressor discharge seal. Radial deflection at the plane of the turbine vanes is further resisted by the following changes to the diffuser case:

- o an increase in strut trailing edge thickness;
- o an increase in strut inner chord;
- o a repositioning of an inner support ring;
- o and an increase in outer shell thickness.

The evolution of the diffuser case-strut design is illustrated in Figure 13.

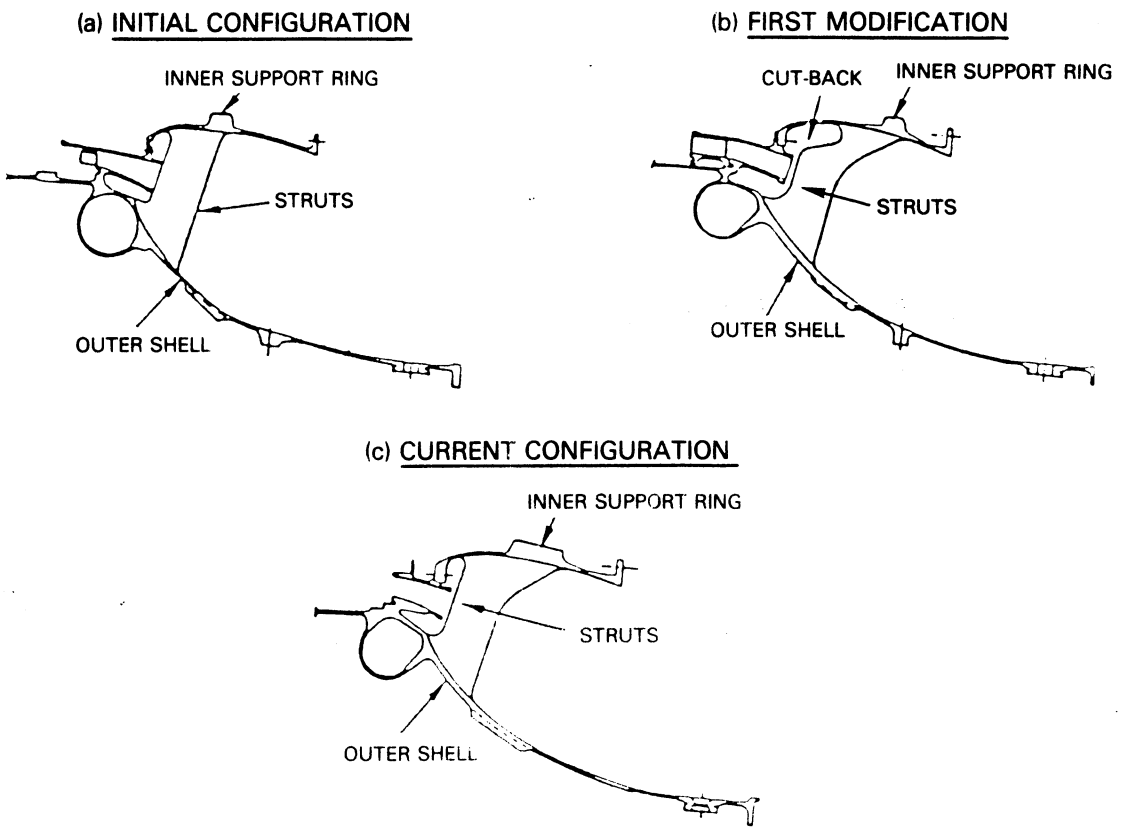

Figure 13 Combustor Diffuser Case Design Evolution

The outer shroud-cantilevered exit guide vane assembly was revised, as shown in Figure 14, and features the following modifications.

- Vanes with integral inner and outer shrouds that are circumferentially separated into groups of five vanes to relieve thermal gradient stresses.
- Decoupled inner and outer prediffuser duct walls.
- A sheet metal seal to minimize leakage through the gap between the vanes and inner prediffuser wall.
- Feather seals to control air leakage through the gaps between vane segments.

The combustor liner segments were reconfigured to two, three, or four panel designs with the panel lengths for three of the segments shortened based on the results of detailed thermal analysis. An optimized convective cooling configuration for the panel cross section was established, including cooling hole diameter and spacing. A maximum wall temperature of 884°C (1624°F) was established for the main zone. Total liner cooling flow is 31 percent of the total combustor airflow. Life analysis for the liner resulted in a predicted 7,200 cycles (or 11,700 hours) before crack initiation in a panel compared to a goal of 8,000 hours.

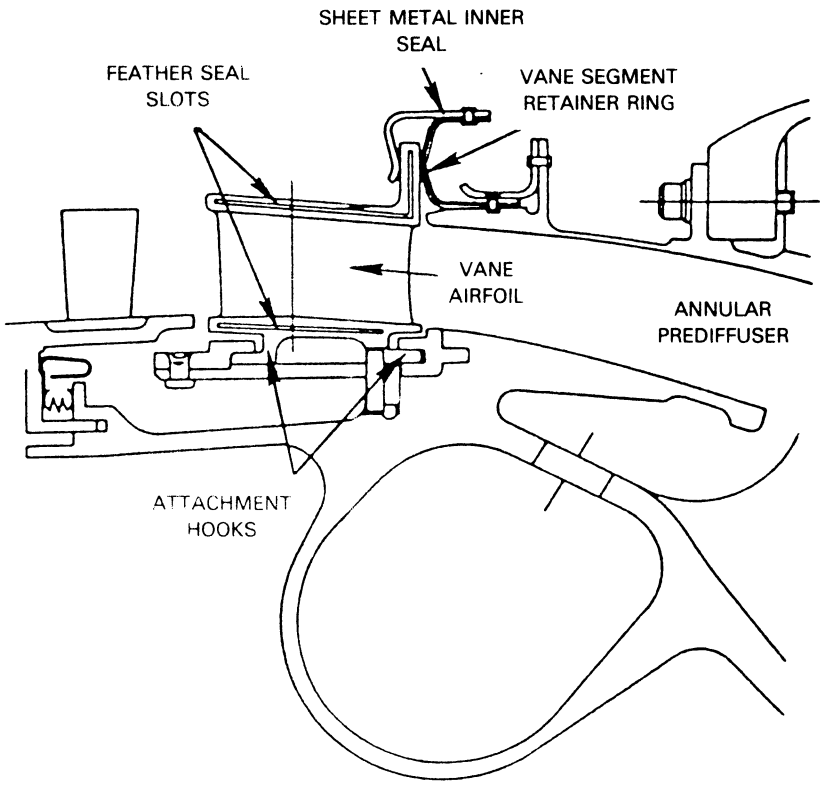

Figure 14 Revised High-Pressure Compressor Exit Guide Vane Assembly

A typical liner segment is shown in Figure 15. The annular combustor contains 120 liner segments. Axial feather seals are on the sides of the segments to control leakage. Cooling is accomplished with the counter-parallel FINWALL technique. This technique consists of a series of axial cooling holes across the segment. Cooling air enters the liner through slots on the liner cold wall. It is then split to flow both counter and parallel to the hot gas flow.

The main zone carburetor tube configuration, shown in Figure 16, incorporates many of the features developed in the Sector Combustor Rig portion of the program. The most prominent include (1) radial inflow swirler vane geometry, (2) co-rotational (secondary) swirler vane geometry, and (3) optimized carburetor tube length. Carburetor tube support lugs are incorporated at the rear of the tube to provide a fully supported design. Refinement of the fuel nozzle support assembly resulted in the selection of casting as the fabrication approach because of the complex geometry of this assembly. The resulting fuel nozzle configuration is illustrated in Figure 17. Fuel manifold system and sealing shroud designs were refined without significant changes from the initial configurations.

Predicted Performance

Table 17 compares combustor performance design goals with the predicted performance for the current design. As shown in Table 17, diffuser and combustor testing confirmed a preliminary pressure loss level of 5.5 percent. Emissions levels for the current flight propulsion system were projected from component testing to be slightly higher than initial estimates for unburned hydrocarbons and carbon monoxide, and slightly lower for oxides of nitrogen. A significant reduction in smoke is currently projected. Analysis confirmed a 99.95 percent combustion efficiency level.

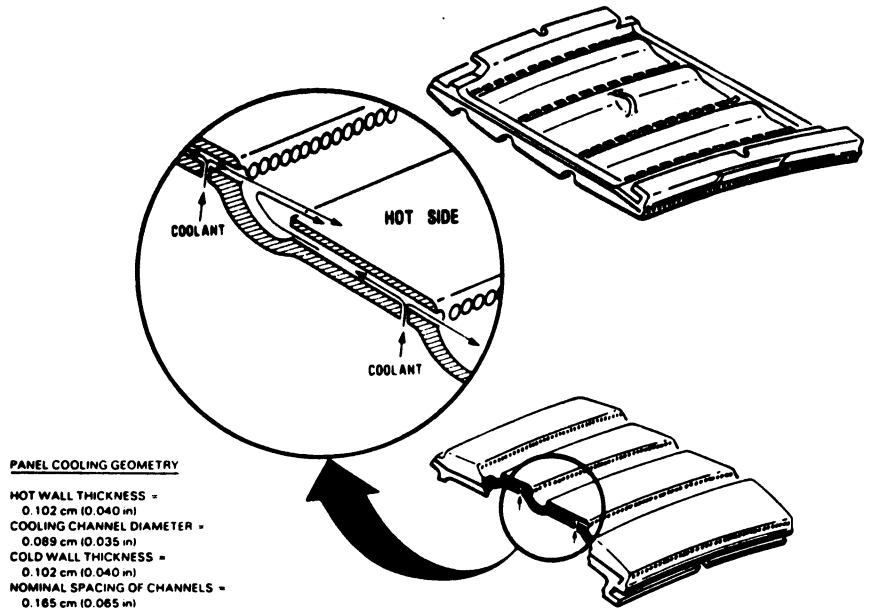

Figure 15 Typical Liner Segment

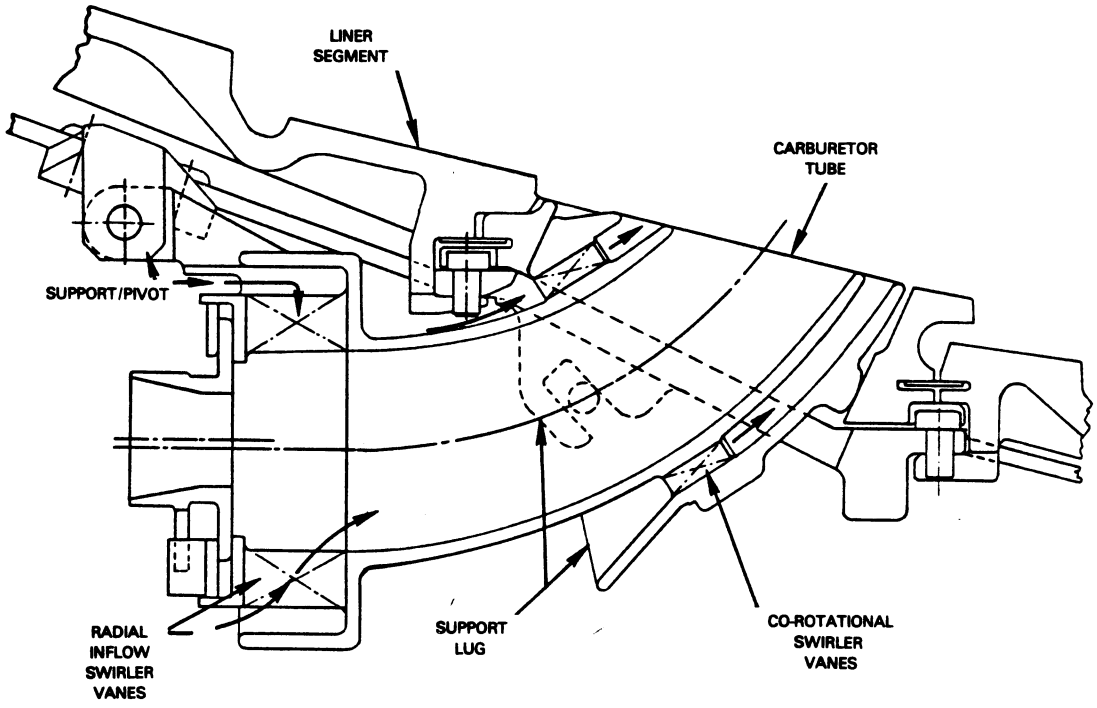

Figure 16 Revised Combustor Carburetor Tube Configuration

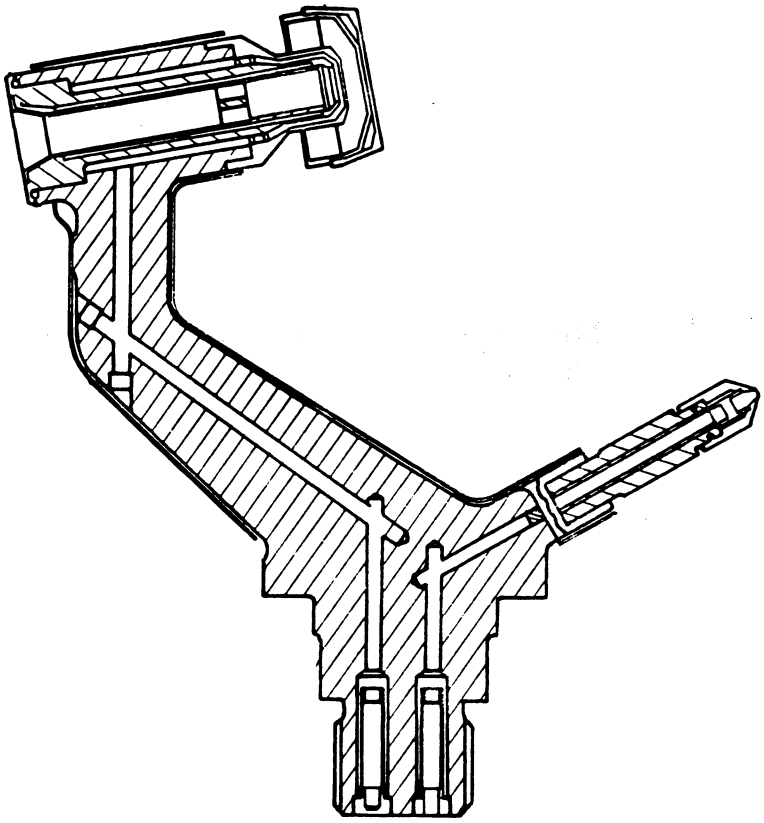

Figure 17 Revised Combustor Fuel Nozzle Configuration

TABLE 17

FLIGHT PROPULSION SYSTEM COMBUSTOR PREDICTED PERFORMANCE

	Design Goal	Initial Design	Predicted Performance Current Design
Overall pressure loss (percent)	5.5	5.5	5.5
Maximum Temperature Pattern Factor	0.37	0.37	0.28
Outer Diameter Skewed Radial Profile Peak Exit Temperature - °C (°F)	121 (250)	121 (250)	104 (220)
Emissions			
Total Unburned Hydrocarbons (HC)*	0.4	0.20	0.32
Carbon Monoxide (CO)*	3.0	1.7	1.8
Oxides of Nitrogen (NO_x)*	3.0	4.6	4.3
Smoke Number (SAE)	20	20	4

* lbm/1000 lbf thrust - hr/cycle

Current and initial aerothermodynamic designs for the combustor differ where parameters have been influenced by sector and full annular rig testing. Included are improvements in temperature pattern factor and radial profile. These aerothermodynamic design parameters were incorporated into the flight propulsion system performance simulation. Updated performance was defined at the aerodynamic design point and at key off-design operating points. Table 18 compares these results to the performance for the initial design. Combustor performance for the initial and current designs is quite similar at each of the key operating conditions. The small differences at takeoff are a result of off-design matching evolution since the initial design. Airflow differences are a result of air bleed quantity changes. Combustor exit temperatures show the effects of philosophies for matching at the aerodynamic design point and rating at the key operating points.

TABLE 18

FLIGHT PROPULSION SYSTEM COMBUSTOR PERFORMANCE PARAMETER COMPARISON

	AERO DESIGN POINT(1)		MAXIMUM CRUISE(2)		MAXIMUM CLIMB(3)		TAKEOFF(4)	
	Initial Design*	Current Design	Initial Design*	Current Design	Initial Design*	Current Design	Initial Design*	Current Design
Corrected Inlet Airflow - (kg/sec)	3.15	3.12	3.16	3.13	3.14	3.11	3.17	3.15
Inlet Pressure - (kg(lb)/6.451 sq.cm.) abs.	92 (203)	92 (203)	89 (197)	89 (197)	96 (213)	96 (212)	201 (444)	206 (456)
Inlet Temperature - °C	481	481	474	472	525	524	568	571
Section Pressure Loss - %	5.50	5.50	5.53	5.53	5.44	5.43	5.54	5.58
Fuel/Air Ratio	.02406	.02420	.02360	.02365	.02628	.02651	.02673	.02667
Exit Temperature - °C	1287	1293	1268	1268	1387	1393	1435	1435
Efficiency - %	99.95	99.95	99.95	99.95	99.95	99.95	99.95	99.95

Design and Off-Design Operating Conditions:

(1) Aerodynamic Design Point - 10675 m (35,000 ft), 0.8 Mn, Standard Day
(2) Maximum Cruise - 10675 m (35,000 ft), 0.8 Mn, Standard Day
(3) Maximum Climb - 10675 m (35,000 ft), 0.8 Mn, Standard Day + 10°C (18°F)
(4) Takeoff - SLTO, 0 Mn, Standard Day + 13.9°C (25°F)

* Values shown are after thrust size of initial engine design was downsized 12 percent.

4.6 High-Pressure Turbine

The flight propulsion system high-pressure turbine is an efficient singlestage system designed to operate at a high velocity ratio and low axial velocity (throughflow) to wheel speed ratio. Major component design features, in addition to the single stage concept (which provides savings relative to initial engine cost, weight and maintenance costs) include low-loss, highly-loaded airfoils and active clearance control for increased aerodynamic efficiency; improved gap and rim sealing for reduced leakage; and oxidation-resistant coated single crystal airfoil material for improved durability. This configuration, with a predicted adiabatic efficiency of 89.1 percent at the aerodynamic design point, is a major contributor to the overall 15 percent improvement in cruise thrust specific fuel consumption for the flight propulsion system as compared to the JT9D-7A reference engine.

The design of the high-pressure turbine utilizes advanced technology in the areas of aerodynamics, structures and materials to enhance efficiency, durability and performance retention. The disk rim region has a five-tooth blade attachment with elliptical cooling air supply holes.

Full-ring side plates seal the disk attachment front and rear regions. To allow the engine to operate safely at high combustor exit temperatures with minimal cooling requirements, the blades and vanes are fabricated from a high-strength, high-temperature single crystal alloy.

Figure 18 compares cross sections of the initial and current designs of the high-pressure turbine while Table 19 summarizes the major design parameters for both. Basic aerodynamic and mechanical design parameters for the initial and current high-pressure turbines are very similar. The differences are attributed primarily to evolution during the detail component design for the integrated core/low spool and are reflected in design updates for the flight propulsion system.

Aerodynamic and mechanical detail designs for the integrated core/low spool high-pressure turbine (see Reference 6) essentially represent those for the flight propulsion system. Performance data used to design the high-pressure turbine for the integrated core/low spool were a combination of flight propulsion system predictions and integrated core/low spool expectations.

While the aerodynamic definition for the high-pressure turbine remained basically unchanged from the initial design, the current mechanical design configuration for the flight propulsion system incorporates numerous changes.

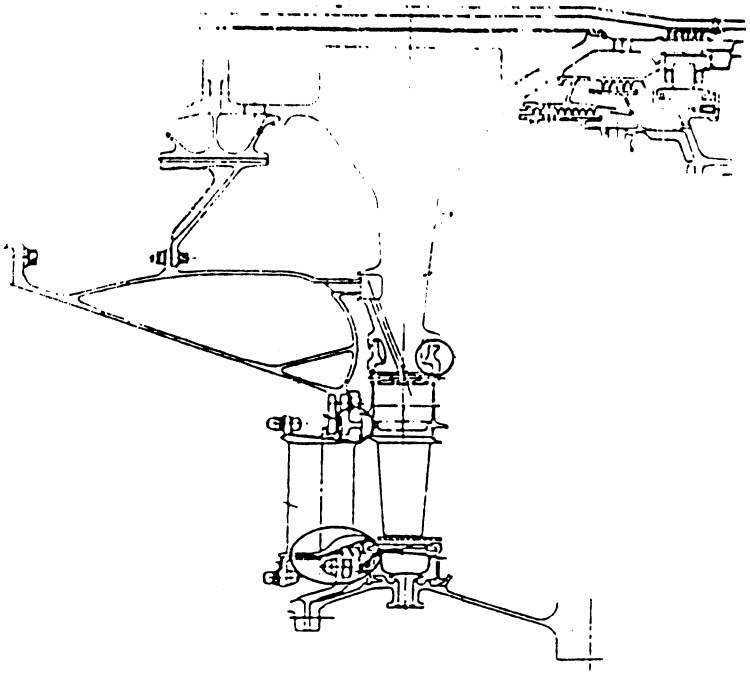

INITIAL HIGH PRESSURE TURBINE CROSS SECTION

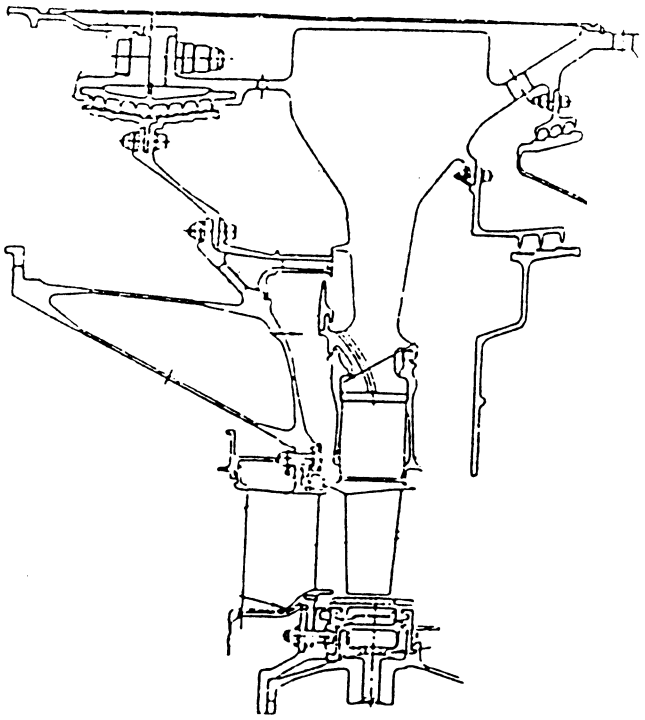

CURRENT HIGH PRESSURE TURBINE CROSS SECTION

Figure 18 Flight Propulsion System High-Pressure Turbine Section Comparison

TABLE 19

FLIGHT PROPULSION SYSTEM HIGH-PRESSURE TURBINE SECTION DESIGN COMPARISON
(Aerodynamic Design Point: 10675 m (35,000 ft), 0.8 Mn, Standard Day)

	Initial Design*	Current Design
Number of Stages	1	1
Pressure ratio	4.03	3.99
Mean velocity ratio	0.56	0.56
(AN^2) max. ~ sq.cm $(rev/min)^2$	316.1×10^9	305.8×10^9
Disk rim speed (max), m(ft)/sec	527 (1730)	521 (1710)
Enthalpy change - SLTO, Btu/N(Btu/lb)	858.5 (193.0)	846.4 (190.3
Mean blade turning, degree	118	117.5
Number of blades	54	54
Number of vanes	24	24
Coolant/leakage flow (percent)	13.25	13.6
Average Reaction (percent)	43.0	43.0

* Values shown are after thrust size of initial engine design was downsized 12 percent.

The high-pressure compressor discharge seal was changed from a wide channel to a nine knife-edge rotating labyrinth configuration since thermal and structural refinement studies on the knife-edged labyrinth seal showed that tight running clearances could be maintained. Felt metal is used as the rubstrip material to accommodate local interferences. Results from these studies are indicated in Table 20.

TABLE 20

PREDICTED HIGH-PRESSURE COMPRESSOR DISCHARGE SEAL RADIAL CLEARANCES

Operating Condition	Gap Location		
Avg. clearance, cm (in)	Front	Center	Rear
Aero. Design Point	0.030 (0.012)	0.035 (0.014)	0.027 (0.011)
Sea Level Takeoff	0.033 (0.013)	0.033 (0.013)	0.033 (0.013)

Optimization of blade cooling, conducted under the High-Pressure Turbine Cooling Model supporting technology program (see Reference 10) resulted in the radial ribs being relocated rearward and thickened toward the root section. Showerhead holes located on the leading edge were eliminated at the root section. Trip strips were added to both sidewalls of the showerhead (front) cavity and to the suction sidewalls of the center cavities. The showerhead cavity was also extended rearward at the tip and trip strips were added to provide proper cooling of the tip. Cooling air is now injected directly from the aft cavity into the trailing edge pedestal cavity, and the number of trailing edge pedestal rows has been increased from 6 to 7. A comparison of internal configurations is shown in Figure 19. These internal blade changes permit blade life goals to be met with the desired cooling airflow level. Predicted life for the current flight propulsion system high-pressure turbine blade is now 3500 missions (16,000 hours) compared to the 2200 missions (10,000 hours) goal established in the initial design.

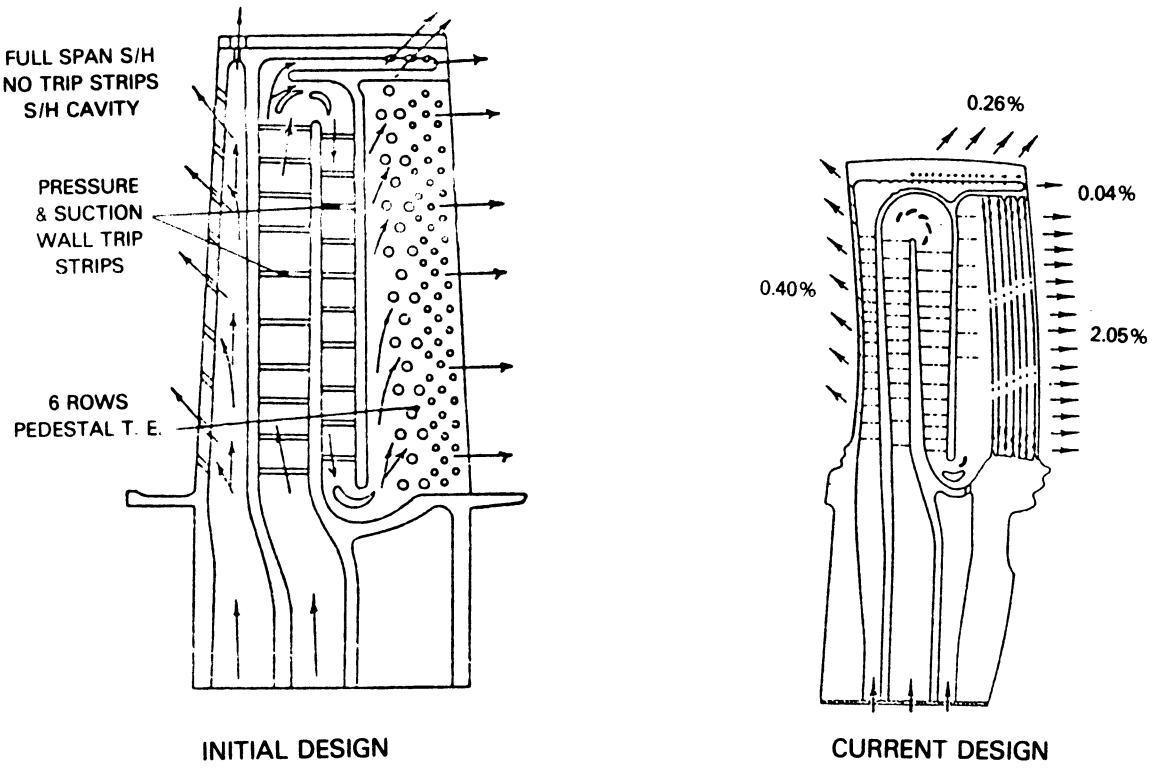

Figure 19 High-Pressure Turbine Blade Cooling Configuration Comparison

The blade attachment configuration was changed from four to five teeth to reduce the disk lug concentrated fillet stress. However, stresses in the disk for the flight propulsion system are still up to twelve percent greater than allowable; whereas, the blade margins are sufficient. Further refinement of the attachment design for the flight propulsion system will achieve the required stress balance between the disk and blade.

To avoid blade natural frequencies in the engine operating speed range, (1) orientation of the secondary axes (rotation angle about the primary or radial axis) of the single crystal blade material is controlled to approximately 25 degrees; and (2) the number of turbine intermediate case struts was reduced from 14 to 11. The 25 degree secondary axis orientation aligns the material's higher modulus of elasticity with the blade's trailing edge mean chord line. The 11E frequency line showed ample margins for the first and second vibratory modes.

Optimization of vane cooling resulted in only minor refinements to the vane internal configuration defined in the initial design. Calculated vane life predictions for oxidation and cracking caused from interacting creep and low cycle fatigue are shown in Table 21. All goals are attainable with one recoating.

TABLE 21

CURRENT HIGH-PRESSURE TURBINE VANE LIFE ESTIMATES

	Flight Propulsion System Goal	Flight Propulsion System Current Design
Oxidation	6,000 hrs.*	7,000 hrs.*
Cracking	10,000 hrs. (2200 missions)	11,000 hrs.(2,500 missions)

* A recoating achieves 10,000 hours

The initial vane attachment configuration was refined to improve structural load paths and reduce airflow leakage. The vane is currently mechanically retained by clamping at the outer attachment and engagement in a slot at the inner attachment. The inner attachment rail fits the inner support slot with minimum clearance to restrict vane twist while accommodating thermal growth. Reaction to vane circumferential loads is taken at the outer attachment to avoid excessive torque loads at the inner support and improper loading of the combustor diffuser case struts. Pressure loads in the axial direction are divided between the inner and outer attachment.

Feather seals, used to close gaps and reduce leakage between the vane platforms, were refined. Two feather seals are incorporated into the turbine vane outer platform, as shown in Figure 20, to replace the original four-piece feather seal configuration. This change was based on cooling air leakage studies and leakage rig testing results made available from the Energy Efficiency Engine High-Pressure Turbine Leakage supporting technology program (Reference 11). The revised configuration eliminates two of the three feather seal intersections that were determined to be high leakage areas. A vane leakage of 1.4 percent for the flight propulsion system was established based on the results of these analyses.

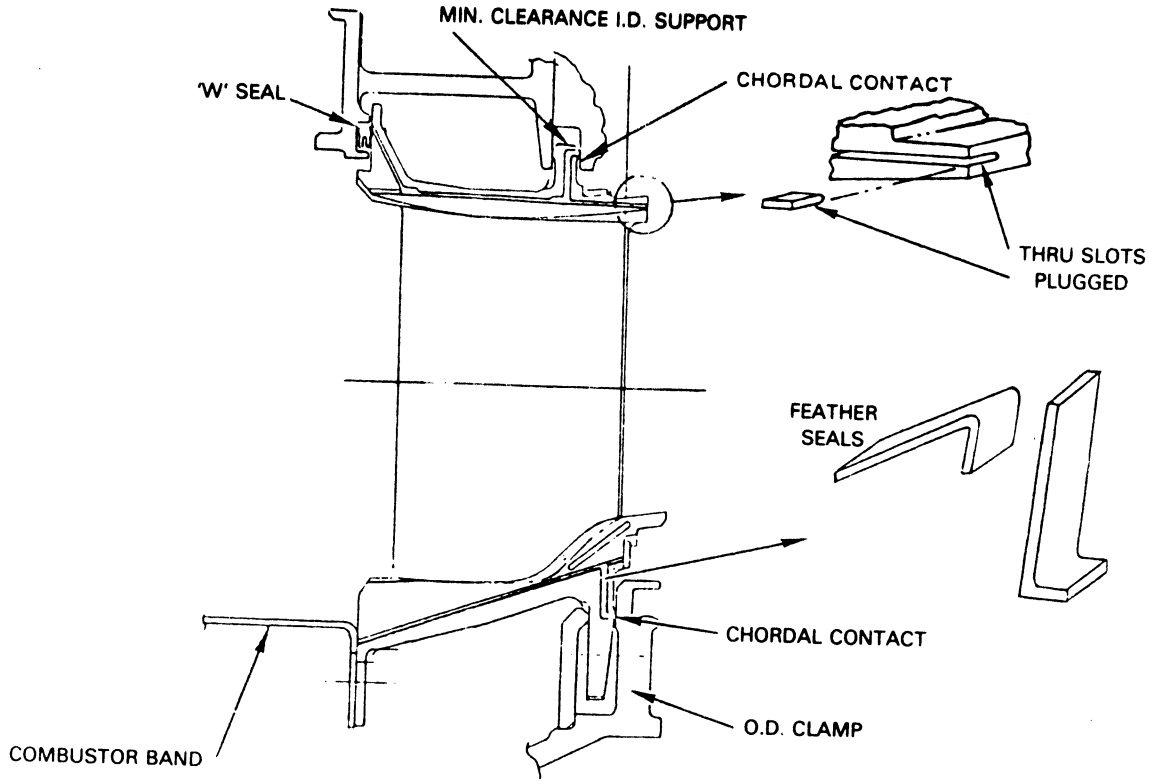

Figure 20 Current Vane Air Leakage Control

Blade and vane fabrication approaches were changed from two-piece, bonded construction to one-piece castings because of manufacturing cost reductions projected for single-piece fabrication.

Refined structural analysis of the high-pressure turbine disk resulted in a boltless sideplate design (Figure 21) which replaced the initial bolted configuration. In the boltless design, the rear sideplate is canted 4 degrees rearward so that centrifugal sideplate loads will resist rearward blade loads and pressure loads caused by the pressure difference between blade cooling air and the disk rear cavity.

Curved, elliptical blade cooling air supply holes in the disk rim (Figure 22) replace the straight, round blade cooling air supply holes of the initial design. The elliptical hole shape improves the rim breakout stress concentration factor relative to a round hole. The curvature improves the flow of stresses in the disk rim by providing increased hole-to-front sidewall thickness.

To further optimize the blade cooling air supply pressure at the root location, a vortex plate was added to the tangential on-board injection (TOBI) system, also shown in Figure 21. Free vortexing of the cooling air was selected as the method for increasing the inlet pressure of the air entering the cooling air supply holes in the disk.

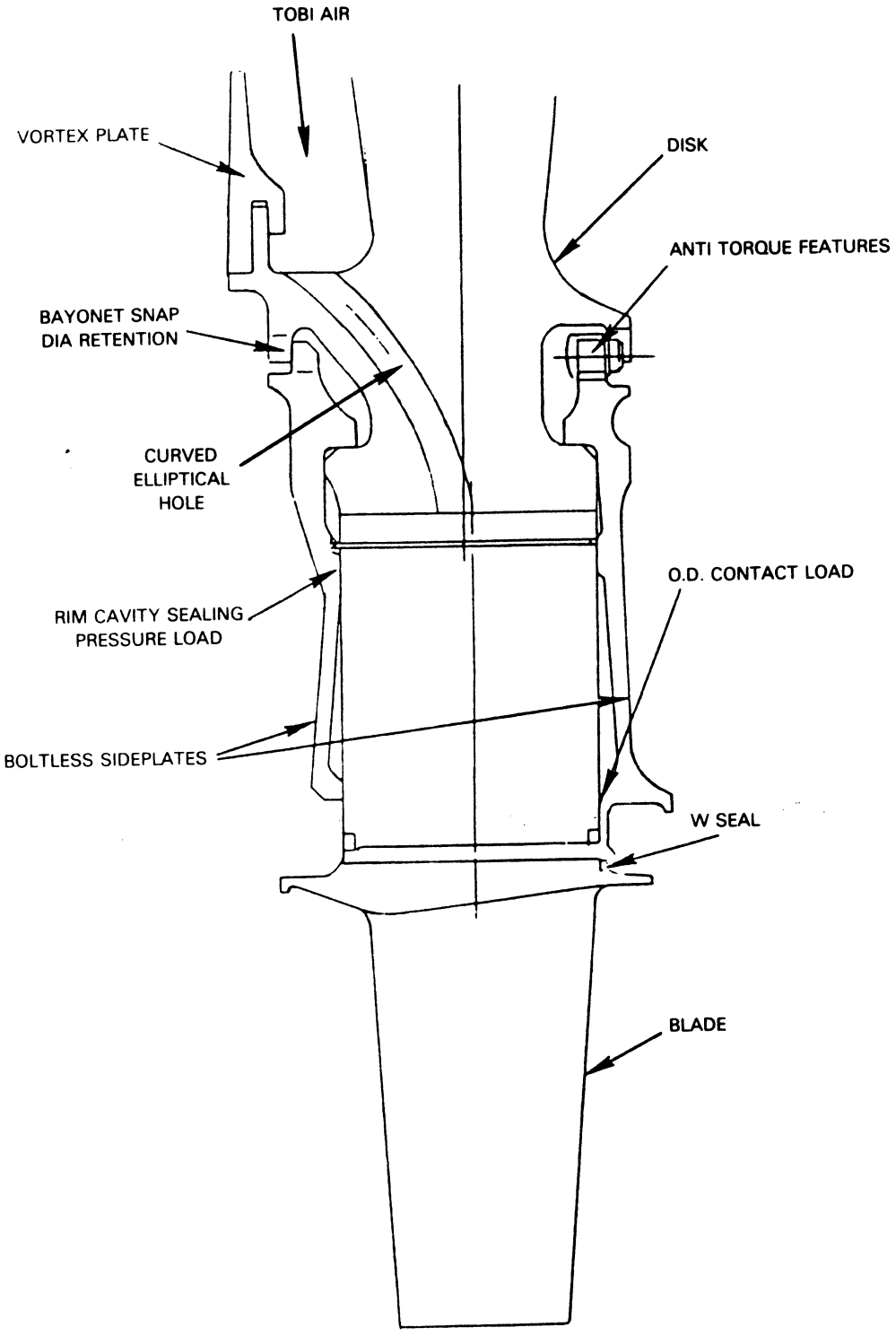

Figure 21 Boltless Sideplate Design

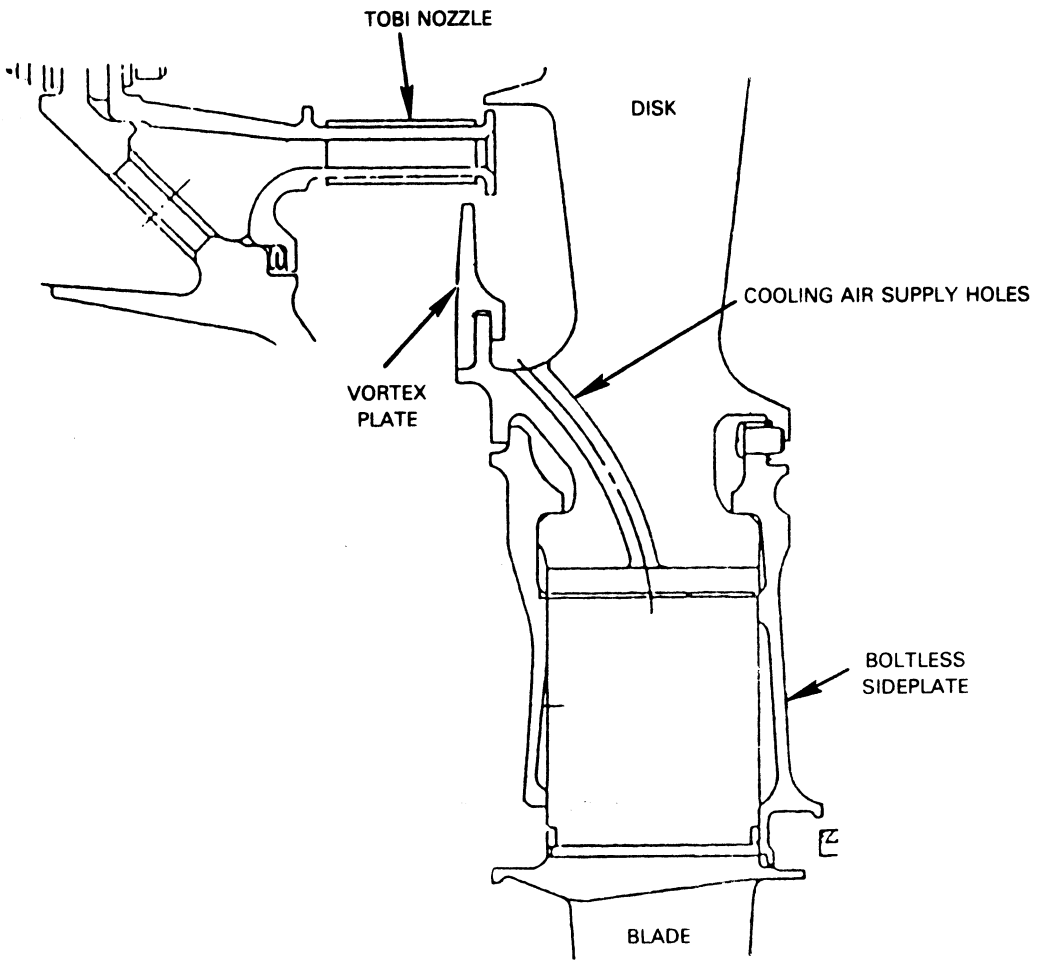

Figure 22 Curved, Elliptical Blade Cooling Air Supply Holes and Tangential On-Board Injection (TOBI) System With Vortex Plate

A 'mini' tangential on-board injection (TOBI) system was incorporated in the disk front rim cavity, as shown in Figure 23. This system reduces windage heat-up by preswirling the air in the front disk rim cavity. The resultant swirl field also provides a radial pressure gradient between the blade supply TOBI system and the gas path static pressure, thus linking the blade supply pressure directly to the inner gas path pressure at the blade leading edge. This linkage keeps the pressure relationship fixed independent of seal leakage, attachment leakage, and blade flow area.

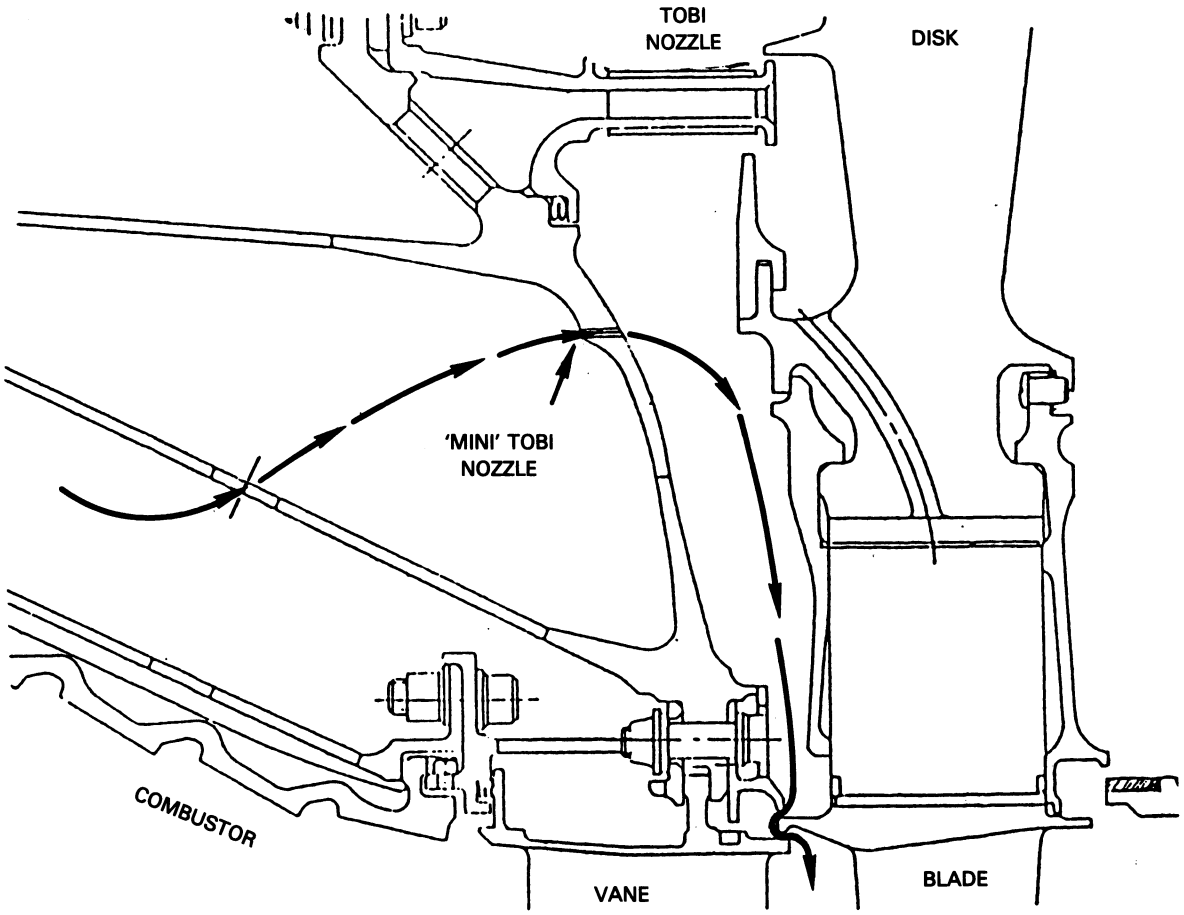

Figure 23 Mini-TOBI Nozzle Configuration

The addition of a seal at the rear of the high-pressure turbine disk and a reduction in high-pressure compressor discharge seal diameter were required for thrust balance. The added seal increased the total pressure in the rear cavity from 18 percent of high-pressure compressor discharge pressure to 22 percent and the reduced diameter high-pressure compressor discharge seal increased forward loading. These seals, along with the No. 4 bearing buffer seal, are shown in Figure 24.

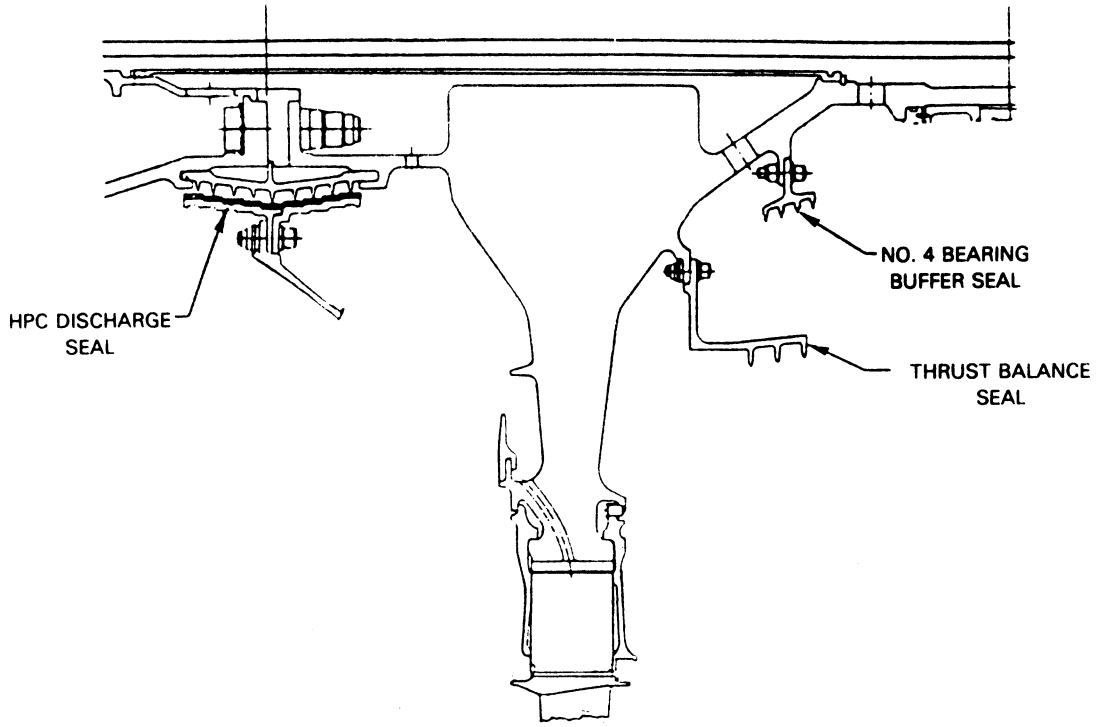

Figure 24 Seal Arrangement for High-Pressure Rotor Thrust Balance

The high-pressure turbine outer air seal configuration is shown in Figure 25. A revised cooling air impingement plate was designed for the outer air seal to reduce leakage. The current configuration is a full ring encircling the active clearance control manifold. A tight fit to the manifold eliminates leakage and reduces complexity of the outer air seal segment design.

Slots are incorporated in the attaching hooks and rails of the seal segments to provide the proper metal flexibility so that the ceramic material will not be overstressed at any condition. Figure 26 shows the resulting air seal segment design.

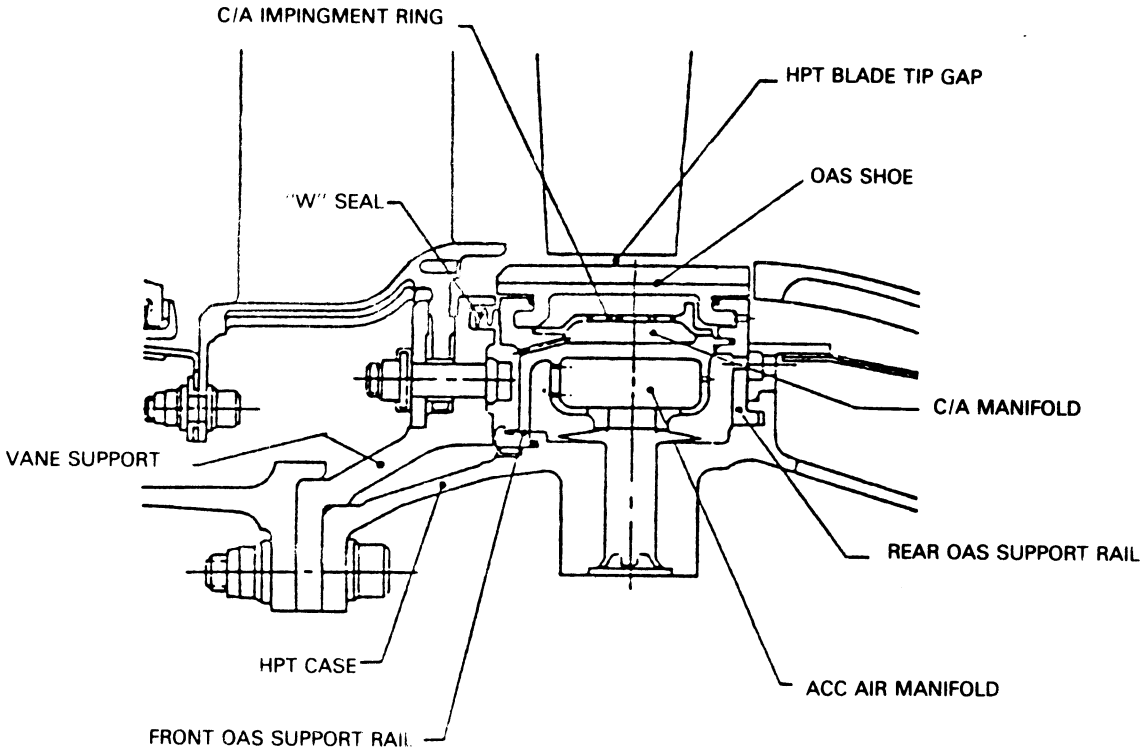

Figure 25 Revised High-Pressure Turbine Case and Outer Air Seal

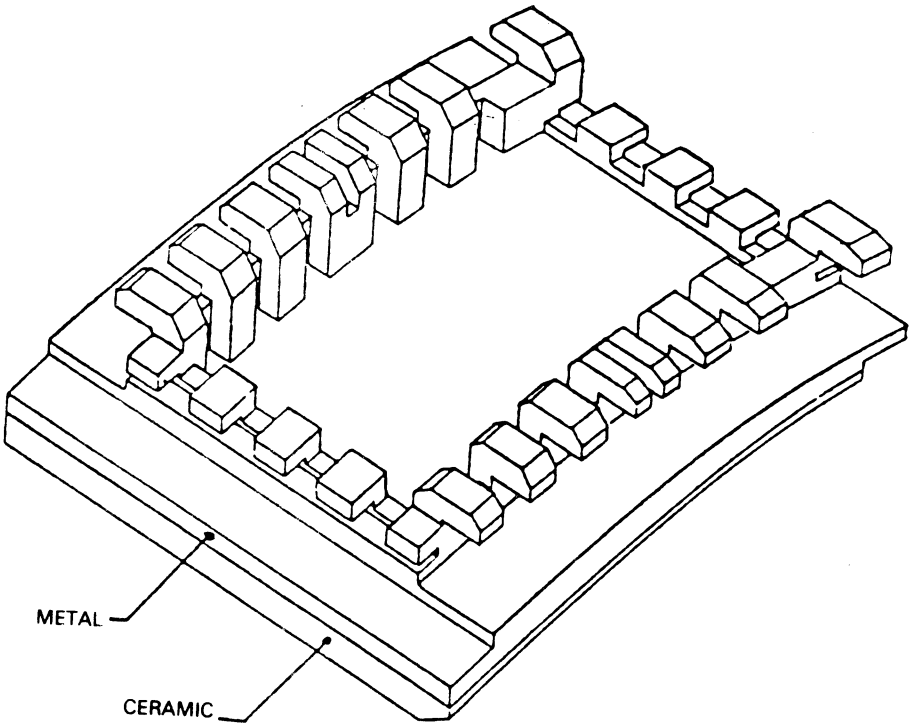

Figure 26 Revised Ceramic Outer Air Seal

Predicted Performance

An assessment was conducted to define current performance predictions for the high-pressure turbine. The current component adiabatic efficiency prediction of 89.1 percent, shown in Table 22 along with its contributing elements, exceeds the 88.2 percent goal level established for the high-pressure turbine at the completion of the initial design. The efficiency predicted for the current high-pressure turbine is based on test results from the high-pressure turbine component (Reference 17). The rig test efficiency at design point conditions was 88.54 percent. Mechanical design results showed a capability to achieve a 0.032 cm (0.0126 in) rotor tip clearance for the flight propulsion system high-pressure turbine compared to the rig clearance of 0.047 cm (0.0186 in). This 0.015 cm (0.006 in) tip clearance improvement was estimated to increase efficiency an additional 0.54 percent.

TABLE 22

CURRENT FLIGHT PROPULSION SYSTEM HIGH-PRESSURE TURBINE
ADIABATIC EFFICIENCY PREDICTION
(Aerodynamic Design Point: 10675 m (35,000 ft), 0.8 Mn, Standard Day)

	Percent
HPT Component Rig (Rig Clearance of 0.047 cm (0.0186 in))	88.54
Airfoil Coating	- 0.09
Cooling/Rematching	+ 0.11
Reduced Tip Clearance	+ 0.54
Predicted Efficiency (Status Clearance of 0.032 cm (0.0126 in))	89.1
Goal Efficiency (Goal Clearance of 0.048 cm (0.019 in))	88.2

Note: Effect of Reynolds number assumed negligible per annular cascade results.

High-pressure turbine maps were reviewed at the completion of the detailed aerodynamic design, and no basic changes were made. Only the flight propulsion system operating points have varied from the initial design.

The current high-pressure turbine aerodynamic design parameters and maps were incorporated into the flight propulsion system performance simulation. Updated performance was defined at the aerodynamic design point and at key off-design operating points. Table 23 compares these results to the performance for the initial design. Current and initial design high-pressure turbine performance is generally similar at each operating point except for differences resulting from high-pressure turbine efficiency improvements. Some differences in parameter values do exist at takeoff because of off-design matching evolution, including the effects of high-pressure turbine tip clearance improvement, since the initial design.

TABLE 23

FLIGHT PROPULSION SYSTEM HIGH-PRESSURE TURBINE PERFORMANCE PARAMETER COMPARISON

	AERO DESIGN POINT(1)		MAXIMUM CRUISE(2)		MAXIMUM CLIMB(3)		TAKEOFF(4)	
	Initial Design*	Current Design	Initial Design*	Current Design	Initial Design*	Current Design	Initial Design*	Current Design
Inlet Flow Parameter - kg °K sq.cm/sec (lb °R sq.in/sec)	7.62 (16.80)	7.57 (16.70)	7.64 (16.85)	7.57 (16.70)	7.62 (16.80)	7.55 (16.65)	7.62 (16.80)	7.55 (16.65)
Rotor Inlet Temperature - °C	1226	1223	1207	1201	1321	1321	1368	1362
Pressure Ratio	4.03	3.99	4.03	3.99	4.02	3.97	4.03	3.98
Adiabatic Efficiency - %	88.2	89.1	88.2	89.1	88.2	89.1	87.3	89.2
Enthalpy Change - Btu/N (Btu/lb)	858.5 (190.3)	858.5 (190.3)	847.3 (190.5)	834.0 (187.5)	911.8 (205.0)	900.7 (202.5)	932.7 (209.7)	928.3 (208.7)
Cooling/Leakage Airflow - %	13.25	13.60	13.25	13.60	13.25	13.60	13.25	13.60
Exit Temperature - °C	837	837	823	818	912	912	954	946

Design and Off-Design Operating Conditions:

(1) Aerodynamic Design Point - 10675 m (35,000 ft), 0.8 Mn, Standard Day
(2) Maximum Cruise - 10675 m (35,000 ft), 0.8 Mn, Standard Day
(3) Maximum Climb - 10675 m (35,000 ft), 0.8 Mn, Standard Day + 10°C (18°F)
(4) Takeoff - SLTO, 0 Mn, Standard Day + 13.9°C (25°F)

* Values shown are after thrust size of initial engine design was downsized 12 percent.

4.7 Turbine Intermediate Case

The turbine intermediate case supports the rear high and low-pressure spool rotors, provides gaspath transition between the high-pressure turbine exit and low-pressure turbine inlet, and transfers engine loads to the aft engine mounts. Figure 27 compares cross sections of the initial and current designs of the turbine intermediate case. In the current case design the structural struts have been reduced in number from 14 to 11 to avoid a 14E resonance on the high-pressure turbine blade. In addition, the struts were canted rearward 11 degrees to accommodate structural loadings imposed by low and high pressure spool rotor thrust balance. Cooling air passage hole exits in the flight propulsion system struts are elliptical to produce a lower stress concentration factor and thus greater life. To meet life requirements, an advanced single crystal alloy (SC2000) is used for the strut fairings. The outer case is a lightweight design that features a polygonal cross section at the strut connection plane with flat plates joined at the tiebolt bosses.

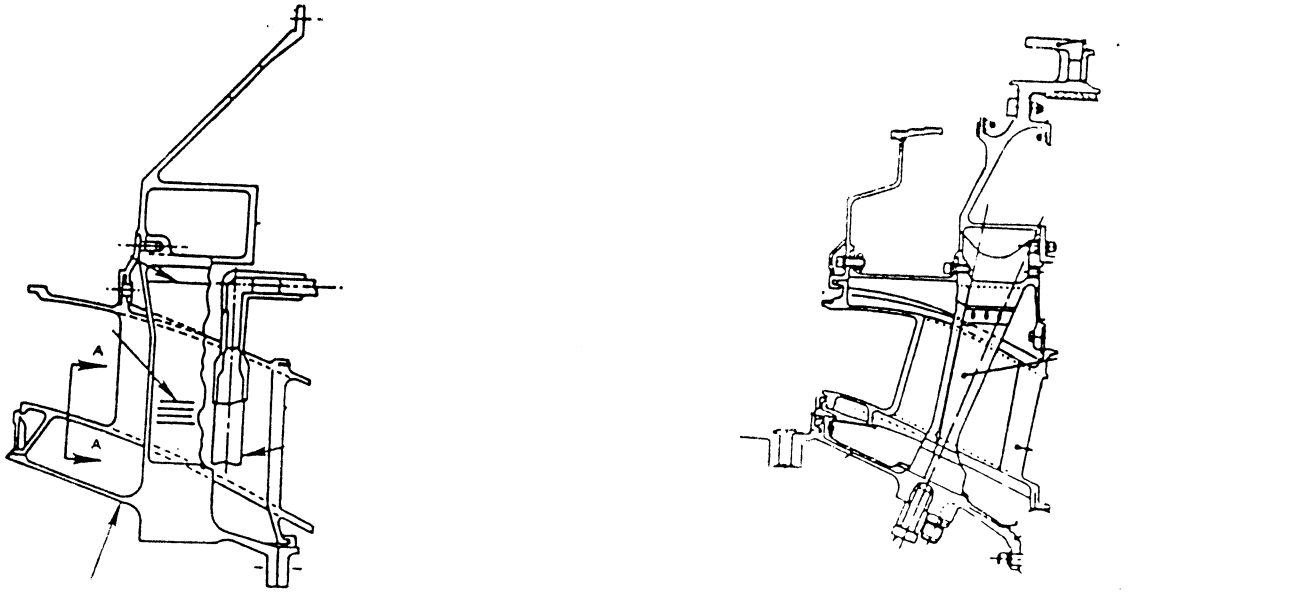

INITIAL TURBINE INTERMEDIATE CASE CROSS SECTION

CURRENT TURBINE INTERMEDIATE CASE CROSS SECTION

Figure 27 Flight Propulsion System Turbine Intermediate Case Section Comparison

Each strut is electron beam welded to the torque ring at the inner diameter, as shown in Figure 28, and fastened to the outer case with a single, high strength tiebolt. Externally removable dowels are installed on either side of each tiebolt to help the struts resist the tightening torque, absorb twisting moments at the end of the strut, and prevent potential shear loads on the tiebolt. Flight propulsion system rear mount lugs are integrally forged with the upper half of the outer case between struts.

The basic aerodynamic requirement of the turbine intermediate case is to duct air from the high-pressure turbine exit to the low-pressure turbine inlet without separation and with minimum loss. The initial aerodynamic design of the flight propulsion system turbine intermediate case remained basically unchanged. Transition duct testing results (see Reference 14), indicated that the flight propulsion system design produced a pressure loss of 0.7 compared to the goal of 1.5 percent while retaining most of the features detailed in the initial design. The initial strut fairing airfoil section was changed from a 65 circular arc to a 400 series to increase incidence range capability. Transition duct length was increased to accommodate high-pressure turbine blade structural considerations.

Based on results from the model testing, the transition duct design for the flight propulsion system is aerodynamically stable and provides the low-pressure turbine rotor inlet with a flowfield that is insensitive to the range of high-pressure turbine exit conditions evaluated. The total pressure loss goal of 0.7 percent P_T/P_T was verified for transition duct design in the flight propulsion system.

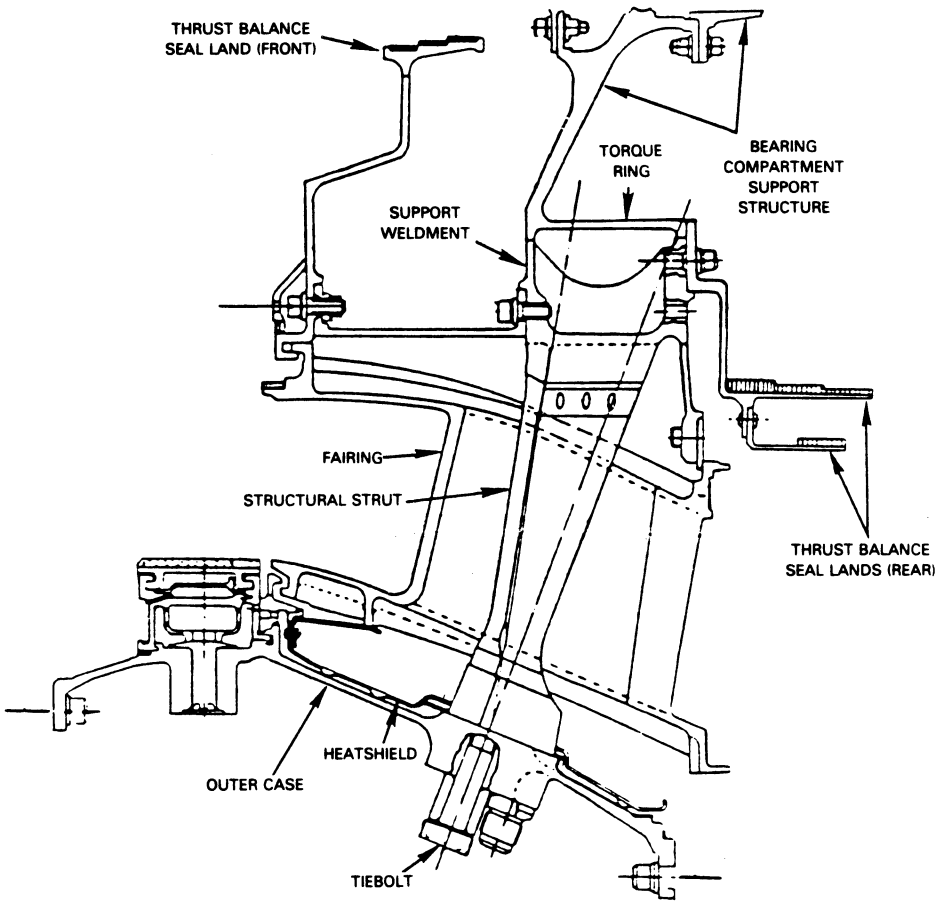

Figure 28 Turbine Intermediate Case Design

Structural analyses of turbine intermediate case struts and fairings confirmed that lives at all strut sections are greater than 20,000 missions and have greater than 30,000 hours capability to 0.1 percent creep. Tiebolt stresses were calculated to be well within the ultimate, and preloads were set at a level to prevent separation of the strut from the outer case under the worst normal load conditions. Strut fairing stresses were found to be primarily bending stresses with highest levels occurring at the fillet areas, where they are still well within limits. Durability goals in the fairings can all be met with application of the required recoating. Predicted lives for cracking and oxidation are 23,000 hours and 9,300 hours (15,000 hr. with one recoating), respectively.

4.8 Low-Pressure Turbine

The flight propulsion system low-pressure turbine is a highly loaded four-stage system designed to operate at a low mean velocity ratio and a low ratio of axial velocity (throughflow) to wheel speed (Cx/U). Major component design features have been incorporated to minimize leakage, improve aerodynamics and reduce weight. Some of these include double wall case construction to accommodate an internal clearance control system for control of blade tip clearances, low loss aft-loaded airfoils with elliptical leading edges, stepped labyrinth inner air seals to control leakage, high-strength high-temperature airfoil materials which eliminate airfoil cooling requirements, and blade leading and trailing edge flow guides to minimize cavity recirculation losses. This configuration, has a predicted adiabatic efficiency of 91.6 percent at the aerodynamic design point.

Figure 29 compares cross sections of the initial and current designs of the low-pressure turbine while Table 24 provides a design summary. Since the initial design effort, a number of changes has been made to the low-pressure turbine. Basic aerodynamic criteria remained essentially unchanged while detail changes in the mechanical design were rather extensive. These modifications are described in the following paragraphs.

TABLE 24

FLIGHT PROPULSION SYSTEM LOW-PRESSURE TURBINE SECTION DESIGN COMPARISON
(Aerodynamic Design Point: 10675 m (35,000 ft), 0.8 Mn, Standard Day)

	Initial Design*	Current Design
Number of Stages	4	4
Pressure Ratio	5.60	5.72
Mean Velocity Ratio	0.47	0.47
Average Throughflow Velocity Ratio (Cx/U)	0.73	0.73
Maximum Rim Speed - m(ft)/sec	198 (650)	199 (652)
Inlet Speed Parameter $N/\sqrt{T}$. - rev/min/$\sqrt{°K}$	87.3	87.3
Inlet Flow Parameter $\frac{W\sqrt{T}}{P}$ - $\frac{kg\sqrt{°K}\ cm^2/sec.}{N}$ where N is newtons	30.4	29.6
Exit Mach Number (Mean Absolute)	0.40	0.45
Enthalpy change - Btu/N(Btu/lb)	773.5 (173.9)	781.1 (175.6)
Number of Airfoils	749	756
Coolant/Leakage Flow (percent)**	2.27	2.55

* Values shown are after thrust size of initial engine design was downsized 12 percent.
** Includes turbine intermediate case flows.

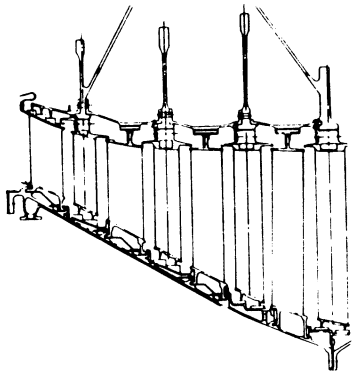

INITIAL LOW PRESSURE TURBINE CROSS SECTION

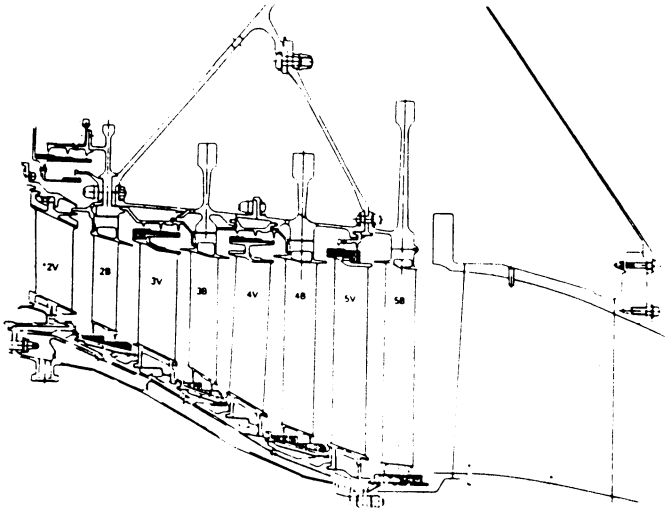

CURRENT LOW PRESSURE TURBINE CROSS SECTION

Figure 29 Flight Propulsion System Low-Pressure Turbine Section Comparison

Test results from the Low-Pressure Turbine Boundary Layer supporting technology program (Reference 15) indicate that the aft-loaded aerodynamic concept provided the lowest loss airfoil design for the turbine. Detailed design studies indicated that airfoil axial gapping had to be increased to accommodate thermal growth of the shaft, cases, blades, and vanes; pressure load deflections of the airfoil, case, shaft, and hub; vibratory deflections; mechanical tolerances and bearing play; and blade meshing criteria. The increase in airfoil axial gapping was absorbed by reducing the gap between the last blade and the turbine exit case vane. Resulting gapping was sufficient for incorporation of flow guides on the airfoil platforms that serve to minimize cavity recirculation losses.

The rotating inner seals were removed from the structural spacers and included as part of the nonstructural spacers, as shown in Figure 30. Analysis of the initial rotor configuration showed that in the event of a heavy rub, secondary damage could result in release of a disk. The current configuration not only ensures rotor integrity, but shields the structural rotor from hot gaspath flow.

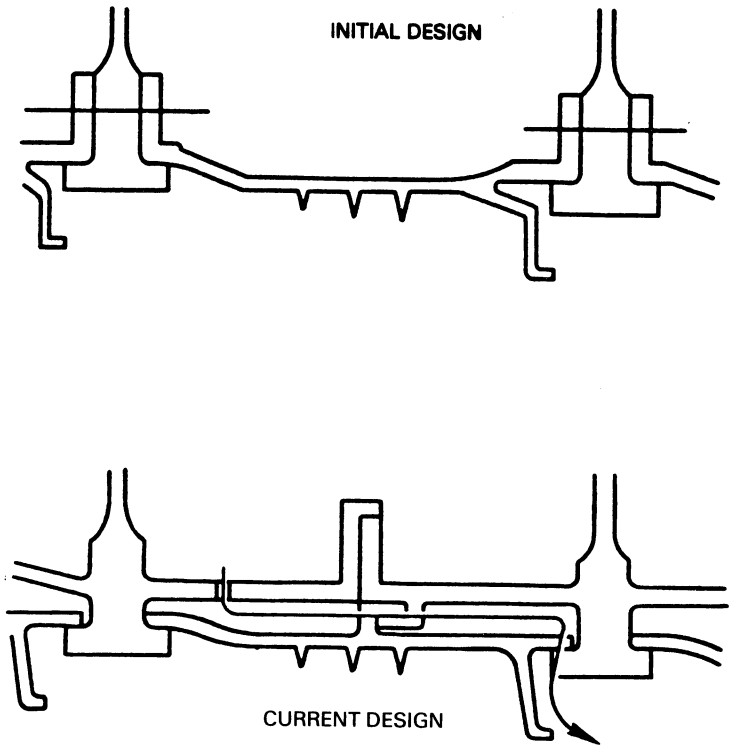

Figure 30 Low-Pressure Turbine Inner Air Seal Concept Comparison

The wide channel configuration for the rotating inner seals was eliminated in favor of a stepped knife edge labyrinth seal with honeycomb lands. This change was made because little, if any, advantage over the more conventional knife edge on honeycomb configuration could be established.

The front and rear hubs are bolted rather than bonded to the second and fifth stage disks, respectively.

A seal was added to the front of the low-pressure turbine rotor for thrust balance reasons. Based on the pressure differential between the gaspath and the front cavity, a dual thrust balance seal configuration was selected featuring a stepped labyrinth seal accommodating three knife edges and a non-stepped seal with two knife edges. This geometry was established to satisfy intermesh criteria and propulsion system transient excursions.

Several revisions were made to the initial double wall design for the low-pressure turbine case. Case cooling was extended rearward from the rear foot of the fourth stage vane to the front foot of the fifth stage vane, with air now introduced at six axial locations for improved radial clearance control. In addition, the design was optimized to use a mixture of eighth and fifteenth stage compressor bleed air instead of all fifteenth stage air at takeoff, and all eighth stage compressor bleed air instead of all tenth stage air at cruise. Use of eighth stage air was estimated to improve thrust specific fuel consumption by 0.28 percent at cruise. Cooling passages in the second stage turbine vane support hook area and the third stage vane front support hook area are filled with insulation. The other vane feet areas are cooled by metering a portion of the cooling flow through holes in the inner turbine case wall to internal manifolds adjacent to the feet. Heat transfer rates are maximized with minimum flows by controlling the gap between the inner case and the sheet metal flow guides. The case design, as modified, is illustrated in Figure 31.

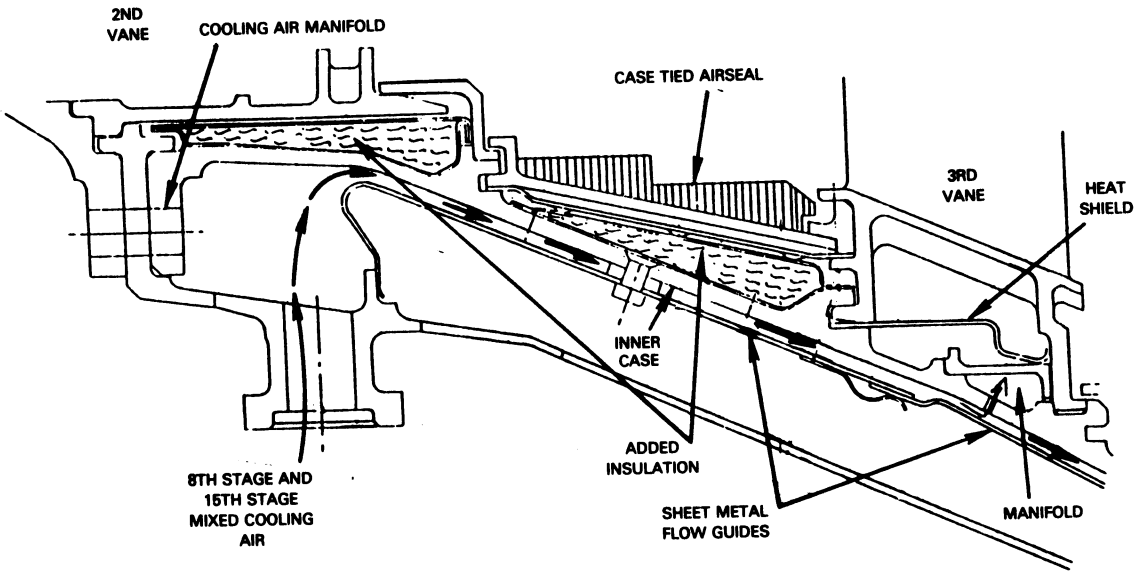

Figure 31 Low-Pressure Turbine Case Modifications

Several structural and life analyses, detailed below, were conducted for the low-pressure turbine of the flight propulsion system during the detailed design effort. Results from these analyses are discussed below.

Predictions were made concerning blade creep strengths and lives. At the limiting span, creep strength margins relative to allowables ranged from a low of 14 percent in the second blade to a high of 50 percent in the fourth blade. The life-limiting second and third blades were estimated to exceed goals by having 20,000 hours available in terms of both cracking and oxidation.

Vibration analysis of the fifth stage for the flight propulsion system indicated that 1st mode frequency margin above the second and third engine orders (i.e., 2E and 3E) is ample at maximum rotor speed with the titanium-aluminide material. Also, 13E with the downstream struts will be well below minimum cruise speed for the first and second modes.

Rotor life analysis indicated that most all areas exceed 100,000 cycles except the four areas noted in Figure 32, two of these areas meeting only the minimum 20,000 cycle goal requirement. Life margins could be added in these areas by a slight refinement to the current design.

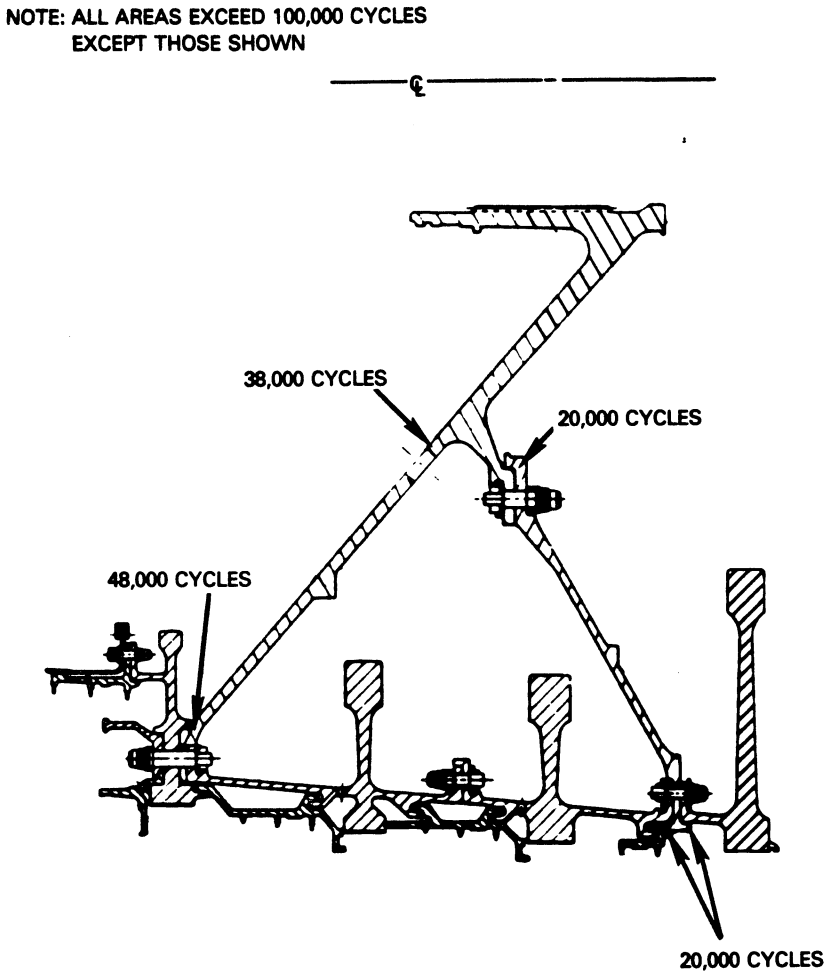

Figure 32 Rotor Low Cycle Fatigue Life

Low cycle fatigue life for the low pressure spool shaft was predicted to exceed the goal of 20,000 cycles in all locations, except for the front spline which had a life of 1,300 cycles. Further analysis showed that this deficiency can be resolved by increasing the pitch diameter by 0.38 cm (0.15 in), increasing the root fillet radius, and crowning the spline to better distribute the loads.

Predictions were made of vane creep strengths and lives. At the limiting span, creep strength margins relative to allowables ranged from a low of 28 percent in the second vane to a high of 75 percent in the fifth vane. Life calculations in terms of cracking showed goals to be exceeded, with 20,000 hours for the life-limiting second, third, and fourth vanes. Surface oxidation lives were estimated at 9,300 hours for the second vanes, 15,000 hours for the third vanes, and 20,000 hours for the fourth vanes. The life goal of 15,000 hours for the second vane can be met with one strip and recoat.

Low-pressure turbine case life was estimated using the resultant of stresses caused by thermal and maneuver loads. Life estimated from this distribution was determined to be in excess of the required 20,000 cycles.

Predicted Performance

An assessment was conducted to define the current performance predictions for the low-pressure turbine. The efficiency estimate is shown in Table 25 below.

TABLE 25

CURRENT FLIGHT PROPULSION SYSTEM LOW-PRESSURE TURBINE
ADIABATIC EFFICIENCY PREDICTION
(Aerodynamic Design Point: 10675 m (35,000 ft), 0.8 Mn, Standard Day)

	Percent
State-of-the-Art Design System (Goal Clearance/Cooling)	90.5
Improved Aerodynamics	+1.4
Cooling/Rematching	+0.1
Increased Tip Clearance	-0.4
Predicted Efficiency (Status Clearance)	91.6
Goal Efficiency (Goal Clearance)	91.5

Current efficiency exceeds the 91.5 percent goal level established for the low-pressure turbine at the completion of the initial design. The efficiency predicted for the low-pressure turbine is based on the level currently estimated for the integrated core/low spool turbine, with adjustments for the reduced inlet annulus area and swirl effects of the flight propulsion system flowpath. This 90.5 percent efficiency base assumes a goal average rotor tip clearance of 0.048 cm (0.019 in) and goal levels of cooling and leakage airflows. Detailed mechanical design results showed a capability to achieve only a 0.088 cm (0.035 in) average rotor tip clearance for the low-pressure turbine of the flight propulsion system compared to the goal clearance of 0.048 cm (0.019 in). Maneuver loads produced these higher than anticipated deflections, particularly in the rear stages. It was determined that reducing their impact would require basic changes in the rotor system support. This major redesign effort was not undertaken since the status efficiency exceeds the goal level.

Low-pressure turbine maps were reviewed at the completion of the detailed aerodynamic design, and no basic changes were made. Only the flight propulsion system operating points have varied from the initial design.

The current low-pressure turbine aerodynamic design parameters and maps were incorporated into the flight propulsion system simulation. Updated performance was defined at the aerodynamic design point and at key off-design operating points. Table 26 compares these results to the performance for the initial design. Low-pressure turbine performance for the current and initial designs is generally similar at each operating point. Differences, especially those at takeoff, have occurred because of design point and off-design matching evolution as detail component designs and flight propulsion system updates have been conducted.

TABLE 26

FLIGHT PROPULSION SYSTEM LOW-PRESSURE TURBINE PERFORMANCE PARAMETER COMPARISON

	AERO DESIGN POINT(1)		MAXIMUM CRUISE(2)		MAXIMUM CLIMB(3)		TAKEOFF(4)	
	Initial Design*	Current Design	Initial Design*	Current Design	Initial Design*	Current Design	Initial Design*	Current Design
Inlet Flow Parameter - $\frac{W\sqrt{T}}{P}$ $\frac{kg\sqrt{°K}\ cm2/sec.}{N}$ where N is newtons	30.43 (67.10)	29.66 (65.40)	30.48 (67.20)	29.71 (65.50)	30.36 (66.95)	29.59 (65.25)	30.48 (67.20)	29.66 (65.40)
Inlet Temperature - °C	837	837	821	818	912	912	954	946
Pressure Ratio	5.60	5.72	5.55	5.66	5.69	5.81	4.91	5.09
Adiabatic Efficiency - %	91.5	91.6	91.4	91.5	91.6	91.7	90.2	90.5
Enthalpy Change - Btu/N (Btu/lb)	773.5 (173.9)	781.1 (175.6)	757.9 (170.4)	762.8 (171.5)	834.9 (187.7)	843.3 (189.6)	794.8 (178.7)	806.0 (181.2)
Cooling/Leakage Airflow - %**	2.30	3.10	2.30	3.10	2.30	3.10	1.80	3.10
Exit Temperature - °C	479	474	470	463	531	527	598	582

Design and Off-Design Operating Conditions:

(1) Aerodynamic Design Point - 10675 m (35,000 ft), 0.8 Mn, Standard Day
(2) Maximum Cruise - 10675 m (35,000 ft), 0.8 Mn, Standard Day
(3) Maximum Climb - 10675 m (35,000 ft), 0.8 Mn, Standard Day + 10°C (18°F)
(4) Takeoff - SLTO, 0 Mn, Standard Day + 13.9°C (25°F)

* Values shown are after thrust size of initial engine design was downsized 12 percent.

** Includes turbine intermediate case flows

4.9 Turbine Exhaust Case

The turbine exhaust case supports the exhaust mixer and tailcone, and transfers loads from the nacelle to the engine. The case includes 24 exit guide vanes to remove the low-pressure turbine discharge residual swirl and redirect the exhaust gas from the turbine into the exhaust mixer without separation and with minimum loss. This assembly comprises an integral ring-strut-ring structure with aerodynamically shaped struts which serve as the low-pressure turbine exit guide vanes. The inner ring supports the tailplug. The outer ring case supports the mixer, carries the loads from the cowl load transfer ring and transfers the load forward through the low-pressure turbine case and to the rear mounts. Figure 33 compares cross sections of the initial and current designs.

The initial design was executed to accommodate exit swirls of 0 and 10 degrees, pending results from the Exhaust Mixer Model support technology program (Reference 8). Model testing showed swirl to improve mixing at the expense of excess pressure loss, so the current case design removes all swirl. Exit guide vanes were changed from the original 65 series airfoil to a controlled diffusion airfoil design to produce an attached boundary layer and attain the desired gas exit angle while minimizing pressure losses. Endwall contours have been defined for compatibility with the latest exhaust mixer design. For loading reasons, the number of exit guide vanes was increased from the original 24 to 30.

Mechanically, the exit guide vanes are hollow for reduced weight, and are fabricated by welding together titanium-aluminide (Ti-Al) sheets. The inner and outer rings are forged from the same material and welded to the vanes.

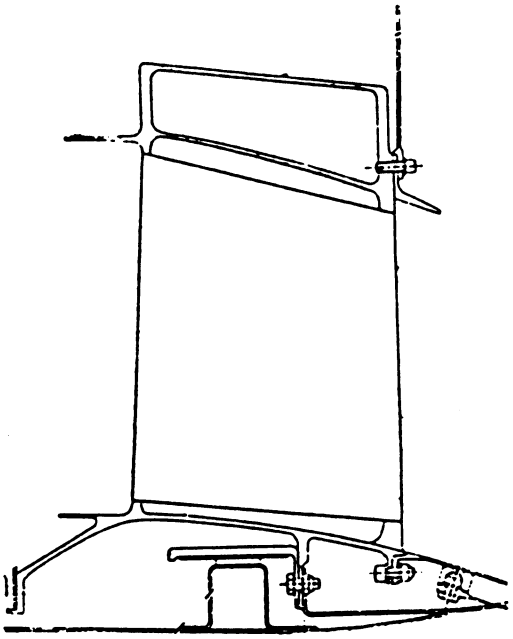

INITIAL TURBINE EXHAUST CASE CROSS SECTION

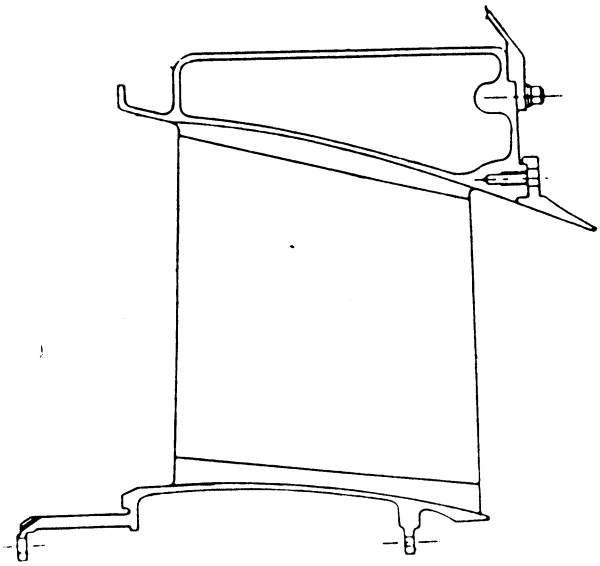

CURRENT TURBINE EXHAUST CASE CROSS SECTION

Figure 33 Flight Propulsion System Turbine Exhaust Case Section Comparison

Predicted Performance

The original 0.9 percent exit guide vane pressure loss at the aerodynamic design point was confirmed during the detailed design effort. Table 27 compares current pressure losses at key operating points to those for the initial design. Matching evolution has caused small differences in loss at off-design conditions.

TABLE 27

FLIGHT PROPULSION SYSTEM TURBINE EXHAUST PERFORMANCE PARAMETER COMPARISON

	AERO DESIGN POINT(1)		MAXIMUM CRUISE(2)		MAXIMUM CLIMB(3)		TAKEOFF(4)	
	Initial Design*	Current Design	Initial Design*	Current Design	Initial Design*	Current Design	Initial Design*	Current Design
Pressure Loss - %	0.90	0.90	0.88	0.87	0.95	0.95	0.66	0.69

Design and Off-Design Operating Conditions:

(1) Aerodynamic Design Point - 10675 m (35,000 ft), 0.8 Mn, Standard Day
(2) Maximum Cruise - 10675 m (35,000 ft), 0.8 Mn, Standard Day
(3) Maximum Climb - 10675 m (35,000 ft), 0.8 Mn, Standard Day + 10°C (18°F)
(4) Takeoff - SLTO, 0 Mn, Standard Day + 13.9°C (25°F)

* Values shown are after thrust size of initial engine design was downsized 12 percent.

4.10 Exhaust Mixer and Nozzle

The initial design of the mixer/exhaust nozzle system has undergone some significant changes. Some of these changes were based on results from the Exhaust Mixer Model supporting technology program (Reference 8). Other changes were a result of additional detailed design work conducted for the integrated core/low spool. These modifications are described in the following paragraphs. Figure 34 compares cross sections of the initial and current designs of the exhaust mixer and nozzle while Table 28 summarizes the major design parameters for both configurations.

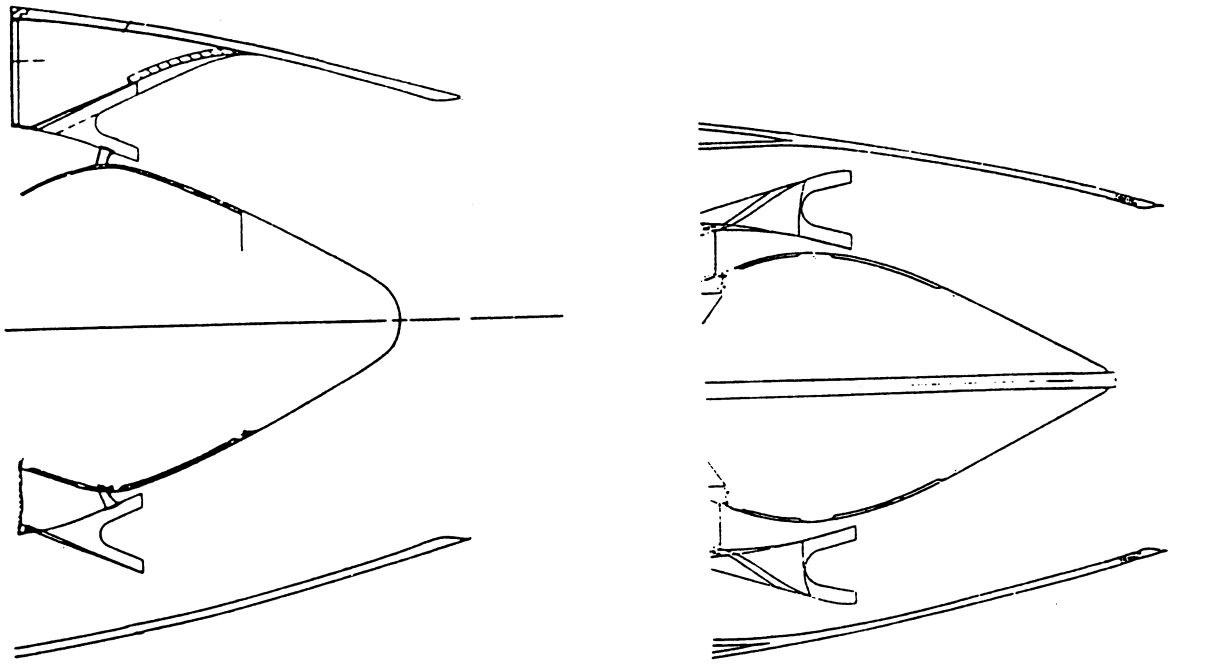

Figure 34 Flight Propulsion System Exhaust Mixer and Nozzle Section Comparison

TABLE 28

FLIGHT PROPULSION SYSTEM EXHAUST MIXER AND NOZZLE SECTION DESIGN COMPARISON
(Aerodynamic Design Point: 10675 m (35,000 ft), 0.8 Mn, Standard Day)

	Initial Design	Current Design
Number of Lobes	12	18
Length/Diameter	0.54	0.61
Penetration (percent)	50	75
Efficiency (percent)	85.0	85.0
Core-to-Duct Stream Temperature Ratio	2.55	2.53
Core-to-Duct Stream Pressure Ratio	0.91	0.91
Core Stream Mach Number	0.42	0.42
Duct Stream Mach Number	0.56	0.56
Inlet Swirl Angle (degree)	0 to 10	0

Aerodynamic-related configurational changes made to the initial design were substantial. Parametric test results from Phase I of the Mixer Model supporting technology program indicated that performance could be improved by increasing the tailpipe length, number of lobes, and amount of penetration. Since these results were for internal performance only, an optimization study was undertaken to factor in the impact of nacelle drag and propulsion system weight. Study results, shown in Figure 35, indicate that an 18-lobe configuration with an increased penetration level is desirable because of equivalent thrust specific fuel consumption improvements caused by thrust coefficient (Cv), weight, and drag effects. However, a significant increase in the length/diameter ratio is not desireable because of the associated nacelle drag and weight debits. More detailed analysis led to the selection of 75 percent penetration and a slight increase in length/diameter to 0.61. The resulting flowpath, presented in Figure 36, was used as the base for testing conducted under Phase II of the Mixer Model supporting technology program. Phase I testing also established the impact of low-pressure turbine exit guide vane swirl on mixed performance. It showed that a 10 degree swirl causes a 0.3 percent loss in thrust specific fuel consumption and led to a decision to remove all swirl into the mixer. Test results also indicated integration of the mixer with the structural pylon in the nacelle to be minor in scope, with very small overall penalties involved.

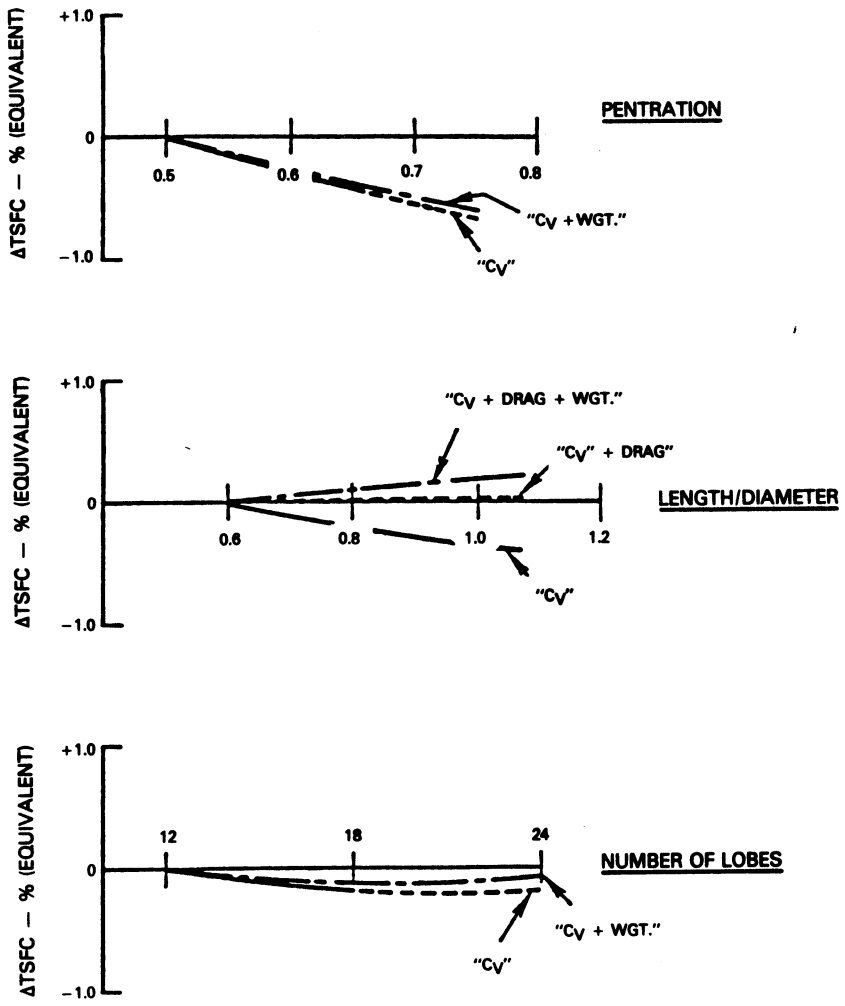

Figure 35 Exhaust Mixer Update Trends

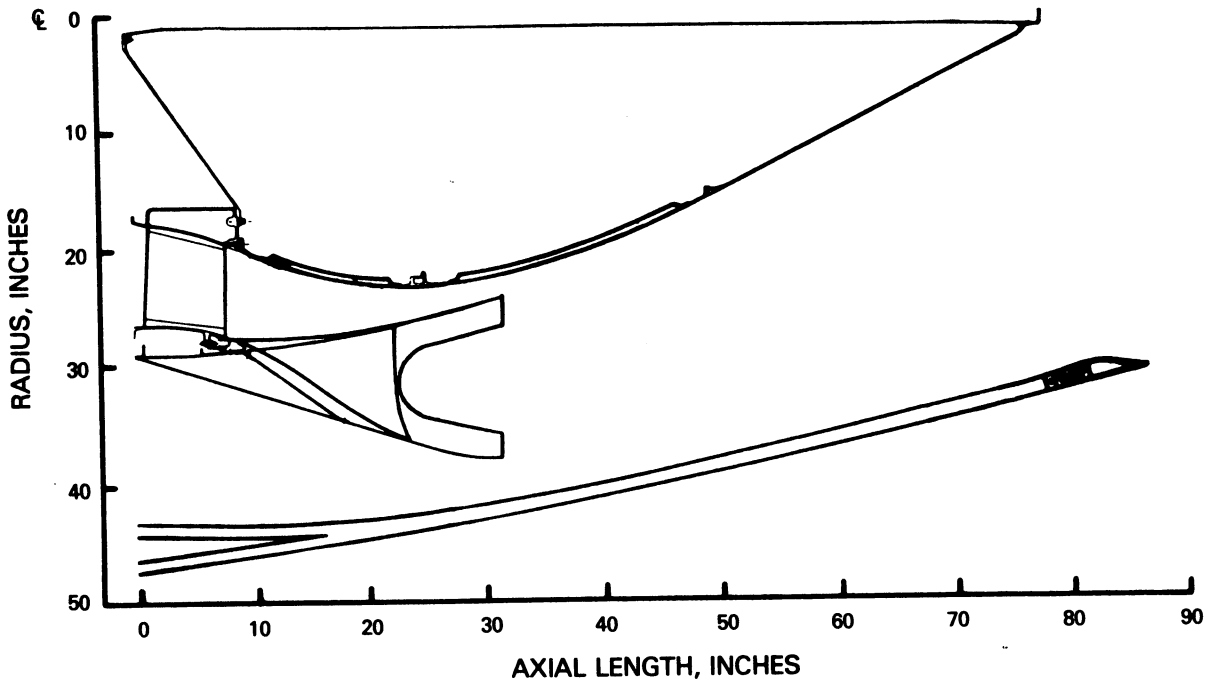

Figure 36 Updated Mixer Flowpath

Phase II testing results substantiated the projections based on Phase I results. Almost 85 percent of the performance improvement goal was accomplished in Phase II testing. It was projected that additional tailoring of the mixer configuration would provide enough improvement in performance characteristics that the design goal of 3.3 percent reduction in thrust specific fuel consumption could be accomplished. Reduction of mixer pressure loss was envisioned by recontouring of the turbine exhaust case and optimization of the mixer lobe length. Mixing efficiency improvement was projected by recontouring lobe exit geometry to further increase penetration without affecting weight. Phase II data analysis led to the incorporation of hoods (sheet metal fairings) attached to the upstream portion of the lobes and a recontoured (reduced diameter, slightly increased length) tailplug to improve the characteristics of the flow.

The introduction of hoods for aerodynamic reasons provided the structural support required to make the mixer lobes self-supporting. This enhancement eliminated the requirement for support struts between the inner portion of the lobes and the tailplug, which improves the characteristic of the gas flow. The vibration dampers on the outer part of the lobe were also eliminated because of the stiffening effects of the outer and inner hoods and the outer rib in conjunction with the damper ring between the inner lobe contour and the structural ring at the rear of the turbine exhaust case. The inner lobes are joined to the outer lobes at a single plane using rivets, which allows thermal freedom between the inner lobe (exposed to hot core stream gas) and the outer lobe (exposed to the relatively cold duct stream).

Predicted Performance

Exhaust mixer and nozzle performance was updated. A comparison of current parameter values with those of the initial design is presented for the aerodynamic design point and key off-design operating points in Table 29. Virtually no performance changes have occurred.

TABLE 29

FLIGHT PROPULSION SYSTEM EXHAUST MIXER AND NOZZLE PERFORMANCE PARAMETER COMPARISON

	AERO DESIGN POINT(1)		MAXIMUM CRUISE(2)		MAXIMUM CLIMB(3)		TAKEOFF(4)	
	Initial Design*	Current Design	Initial Design*	Current Design	Initial Design*	Current Design	Initial Design*	Current Design
Efficiency - %	85	85	85	85	85	85	85	85
Core Stream Pressure Loss - %	0.24	0.24	0.24	0.23	0.25	0.25	0.19	0.19
Duct Stream Pressure Loss - %	0.18	0.18	0.18	0.18	0.18	0.18	0.17	0.17
Nozzle Pressure Loss - %	0.34	0.34	0.340	0.34	0.34	0.34	0.29	0.29
Gross Thrust Coefficient (Cv)	0.9958	0.9958	0.9960	0.9960	0.9956	0.9957	0.9904	0.9905

Design and Off-Design Operating Conditions:

(1) Aerodynamic Design Point - 10675 m (35,000 ft), 0.8 Mn, Standard Day
(2) Maximum Cruise - 10675 m (35,000 ft), 0.8 Mn, Standard Day
(3) Maximum Climb - 10675 m (35,000 ft), 0.8 Mn, Standard Day + 10°C (18°F)
(4) Takeoff - SLTO, 0 Mn, Standard Day + 13.9°C (25°F)

* Values shown are after thrust size of initial engine design was downsized 12 percent.

4.11 Nacelle

Initial nacelle design requirements were established on the basis of engine, installation, and overall performance considerations. It was determined that the nacelle system for the Energy Efficient Engine must provide high performance, tolerate high angles of attack so as to minimize inlet distortion, and be fully treated accoustically to reduce noise. The nacelle must also be installable on representative aircraft without sacrificing benefits in performance and weight. The nacelle configuration comprises an inlet duct, cowl duct section, a 'D' duct section and a tailcone. The inlet duct is bolted to the fan case just forward of the fan blades. The cowl doors are located just behind the inlet and provide accessibility to the oil tank, and electronic fuel control. The cowl doors are hinged on both sides of the pylon and latched at the bottom. Aft of the cowl doors are the 'D' shaped ducts which house the thrust reverser and provide the load path between the front and rear mounts through the nacelle. The tailcone is a full body of revolution and remains with the pylon when the engine is removed. The 'V' shaped groove at the aft end of the 'D' duct fits into a circumferential groove at the front of the tailcone. When the 'D' ducts are opened, the tailcone is supported by a 'T' shaped track bolted to the underside of the pylon.

The engine mount system is designed to minimize engine case distortion and bending for reduced tip gap clearances in the fan, compressors, and turbines. This approach optimizes performance retention while improving overall engine efficiency. The front mount, its plane being the aft face of the compressor intermediate case, transfers vertical, side, and thrust loads from the engine to the pylon. With its plane located at the turbine intermediate case, the rear mount transfers the vertical, side and torque loads.

The current and initial designs of the nacelle are shown in Figure 37 with a summary of the current design presented in Table 30. A design comparison shows changes to the initial design to be minimal. Only two basic revisions have been made to the nacelle. It has been lengthened and aerodynamically updated, and some of the construction has been revised.

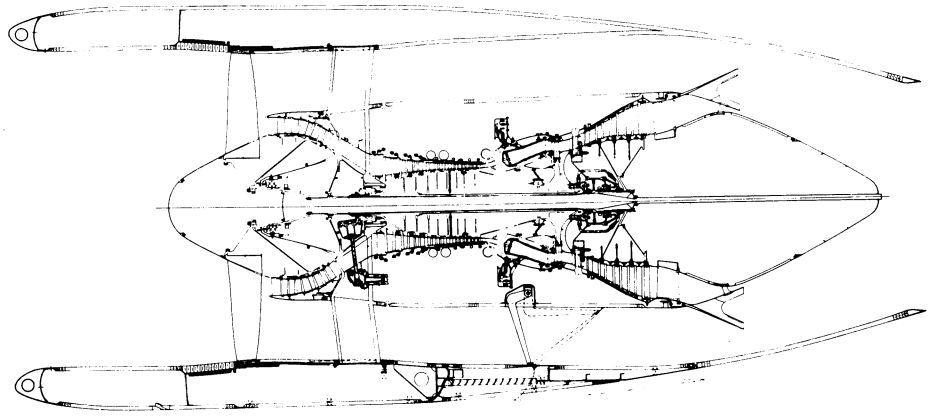

INITIAL NACELLE CROSS SECTION

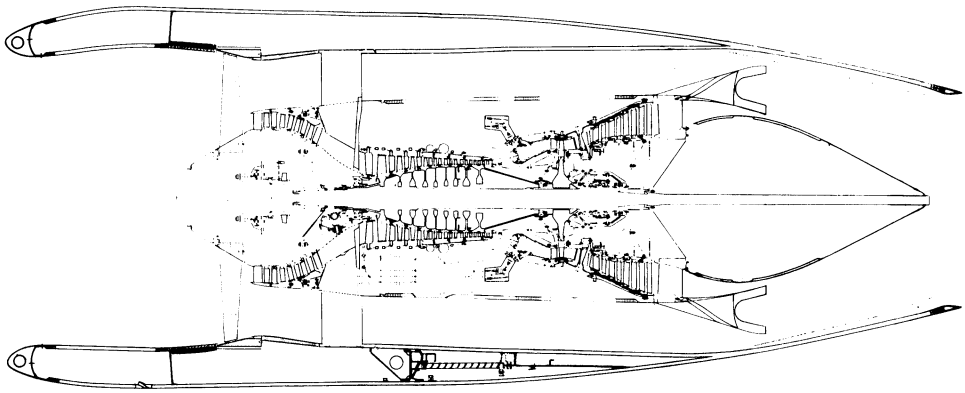

CURRENT NACELLE CROSS SECTION

Figure 37 Flight Propulsion System Nacelle Section Comparison

TABLE 30

FLIGHT PROPULSION SYSTEM NACELLE DESIGN COMPARISON
(Aerodynamic Design Point: 10675 m (35000 ft), 0.8 Mn, Standard Day)

	Initial Design	Current Design
Hilite-to-Maximum Diameter Ratio (Dh/Dmax)	0.83	0.83
Hilite-to-Throat Area Ratio (Ah/At)	1.25	1.25
Maximum Diameter Location - % of Maximum Diameter Downstream of Inlet Leading Edge	40	40
Acoustic Treatment Length-to-Fan Diameter Ratio	0.5	0.56
Inlet Airflow Capacity (Relative to Nominal Maximum Airflow) - %	8	8
Acoustic Treatment		
Inlet	All Surfaces	All Surfaces
Duct	All Surfaces Except Mixer	All Surfaces Except Comp. Intermediate Case & Mixer
Reverse Thrust - % Forward Thrust	35	35

The nacelle configuration and performance were updated to reflect length increases caused by lowand high-pressure compressor and exhaust mixer and nozzle flowpath changes. Figure 38 shows the revised nacelle. Nacelle design parameters are generally unchanged. The nacelle length has been increased by 23.3 cm (9.2 in) due to (1) an increase in length caused by low-pressure compressor rotor-to-stator gapping requirements, (2) an increase in length caused by high-pressure compressor aerodynamic revisions and (3) an increase in exhaust tailpipe length as a result of exhaust mixer length/diameter increase based on mixer model test results. A total external drag increase of 106 N (24 lb.) resulted.

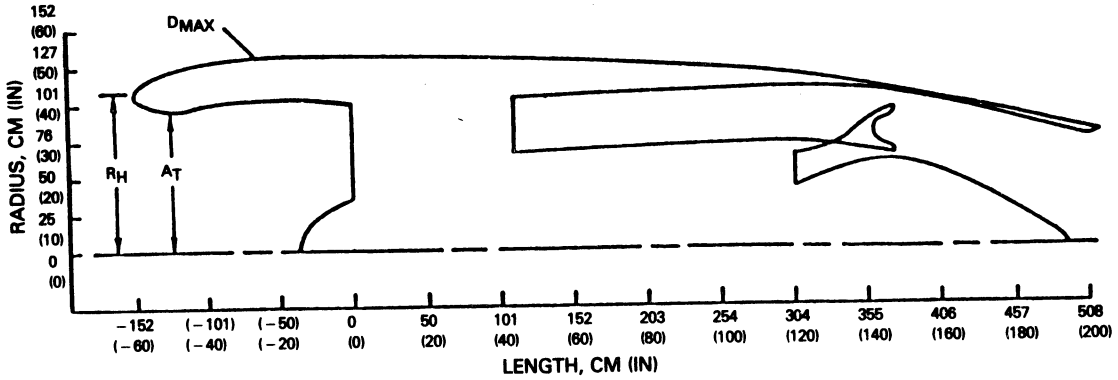

Figure 38 Updated Mixed Flow Nacelle

A review of the nacelle inlet requirements was completed as part of the detail design effort for the integrated core/low spool. The results of this review indicated that the design parameters established during the initial design of the flight propulsion system should be retained, with the inlet designed for 8 percent growth capability. The length already established was projected to provide an acoustical treatment length-to-fan diameter ratio of 0.56.

A materials reassessment showed that the low temperatures in the tailpipe region of the updated mixer/exhaust nozzle configuration could permit the use of graphite polyimide honeycomb in place of the aluminum brazed titanium honeycomb of the initial design. A 36 kg (80 lb.) weight reduction resulted from this substitution.

Other changes in nacelle construction resulted from updated noise predictions which led to (1) acoustic material thickness changes in the inlet, fan case, and fan duct and (2) the deletion of treatment altogether on the duct walls of the compressor intermediate case.

Predicted Performance

Internal and external nacelle performance was updated. A comparison of current parameter values with those of the initial design is presented for the aerodynamic design point and key off-design operating conditions in Table 31. Except for the increase in drag resulting from the increased length of the nacelle, performance remains unchanged.

TABLE 31

FLIGHT PROPULSION SYSTEM NACELLE PERFORMANCE PARAMETER COMPARISON

	AERO DESIGN POINT(1)		MAXIMUM CRUISE(2)		MAXIMUM CLIMB(3)		TAKEOFF(4)	
	Initial Design*	Current Design	Initial Design*	Current Design	Initial Design*	Current Design	Initial Design*	Current Design
Inlet Pressure Recovery (P_{T2}/P_{T0})	0.9966	0.9966	0.9966	0.9966	0.9966	0.9966	0.9925	0.9925
Fan Duct Pressure Loss - %	0.60	0.60	0.61	0.61	0.59	0.59	0.54	0.54
Fan Stream Pressure Loss - %	1.12	1.12	1.13	1.13	1.10	1.10	1.01	1.01
Core Stream Pressure Loss - %	0.58	0.58	0.57	0.57	0.60	0.60	0.45	0.46
External Drag - N	1605	1712	1605	1712	1605	1712	0	0

Design and Off-Design Operating Conditions:

(1) Aerodynamic Design Point - 10675 m (35,000 ft), 0.8 Mn, Standard Day
(2) Maximum Cruise - 10675 m (35,000 ft), 0.8 Mn, Standard Day
(3) Maximum Climb - 10675 m (35,000 ft), 0.8 Mn, Standard Day + 10°C (18°F)
(4) Takeoff - SLTO, 0 Mn, Standard Day + 13.9°C (25°F)

* Values shown are after thrust size of initial engine design was downsized 12 percent.

4.12 SUBSYSTEM DESIGN UPDATE

4.12.1 Mainshaft Bearings and Seals

Mainshaft bearings were selected on a preliminary basis during the initial design, as described in Reference 1. Additional analyses for the flight propulsion system refined these preliminary bearing definitions due to updated thrust balance, rotor vibration control, and life considerations. A comparison of current and initial bearing sizes for the flight propulsion system is presented in Table 32. Revisions in size are observed to be relatively small. As a result, bearing surface speeds, as measured in terms of DN - the product of bearing inner diameter (mm) and maximum rotor speed (rev/min), are virtually unchanged. Maximum DN's remain at approximately 2.3 million for high pressure spool number 3 and 4 bearings.

TABLE 32

FLIGHT PROPULSION SYSTEM MAIN SHAFT BEARING SIZE COMPARISON

Bearing Number	Inner Diameter (mm)		Outer Diameter (mm)	
	Initial	Current	Initial	Current
1	270	269	380	385
2	135	130	195	190
3	170	160	260	250
4	170	160	260	250
5	170	160	240	230

Bearing compartment seal designs were changed in several instances as results from more detailed analyses became available. Table 33 summarizes the types of seals incorporated in the current flight propulsion system and compares them to the seals selected in the initial flight propulsion system design. No changes were made to the types of seals in the front bearing compartment of the flight propulsion system except for the front intershaft seal where four knife edges were added to the original six knife edge labyrinth seal configuration to further reduce breather flow rate. The number 4 bearing seal was changed from a labyrinth to a carbon type seal to minimize breather flow. The rear intershaft seal was also changed from a labyrinth to a back-to-back carbon seal configuration. The number 5 bearing carbon type seal remained the same for the current system. The seal types listed in Table 33 for the current flight propulsion system are also used in the integrated core/low spool.

TABLE 33

BEARING COMPARTMENT MAINSHAFT SEAL COMPARISON

Seal Location	Seal Type	
	Initial Flight Propulsion System	Current Flight Propulsion System
No. 1 (Front)	Carbon	Carbon
No. 3 (Rear)	Six Knife Edge Labyrinth Seal	Six Knife Edge Labyrinth Seal
No. 4 (Front)	Five Knife Edge Labyrinth Seal	Carbon
No. 5 (Rear)	Carbon	Carbon
Front Intershaft	Six Knife Edge Labyrinth Seal	Ten Knife Edge Labyrinth Seal
Rear Intershaft	Six Knife Edge Labyrinth Seal	Back-to-back Carbon

4.12.1.1 Buffer/Breather System

The buffer/breather system utilizes buffer air bled from the inner diameter of the high-pressure compressor inlet. The lower temperature of this air permits the use of labyrinth seals. Dry face carbon seals for the number 1 bearing front compartment and number 5 bearing rear compartment control the breather flow and oil consumption. The spent buffer air is carried through a deareator mounted on the low shaft out to the engine exhaust. The cooler compartment environment reduces engine heat rejection, and the breather vent to sub-ambient pressure ensures improved resistance to oil weepage during idle and windmilling operations.

Bearing compartment buffer and breather configurations defined in the initial design were retained in concept. Figure 39 shows the current design. The major revision, in addition to the seal changes mentioned in the previous paragraph, was to eliminate the deoiler in the rear compartment and to scavenge the air and oil together through the turbine transition duct strut to the front bearing compartment. Rear and front compartment air are serviced together before being discharged through the center vent exhaust system.

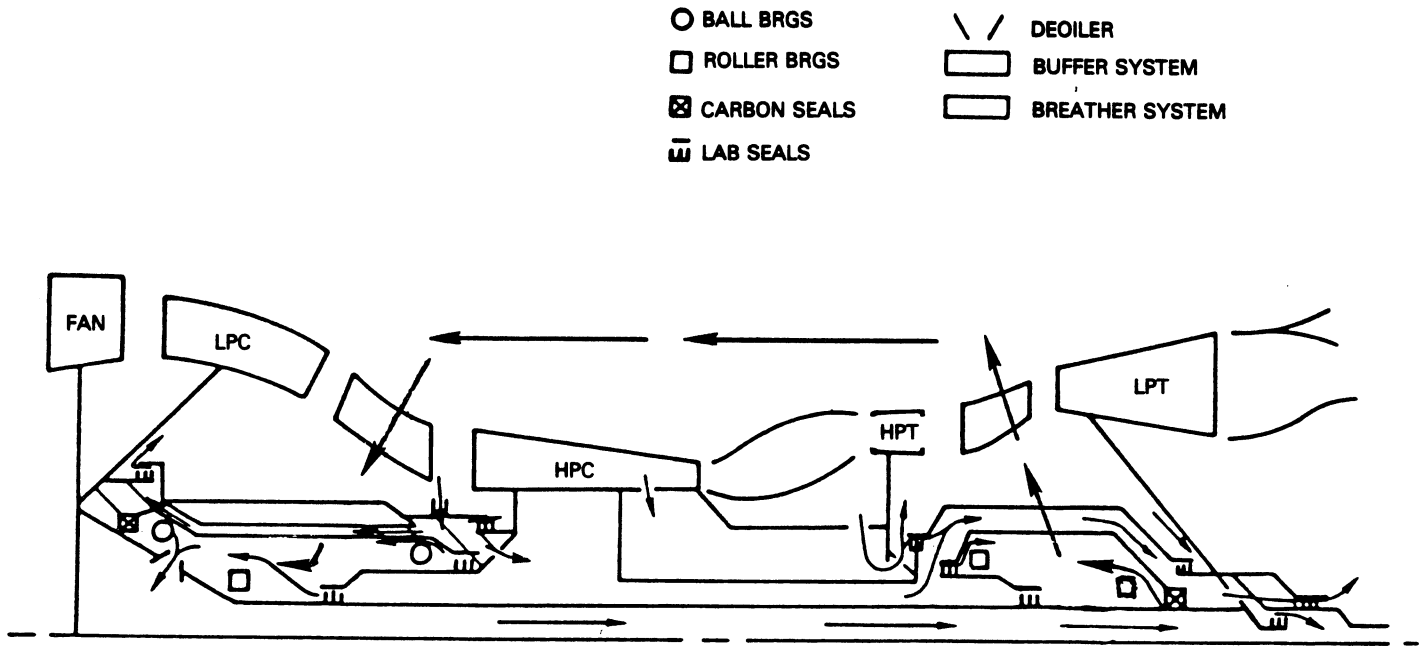

Figure 39 Current Flight Propulsion System Bearing Compartment Buffer/Breather

4.12.1.2 Lubrication System

The lubrication system, as initially designed, features a non-regulated oil supply system, a conventional scavenge system, and a low shaft-mounted rotary deareator. Successful efforts to minimize oil flow while optimizing oil distribution for minimum bearing and seal heat generation has eliminated the requirement for an air/oil heat exchanger without compromise to mainshaft bearing and seal durability.

This initial design of the lubrication system has been retained, in concept, for the flight propulsion system. The major change was to eliminate the deareator in the rear compartment and to scavenge the oil (and air) to the front compartment. As in the initial configuration, the current system features positive oil management to provide the necessary cooling and lubrication flows. A main feature of the current system is self-regulation which simplifies the plumbing, reduces the size and number of scavenge pumps, and eliminates the need for a pressure regulating valve. It also features a blowdown system in the rear compartment whereby oil and air are scavenged together through a turbine transition duct strut to the front bearing compartment. A single low rotor deoiler in the front compartment is used to separate the oil mist from all the breather air.

4.12.2 Secondary Airflow System

The secondary airflow system provides air for component cooling, bearing compartment buffers/breathers, rotor thrust balance control, aircraft/engine service bleeds, and active clearance control coolant. This system comprises six distinct design features which exercise partial control over the major coolant sources by setting the operational pressures, the flow rates, and/or temperature. These features include solid body tubes, knife edge labyrinth seals, a tangential on-board injection (TOBI) supply system, a preswirl mini-TOBI system, windage flow separator, and mid-turbine trip strips. Reference 1 contains a complete description of each feature, as initially designed.

Considerable updating of the secondary flow system was accomplished as a result of detail design efforts directed toward integrated core/low spool demonstrator components and updates of the initial design for the flight propulsion system. Updating of specific main design features presented in Reference 1 is discussed in other sections of this report. Specifically, solid body bleed tube changes are discussed under Section 4.4; the knife edge labyrinth seal, tangential-on-board injection supply system, preswirl 'mini' tangential-on-board injection system, and windage flow separator changes are discussed under Section 4.6 along with mid-turbine blade trip strips and updated turbine airfoil cooling schemes. Section 4.13 reports current revisions to the active clearance control system. Updates of rotor thrust balance control and secondary airflow rate, pressure, and temperature predictions are discussed in the following paragraphs.

4.12.2.1 Rotor Thrust Balance

Refined analysis of the low rotor thrust balance indicated that rearward thrust was unacceptable for the No. 1 bearing. Therefore, the cavity in front of the low-pressure turbine was depressurized in order to reduce loading. Depressurization was accomplished by adding a nonstepped, two knife-edge seal to the front of the low-pressure turbine. The resultant rearward load on the No. 1 bearing was acceptable.

Rearward loading in the high pressure rotor was also found to have increased, primarily as a result of reduced reaction in the high-pressure compressor design. To minimize the load on the No. 3 bearing, a multi-stepped knife edge seal was added to the rear of the high-pressure turbine and the diameter of the high-pressure compressor discharge seal was reduced.

The resulting thrust balance system was refined following completion of the fan, low-pressure compressor, and low-pressure turbine component detailed designs. High pressure rotor thrust balance load remained essentially unchanged at the sea level takeoff condition because no configuration changes were made. The low pressure rotor load, however, was predicted to increase at sea level takeoff.

To accommodate the revised thrust loads on the low and high pressure rotors and still maintain acceptable axial and radial spring rates, the turbine intermediate case struts were canted 11 degrees rearward.

4.12.2.2 Airflow Rate, Pressure, and Temperature

The secondary air flow system model developed during the initial design was updated to reflect changes induced by the following:

- o turbine airfoil cooling and leakage based on life analysis and high-pressure turbine supporting technology program results;
- o high and low pressure spool seal provisions for improved thrust balance;
- o rear intershaft seal and buffer system revisions to reduce oil leakage;
- o low-pressure turbine inner cavity cooling refinement;
- o refinement of active clearance control requirements for the high- and low-pressure turbines to optimize clearances and deterioration;
- o high-pressure compressor bleed source revisions to supply system air at the lowest possible penalties.

The initial flight propulsion system secondary airflow map of airflows, pressures, and temperatures is presented in Figure 40. Figure 41 provides a current system map indicating parametric values reflecting the above changes.

Table 34 compares current and initial airflow levels at the aerodynamic design point. As the design effort evolved, system airflow increases were generally experienced. However, as indicated by the totals, the magnitude of these increases was not large.

TABLE 34

FLIGHT PROPULSION SYSTEM SECONDARY AIRFLOW SYSTEM COMPARISON
(Aerodynamic Design Point: 10675 m (35000 ft), 0.8 Mn, Standard Day)

	Quantities - % Core Airflow	
	Initial Design	Current Design
High Pressure Turbine		
Disk		
Front Rim Cavity	0.48	0.61
Rear Rim Cavity	0.43	0.54
Blade		
Airfoil Cooling	2.57	2.74
Sideplate Cooling	0.23	-
Leakage	0.17	0.24
Vane		
Airfoil Cooling	6.14	6.41
Platform Cooling	0.90	0.81
Leakage	1.03	1.40
Case		
Outer Airseal Cooling	1.24	0.85
Flange Leakage	0.06	0.09
Sub Total:	13.25	13.69
Low Pressure Turbine		
Intermediate Case	0.25	0.64
Disks/Inner Seals	1.02	0.99
Case/Outer Seals	1.00	0.89
Flange Leakage	-	0.03
Sub Total:	2.27	2.55
Buffer System	0.43	0.49
High Pressure Compressor Active Clearance Control	0.50	0.50
TOTAL:	16.45	17.23

The detailed design of the secondary airflow system culminated in (1) refinement of controlling areas in the highand low-pressure turbine and rear bearing compartment regions, (2) refinement of clearances in the front intershaft seal, rear bearing compartment rear buffer seal and the low-pressure turbine front thrust balance seal, and (3) extension of the center vent pipe beyond the exit of the exhaust nozzle.

Current secondary airflow system controlling areas for the flight propulsion system are shown in Table 35. The first turbine blade compartment orifices were sized to provide the required amount of airfoil cooling. The 'mini' tangential on-board injection area was sized to provide 0.50 percent core airflow to reduce windage in front of the first turbine disk. Sizing of the turbine intermediate case outer rear seal was done to supply 0.15 percent core airflow to the second vane outer support in order to reduce thermal stresses. Third and fourth turbine blade cooling holes located in the rotor forward of the respective disks were designed to supply the attachments with the necessary cooling air. Holes in the center vent knife edge seal support were set to reduce the back pressure in the rear bearing compartment buffer system.

TABLE 35

CURRENT FLIGHT PROPULSION SYSTEM
SECONDARY AIRFLOW SYSTEM CONTROLLING AREAS

Location	Area, sq.cm (sq.in)
First Turbine Blade Showerhead Orifice	5.03 (0.780)
First Turbine Blade Multipass Orifice	17.10 (2.650)
Mini Tangential On-Board Injection Holes	1.19 (0.184)
Intermediate Case Outer Rear Seal	4.76 (0.738)
Third Turbine Blade Front Cooling Holes	6.45 (1.000)
Fourth Turbine Blade Front Cooling Holes	2.58 (0.400)
Center Vent Knife Edge Support Holes	31.42 (4.870)

Current clearances for the critical controlling seals are shown in Table 36. The front bearing compartment intershaft seal clearance was set at the minimum possible level at ground idle, based on deflection and deterioration analyses, to ensure that flow through the seal is always into the compartment. Similarly, the clearance of the rear buffer seal in the rear bearing compartment was minimized to prevent reverse flow of the oil/air mixture from the compartment. Clearance of the low-pressure turbine front seal was defined at the takeoff condition to provide the pressure drop and flow quantity required for low rotor thrust balance.

TABLE 36

CURRENT FLIGHT PROPULSION SYSTEM
SECONDARY AIRFLOW SYSTEM CONTROLLING SEAL CLEARANCES

Location	Flight Condition	Clearance - cm (in)
Front Intershaft	Sea Level, 0 Mn, Std. + 13.9°C (25°F) Idle	0.050 (.020)
Rear Bearing Compartment Rear Buffer	Sea Level, 0 Mn, Std. + 13.9°C (25°F) Idle	0.050 (.020)
Low Pressure Turbine Front Thrust Balance	SLTO, 0 Mn, Std. + 13.9°C (25°F)	0.055 (.022)

To provide the bearing compartment buffer system with an ambient vent pressure, the center vent pipe is extended past the end of the tailpipe. Secondary flow system analysis with the pipe terminating at the tailpipe exit showed vent pressure to be above ambient at the aerodynamic design point.

4.12.3 Electronic Engine Control

The electronic engine control is a full authority digital system designed to manage fuel for the flight propulsion system's two-stage combustor and provide control of variable high-pressure compressor vanes, start bleeds, intercompressor surge bleeds, and air valves for active clearance control. The control system regulates hydraulic pressure for stator vanes and bleed actuators with minimum fuel temperature rise and at minimum system cost and weight. Fuel flow management entails separate metering of fuel flows to the pilot zone and main zone fuel nozzles. The engine control system is unchanged from the initial flight propulsion system design.

4.13 SPECIAL DESIGN CONSIDERATIONS

4.13.1 Materials

Changes made in materials for the flight propulsion system since the initial design are not extensive, as shown by a comparison presented in Appendix A. Most revisions were made as a result of the detailed designs of the components indicating that material strengths could be downgraded, allowing lower cost alloys to be substituted without loss of performance. A few areas, such as the turbine section, did require revisions to higher strength materials to meet established life criteria. No new advanced technology alloys were required, or identified as desirable, during the updating efforts for the flight propulsion system.

4.13.2 Clearance Control

The objective of clearance control is to minimize rotor blade tip-to-case radial clearance at all operating conditions to optimize performance without incurring rubs during normal flight.

Clearance analyses were updated for each component during the detail design efforts. The analytical procedures used, clearance criteria considered, and the clearance control design features involved were unchanged from those described in Reference 1 for the initial design. The general philosophy for establishing tip gaps was reviewed separately for each component, and optimization of the active clearance control system was completed.

Tip gap philosophies were defined so that cold clearances could be established to best meet the initial and deteriorated thrust specific fuel consumption goals. For example, assessments made for the high-pressure compressor and high-pressure turbine showed that the performance goals can be met or exceeded if the gaps are set to prevent rubbing at all running conditions except severe maneuvers. In addition, active clearance control must be used in both components to achieve the desired relationship between pinch point, cruise, and takeoff clearances. All compression system components were designed to allow the blade tips to be on-line with the flowpath wall at the aerodynamic design point by running over shallow trenches in the rubstrips that allow for normal operating excursions. Fan tip gap philosophy allows hardware tolerances and severe maneuvers to rub-in. Rub-in from hardware tolerances, case ovalization, and severe maneuvers was the philosophy selected for the low-pressure compressor. Allowing tolerances to rub-in is also the philosophy for the low-pressure turbine, which also requires active clearance control. Finally, all component blade tips will be machined at assembly to minimize the effect of tolerances on tip gap. This approach eliminates the 'long' blade rub problem and allows for more accurate mating of the rotor with the case during component assembly.

A summary of current tip clearance estimates for flight propulsion system components is presented in Table 37. Goals and clearances established during the initial design are included for comparison. The effects of active clearance control are incorporated where applicable. Results indicate that the current component designs have blade tip clearances that are better than the goals established for the aerodynamic design point (consistent with maximum cruise) and takeoff operating points with the exception of the low-pressure turbine. Extensive case analysis and modifications to the active clearance control system improved low-pressure turbine tip clearances relative to the initial design. However, maneuver deflections could not be controlled well enough with the current configuration to provide goal level clearances.

TABLE 37

FPS COMPONENT TIP CLEARANCE COMPARISON

	AERODYNAMIC DESIGN POINT			TAKEOFF		
	Goal*	Initial Design*	Current Design	Goal*	Initial Design*	Current Design
Fan - cm	0.205	0.228	0.139	-	0.185	0.152
Low Pressure Compressor (Avg.) - cm	0.053	0.053	0.048	-	0.071	0.091
High Pressure Compressor (Avg.) - cm	0.033	0.025	0.030	0.045	0.030	0.035
High Pressure Turbine - cm	0.048	0.027	0.035	0.068	0.063	0.033
Low Pressure Turbine (Avg.) - cm	0.048	0.096	0.088	0.142	0.193	0.147

* Values shown are after thrust size of initial engine design was downsized 12 percent.

Notes:
(1) Clearances at MAXIMUM CRUISE are the same as those at the AERODYNAMIC DESIGN POINT.
(2) System performance for the initial design assumes goal level clearances in each component.

Stage-by-stage tip clearances for the multi-stage components are given in Tables 38, 39, and 40 for the lowand high-pressure compressors and the low-pressure turbine, respectively. The effects of active clearance control are incorporated where applicable. Current clearances for the low-pressure compressor are lower than those predicted for the initial design because of increased stiffness in the compressor intermediate case. High-pressure compressor clearances are essentially equivalent to those of the initial design, with active clearance control incorporated, because initial design concepts of rotor and case construction and material compatibility provided the best clearance control possible. Tip clearances for the low-pressure turbine were improved in the rear stages, principally because of detailed tailoring of the case/rotor designs and the active clearance control system.

TABLE 38

CURRENT FLIGHT PROPULSION SYSTEM LOW-PRESSURE COMPRESSOR BLADE TIP CLEARANCES - cm (in)

	Rotor 2	Rotor 3	Rotor 4	Rotor 5
Aerodynamic Design Point and Max. Cruise Clearances	0.033 (0.013)	0.033 (0.013)	0.053 (0.021)	0.078 (0.031)
Takeoff	0.096 (0.038)	0.086 (0.034)	0.093 (0.037)	0.088 (0.035)

TABLE 39

CURRENT FLIGHT PROPULSION SYSTEM HIGH-PRESSURE COMPRESSOR BLADE TIP CLEARANCES - cm (in)

Rotor	Aerodynamic Design Point (and Max. Cruise Clearances)	Takeoff
6	0.035 (0.014)	0.040 (0.016)
7	0.040 (0.016)	0.038 (0.015)
8	0.050 (0.020)	0.035 (0.014)
9	0.033 (0.013)	0.035 (0.014)
10	0.027 (0.011)	0.033 (0.013)
11	0.027 (0.011)	0.030 (0.012)
12	0.025 (0.010)	0.030 (0.012)
13	0.025 (0.010)	0.040 (0.016)
14	0.025 (0.010)	0.035 (0.014)
15	0.022 (0.009)	0.033 (0.013)

TABLE 40

CURRENT FLIGHT PROPULSION SYSTEM LOW-PRESSURE TURBINE BLADE TIP CLEARANCES - cm (in)

	Rotor 2	Rotor 3	Rotor 4	Rotor 5
Aerodynamic Design Point and Max. Cruise Clearances	0.055 (0.022)	0.068 (0.027)	0.093 (0.037)	0.134 (0.053)
Takeoff	0.124 (0.049)	0.132 (0.052)	0.160 (0.063)	0.172 (0.068)

Substantial improvement in fan tip clearance was projected because of increased stiffness in the compressor intermediate case. In addition, careful tailoring of the active clearance control system resulted in reduced running clearance at takeoff for the high-pressure turbine.

The external active clearance control approach, with air for the high-pressure compressor impinging from pipes on the case at critical flange locations, was selected because it eliminates the complex design problems of an internal system. Compared to the internal system, it provides the best means for optimizing blade tip clearance by case-rotor thermal matching without the complexity of double wall construction and with fewer leaks. It can be tailored to varied stage-to-stage clearance control movement, and its characteristics are analytically more predictable than those of the internal configuration.

The hub configuration of the low-pressure turbine was evaluated because of concerns for deflections and weight. Figure 42 depicts the concepts evaluated while Table 41 presents the radial and axial deflections under a simulated 0.2 rad/sec gyro maneuver for each configuration. Results of this evaluation confirmed the selection of the double hub or 'A' frame configuration from the initial design as the most tolerant to radial and axial deflections.

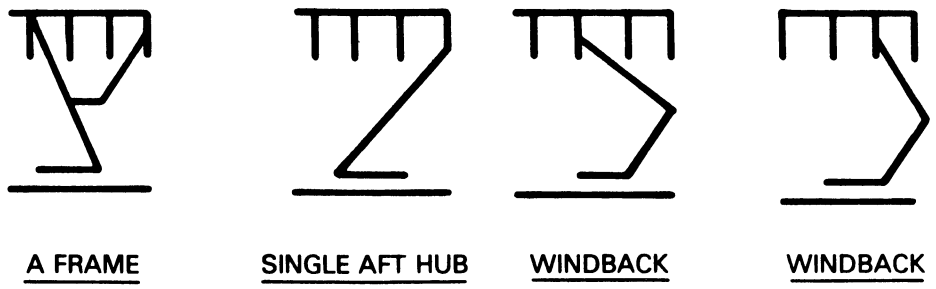

Figure 42 Low-Pressure Turbine Rotor Hub Configurations

TABLE 41

ROTOR RADIAL AND AXIAL DEFLECTION STUDY RESULTS

	A Frame	Single Aft Hub	Windback	Windback
Radial Deflection - cm (in)				
Stage 2	0.0396	0.0500	0.0853	0.0411
	(0.0156)	(0.0197)	(0.0336)	(0.0162)
Stage 5	-0.0259	-0.0497	-0.0660	-0.0289
	(-0.0102)	(-0.0196)	(-0.0260)	(-0.0114)
Axial Deflection - cm (in)				
Stage 2	0.0746	0.1259	0.1971	0.0871
	(0.0294)	(0.0496)	(0.0776)	(0.0343)
Stage 5	0.0988	0.1480	0.2225	0.1069
	(0.0389)	(0.0583)	(0.0876)	(0.0421)

A schematic of the current active clearance control system is shown in Figure 43. Like the initial system design, it is used to control clearances in the rear stages of the highpressure compressor, in the high-pressure turbine, and in the front stages of the low-pressure turbine. For improved clearance control in the rear of the low-pressure turbine, the system was extended rearward from the rear foot of the fourth stage vane in the initial design to include the front foot of the fifth stage vane in the current design. This system incorporates a combination of external fan air impingement on the compressor case during cruise operation and a dual compressor bleed manifold system which supplies the internally cooled turbine cases with different temperature air between takeoff and cruise. This approach reflects the initial design concept except for redefinition of the mixture quantities and a change in compressor stage bleed source for the low-pressure turbine.

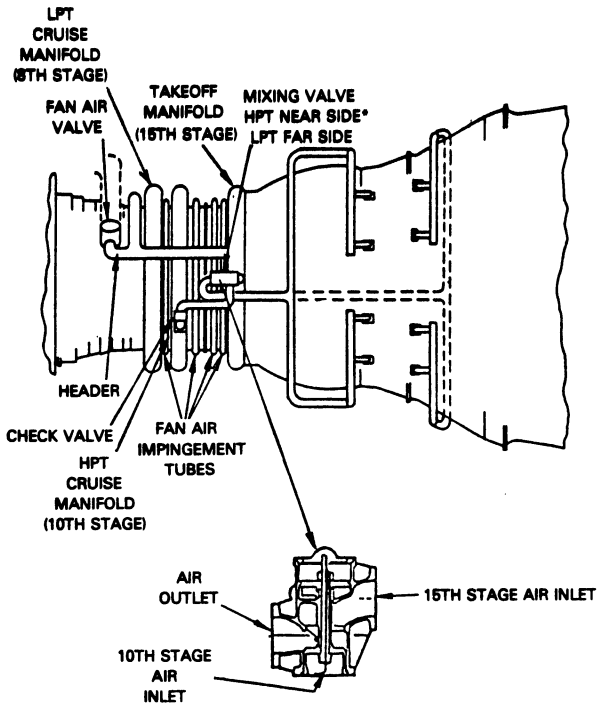

Figure 43 Current Flight Propulsion System Active Clearance Control System

Detailed design of the high-pressure compressor active clearance control system resulted in the addition of a fifth impingement tube to the rear case to adequately cover all flanges and shroud hooks. Air bleed scheduling requirements were established, taking into account both steady state and transient propulsion system operation and minimum gapping requirements. The resultant air scheduling system produces minimum clearance pinch points for each compressor stage at the operating conditions shown in Table 42. Active clearance control was determined to reduce average tip clearance by 0.007 cm (0.003 in). A 0.030 cm (0.012 in) average clearance was obtained at altitude using 0.5 percent fan air bleed.

TABLE 42

CURRENT HIGH-PRESSURE COMPRESSOR DESIGN PINCH POINTS

Stage Number	Pinch Point Condition
6	Sea Level Takeoff
7	Deceleration
8	Sea Level Takeoff
9	Acceleration
10	Begin Cruise
11	Begin Cruise
12	Acceleration
13	Acceleration
14	Deceleration
15	Deceleration

As a result of detailed analysis of the active clearance control system for the high-pressure turbine, the initial design was refined. A scheduled mixture of tenth and fifteenth stage compressor bleed air is used to cool full ring rails, which control the clearances of the outer air seal. The thermal environment of the front and rear rails is carefully matched to prevent unequal thermal gradients, which could result in tilting. The air scheduling is accomplished through a valving arrangement incorporating a check valve and a regulating valve. Although a mixing valve was part of the arrangement in the initial design, the most current analysis of the secondary airflow system included active clearance control requirements and indicated that desired tip clearances can be maintained without mixing. A bleed quantity of 0.22 percent of core airflow is taken from either the fifteenth or tenth stage of the high-pressure compressor, depending on flight condition, to control blade tip clearance. Air scheduling is such that the pinch point occurs early in an acceleration, clearances during takeoff and climb do not unduly penalize performance, and clearance at cruise is minimized to provide the best combination of initial and long time performance. Current active clearance control bleed air schedule requirements are shown in Table 43.

TABLE 43

CURRENT HIGH-PRESSURE TURBINE ACTIVE CLEARANCE CONTROL AIRBLEED REQUIREMENTS

Bleed Quantity Is 0.22 Percent of Core Airflow

Flight Condition	Bleed Source (HPC Stage)
Idle	15
Acceleration	15
Takeoff	15
Climb	
less than 6,096 m	15
(20,000 ft) and above	10
Cruise	10

Detailed analysis of the active clearance control for the low-pressure turbine resulted in (1) extending control rearward to include the front foot of the fifth stage turbine vane, (2) changing the lower temperature compressor bleed source to the eighth stage, and (3) carefully refining the details of the initial design. Control is provided by a convectively cooled chamber positioned between a double-walled case with air progressively leaked into the main gaspath as it cools the vane outer attachments and case hardware. Air scheduling is accomplished through a valving arrangement incorporating a check valve, regulating valve, and mixing valve. Air scheduling is such that the pinch point occurs early in an acceleration and clearances during takeoff, climb, and cruise are controlled to provide the best combination of initial and long time performance. Current active clearance control bleed air schedule and quantity requirements are shown in Table 44.

TABLE 44

CURRENT LOW-PRESSURE TURBINE ACTIVE CLEARANCE CONTROL AIRBLEED REQUIREMENTS

Flight Condition Bleed Quantity - % Core Airflow	Bleed Source (HPC Stage)	
Acceleration	8/15	0.48/0.32
Takeoff	8/15	0.48/0.32
Climb - less than		
6,096 m (20,000 ft)	8/15	0.48/0.32
and above	8	0.80
Cruise	8	0.80

4.13.3 Performance Retention

Two major causes for current in-service performance degradation are clearance increases caused by internal engine rubs and erosion of gaspath parts. Design features incorporated in the flight propulsion system during the initial design were refined during the detailed designs of the components. Details are reported in References 1 and 3 through 7. During these design efforts, emphasis was placed on ensuring case and rotor stiffness and the proper sharing of the imposed loads between the nacelle duct (cowl) walls and the engine cases. The rotor-frame model was refined in order to reflect the final designs, and rotor tip clearances were evaluated. Clearances in each component were set to maximize initial performance while still meeting long term (deteriorated) performance goals. Desired abradability standards for seals throughout the engine were met by careful design and materials selection. Loss of performance caused by erosion of compressor airfoils was further reduced by more extensive use of controlled diffusion airfoils that incorporate thick leading edges. Turbine airfoil attachment designs were refined as a result of analyses aimed at minimizing distortions during operation.

4.13.4 Rotor Vibration Control

Basic anti-vibration features incorporated in the initial design of the flight propulsion system were refined during the detailed designs of the components. Details are reported in References 1 and 3 through 7. These detailed analyses did indicate the necessity for improved rotor control so that all rotor dynamics criteria could be met. The most significant improvements included the addition of oil dampers to the front thrust (number 3) bearing on the high pressure rotor and the rear (number 5) bearing on the low-pressure rotor. The current rotor support configurations are shown in Figures 44 and 45.

The initial rotor-frame analytical model was revised to reflect the addition of oil dampers and refined to account for all linear and torsional springs and damping by support structures between the high and low-pressure rotors, the core component cases, and the inner and outer fan ducts. Figure 46 shows the refined model.

The current design configuration of the flight propulsion system was analyzed with the revised and refined rotor-frame model. Results for the low and high pressure rotors are shown in Figures 47 and 48, respectively. All modes meet the design criteria. The most serious critical speed modes are the free-free shaft modes with high strain energies. These modes occur well above maximum rotor speeds and the low-pressure shaft mode is well below idle speed for the high-pressure rotor. The other high pressure rotor modes are adequately below idle-speed for the high pressure rotor. The tailplug mode is adequately above maximum low-pressure rotor speed. Fan and low-pressure turbine modes for the low-pressure rotor, although in the operating region between idle and minimum cruise speeds, are acceptable because of low strain energy levels.

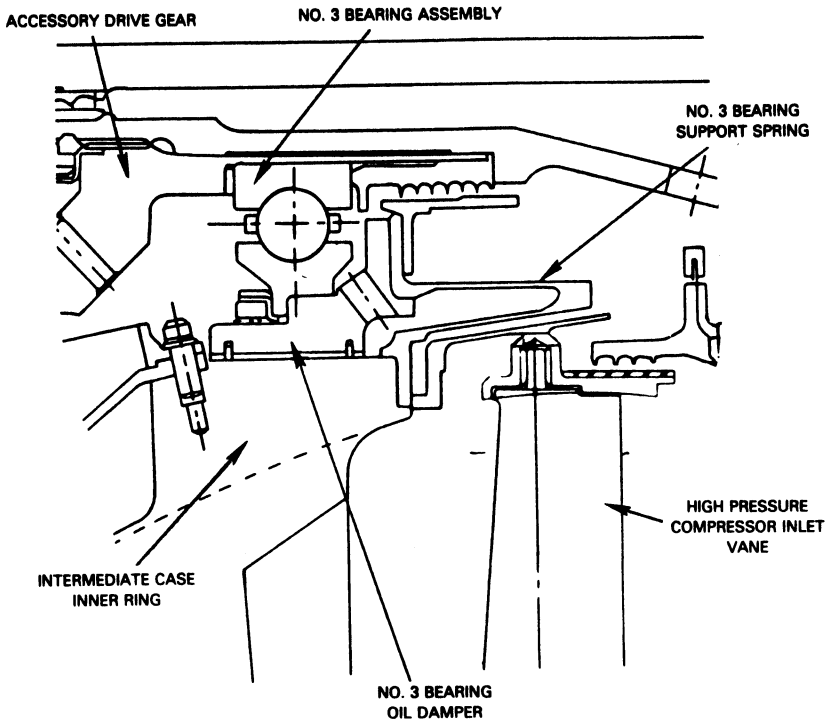

Figure 44 Current Flight Propulsion System No. 3 Bearing Compartment Configuration

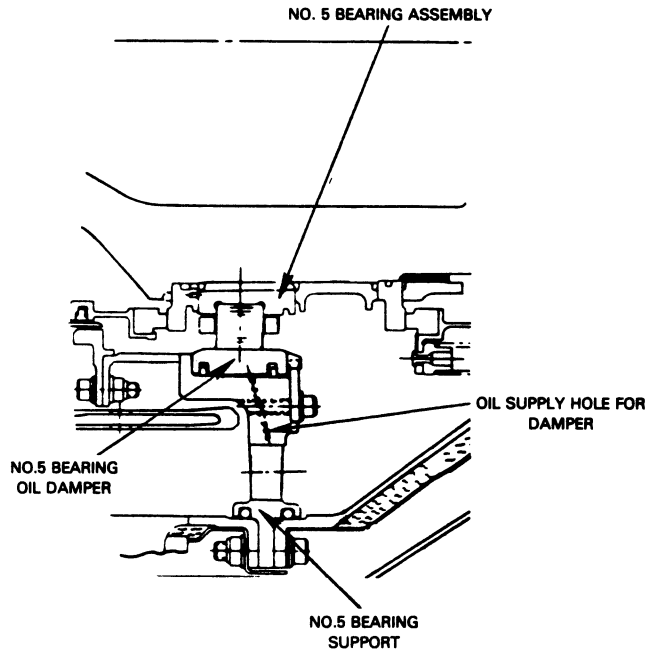

Figure 45 Current Flight Propulsion System No. 5 Bearing Compartment Configuration

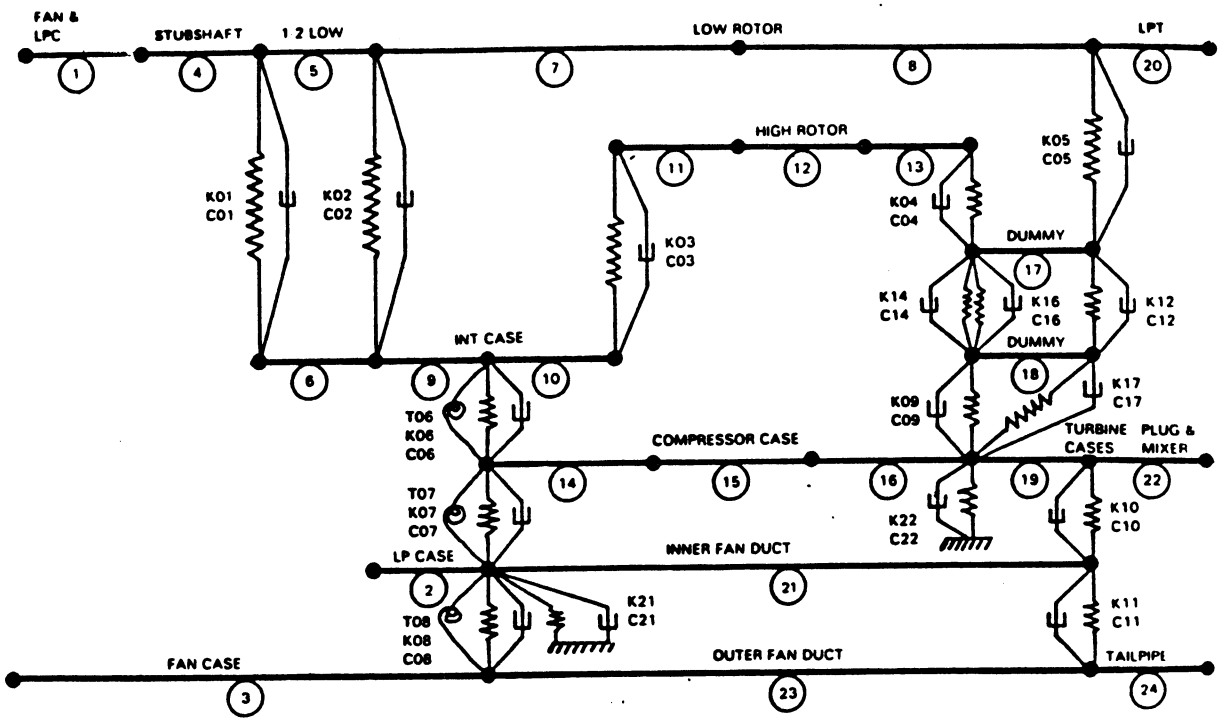

Span	Description	Spring Number	Description
1	Fan/LPC Rotor	K01*	#1 Bearing
2	LPC Case	K02*	#2 Bearing
3	Fan Case	K03*	#3 Bearing & Support (Equivalent)
4	Stubshaft	K04*	#4 Bearing
5	1-2 Low Shaft	K05*	#5 Bearing
6	#1 Bearing Support Cone		#5 Bearing
7	Low Shaft Forward	K06	Fan Intermediate Case-Linear
8	Low Shaft Aft	T06	Fan Intermediate Case-Trunnion
9	#2 Bearing Support	K07	Fan I/C Struts Linear
10	#3 Bearing Support	T07	Fan I/C Struts Trunnion
11	High Rotor	K08	Fan Exhaust Case-Linear
12	High Rotor	T08	Fan Exhaust Case-Trunnion
13	High Rotor	K09	Turbine Intermediate Case
14	High Compressor Case	K10	Fan Duct/Turbine Case Connector
15	High Compressor Case	K11	Fan Duct Bifurcation Beam
16	Diffusion/HPT Case	K12*	#5 Bearing Viscous Damper
17	Dummy	K14*	#4 Bearing Viscous Damper
18	Dummy	K16	#4 Bearing Centering Spring
19	Low Turb & Exhaust Case	K17	Turbine Intermediate Case
20	Low Pressure Turbine Rotor	K21	Front Mount
21	Inner Fan Duct	K22	Rear Mount
22	Plug Mixer		
23	Outer Fan Duct		
24	Tail Pipe		

* Springrates are a function of the type of load.

Figure 46 Current Flight Propulsion System Rotor-Frame Critical Speed Model

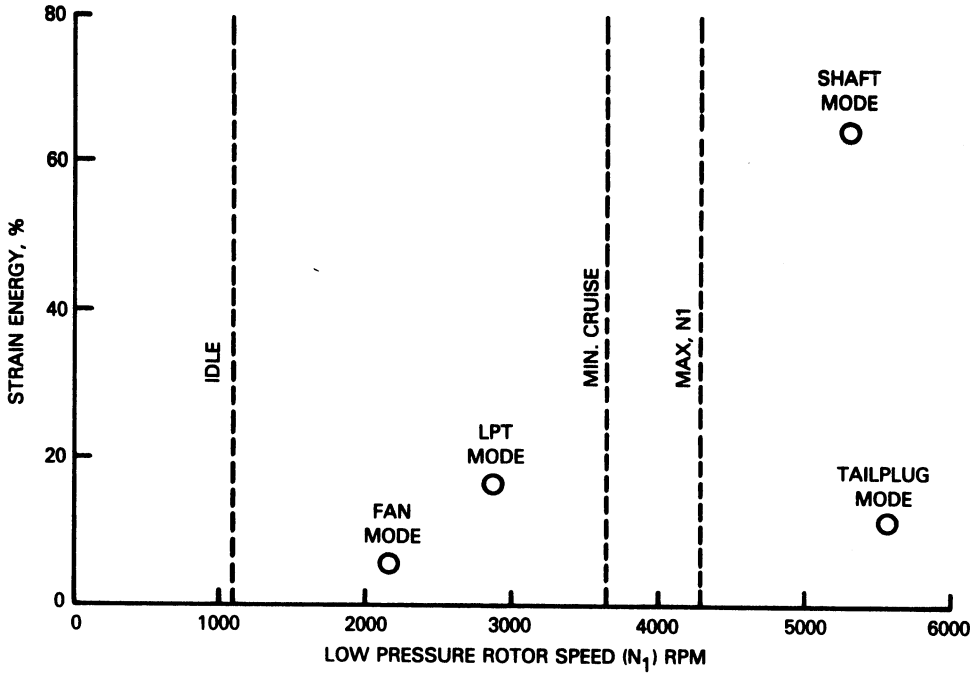

Figure 47 Current Flight Propulsion System Critical Speed Analysis Results - Low-Pressure Rotor

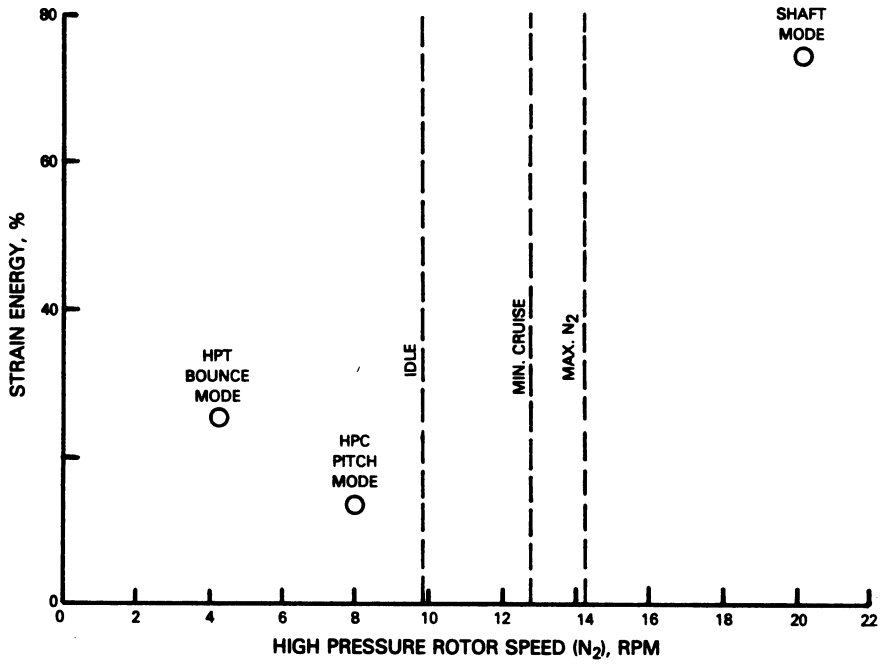

Figure 48 Current Flight Propulsion System Critical Speed Analysis Results - High-Pressure Rotor

Acceptable bowed rotor starting characteristics are achieved with the aid of the viscous film oil dampers on the outer races of the number 3 and number 4 bearings.

4.14 SYSTEM PERFORMANCE AND ECONOMIC ANALYSES

This section presents performance design goals and operating economic data based on installation of the updated flight propulsion system into representative future commercial aircraft. Included in this discussion are the major factors which influenced the evolutionary improvement of thrust specific fuel consumption for the flight propulsion system, updated weight estimates as dictated by current design and configuration modifications, updated manufacturing and maintenance cost estimates, and flight performance and operating economics for future commercial airplanes employing the flight propulsion system. The criteria assessed during this evaluation include fuel burn, direct operating cost, performance deterioration, noise, and emissions.

4.14.1 Fuel Consumption

The performance simulations for the flight propulsion system have been periodically updated throughout the program, as described in Sections 3.2 through 3.4 of this report. These updates have been conducted to evaluate the effects of subsequent design and configuration changes. The primary emphasis in these updates has been the projection of status thrust specific fuel consumption for the flight propulsion system. A comparison of thrust specific fuel consumption at the maximum cruise rating between the flight propulsion system, as it has evolved, and the JT9D-7A reference engine is presented in Figure 49. In this comparison, the JT9D-7A is scaled to the airflow size of the flight propulsion system and both are installed in isolated nacelles without customer service airbleed or power extraction. The comparison shows status thrust specific fuel consumption has been better than the Energy Efficient Engine Program goal of twelve percent reduction throughout the program. The current level of 15 percent improvement relative to the JT9D-7A reference engine shows favorably against the 14.9 percent improvement projected for the initial design.

Several major factors influenced the evolution of thrust specific fuel consumption for the flight propulsion system. Changes affecting the level between the May 1979 and October 1979 status updates include improving performance by using a more suitable design point location on the fan rotor map and by reducing losses from the fan duct exit guide vanes. A revision to the secondary airflow system, however, resulted in a net loss. The improvement made between October 1979 and March 1980 was a result of improvements in high-pressure compressor and high-pressure turbine rotor tip clearances, revisions in high-pressure turbine tip seal and low-pressure turbine cooling and leakage airflow, and a drag increase caused by length increases associated with high-pressure compressor and exhaust mixer design changes. The June 1981 and current thrust specific fuel consumption level evolved from a variety of design changes occurring since March 1980. These changes include:

- improved fan and low-pressure compressor tip clearances;
- worse low-pressure turbine tip clearance and secondary airflow;
- incorporation of a shroud on the fan blade;

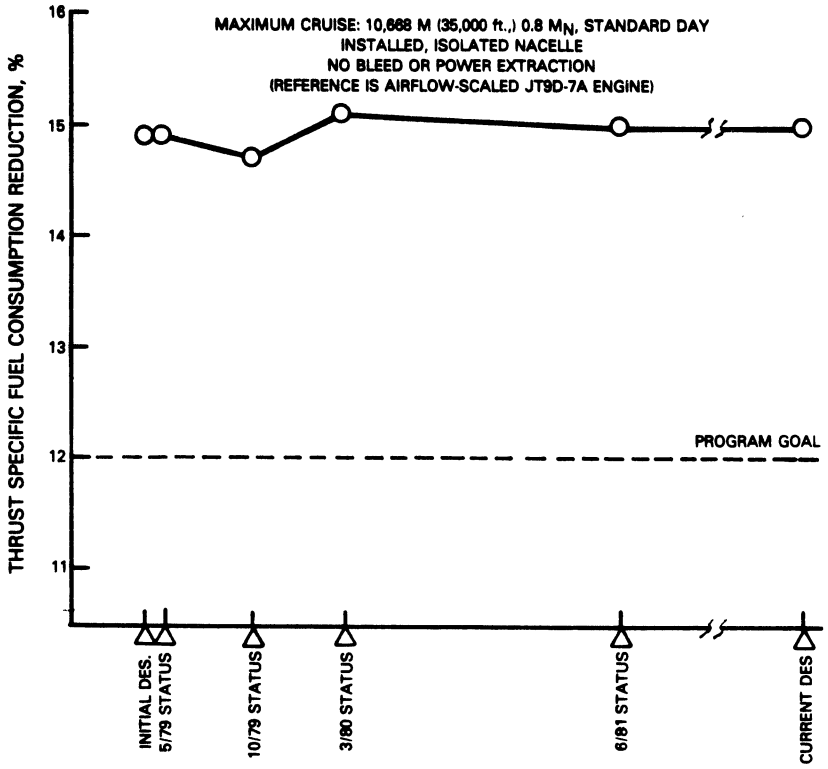

Figure 49 Flight Propulsion System Thrust Specific Fuel Consumption Evolution

- o an improved fan map;
- o high-pressure turbine improvements due to cooling air revisions, secondary airflow reduction, and rematching;
- o reduced turbine transition duct losses;
- o improved low-pressure turbine aerodynamics;
- o and generally increased secondary system and turbine cooling airflows.

The major elements contributing to the initial and current thrust specific fuel consumption advantages are compared in Table 45.

TABLE 45

FLIGHT PROPULSION SYSTEM THRUST SPECIFIC FUEL CONSUMPTION COMPARISON
(Aerodynamic Design Point: 10675 m (35,000 ft), 0.8 Mn, Standard Day)

(Reference is Airflow-Scaled JT9D-7A Engine)

Contributor	TSFC Change - Percent	
	Initial Design	Current Design
Low Pressure Spool	- 5.8	- 5.8
High Pressure Spool	- 3.5	- 3.8
Cycle	- 3.2	- 3.2
Mixing/Installation	- 2.4	- 2.2
Total	-14.9	-15.0

A comparison of installed and uninstalled thrust specific fuel consumption (and thrust) for the initial and current designs of the flight propulsion system is given at the key rated operating conditions in Table 46. Evolution of the design has resulted in a small thrust loss of about 0.8 percent at the altitude conditions, but a thrust gain of 2.3 percent at takeoff. Thrust specific fuel consumption has improved 0.1 percent at maximum cruise and 0.5 percent at takeoff. Conversely, it has increased 0.5 percent at the maximum climb condition.

4.14.2 Weight

Flight propulsion system weight was updated periodically as design and configuration changes dictated. Optimization of weight was not pursued as diligently for the flight propulsion system as it would be in the development of an engine for ultimate production. A comparison of weight evolution for the flight propulsion system against the weight of the JT9D-7A reference engine scaled to the flight propulsion system airflow size is presented in Figure 50. Neither the scaled JT9D-7A reference engine nor the flight propulsion system weight in this comparison includes the nacelle and associated subsystems. The current design of the flight propulsion system is estimated to be 1.9 percent heavier than the scaled JT9D-7A; whereas, the weight of the initial design was estimated to be 2.5 percent lighter than the JT9D-7A.

Several factors have caused the weight of the flight propulsion system to change as the design has evolved. The weight increase between the initial design and May 1979 was caused primarily by revision of the fan hub to accommodate blade loss, incorporation of a vortex plate to improve the tangential on-board injection system, and high pressure rotor bearing and support changes to improve rotor vibration control. An additional weight increase was incurred between May 1979 and October 1979 because of an increased diameter No. 1 bearing required for thrust balance, a longer high-pressure compressor with modifications for reduced aerodynamic risk, the addition of seals to the highand low-pressure turbines for thrust balance, and a redesigned turbine intermediate case for increased axial loading. A weight reduction was experienced between October 1979 and the current design, despite design revisions which increased weight. This weight reduction was primarily the result of incorporating a shrouded fan blade in place of the heavier shroudless blade configuration. Other design revisions offsetting weight include the addition of a viscous damper to the No. 5 bearing, recontouring of the diffuser struts to take increased blow-off loads, and increased penetration along with additional lobes for improved exhaust mixer performance.

The initial nacelle design weight was reduced by substitution of graphite polyimide honeycomb for aluminum brazed titanium honeycomb in the tailpipe.

TABLE 46

FPS FUEL CONSUMPTION AND THRUST COMPARISON

	AERO DESIGN POINT[1]		MAXIMUM CRUISE[2]		TAKEOFF[3]	
	Initial Design*	Current Design	Initial Design*	Current Design	Initial Design*	Current Design
Thrust Specific Fuel Consumption kg/hr/kg						
Uninstalled	0.2497	0.2487	0.2580	0.2587	0.1492	0.1483
Installed	0.2612	0.2610	0.2689	0.2703	0.1505	0.1499
Thrust - N						
Uninstalled	39967	39744	44570	44304	160935	164694
Installed	38076	37742	42,635	42280	158378	162047

Off-Design Operating Conditions:

(1) Maximum Cruise - 10675 m (35,000 ft), 0.8 Mn, Standard Day
(2) Maximum Climb - 10675 m (35,000 ft), 0.8 Mn, Standard Day + 10°C (18°F)
(3) Takeoff - SLTO, 0 Mn, Standard Day + 13.9°C (25°F)

* Values shown are after thrust size of initial engine design was downsized 12 percent.

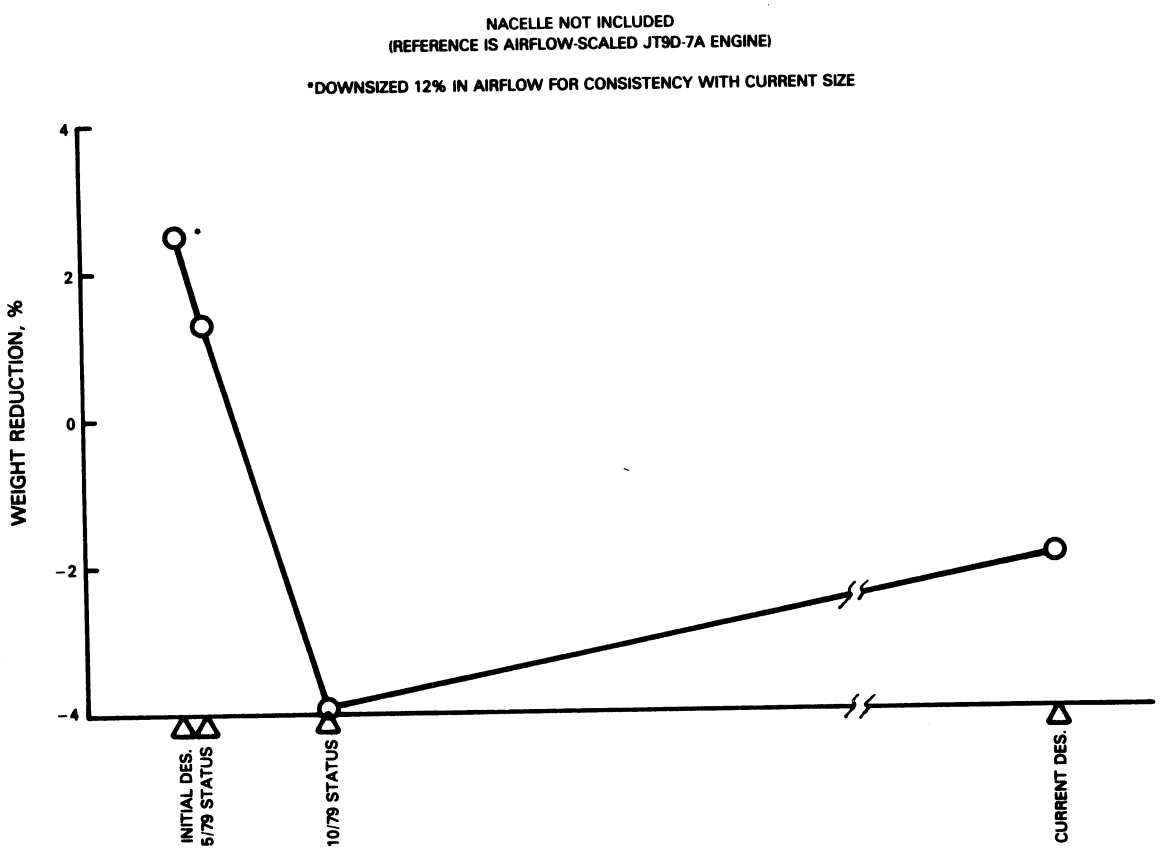

Figure 50 Flight Propulsion System Weight Evolution

4.14.3 Manufacturing Cost/Maintenance Cost

Flight propulsion system manufacturing and maintenance cost estimates were updated at the same intervals as weight updates. These updates were made as design and configuration changes dictated. For similar reasons as weight, optimization of manufacturing and maintenance costs was not pursued as diligently for the flight propulsion system as it would be in the development of an engine for ultimate production. The evolution of these costs for the flight propulsion system compared to those for the JT9D-7A reference engine scaled to the flight propulsion system airflow size are shown in Figures 51 and 52. Both manufacturing cost and maintenance cost are directly compared in terms of 1977 dollars, the economic base for the initial design. Current manufacturing cost of the flight propulsion system is estimated to be 0.4 percent higher than the scaled JT9D-7A, compared to the initial design being 1.8 percent lower in cost. The current flight propulsion system maintenance cost is estimated to be 5.4 percent lower than reference engine maintenance cost; whereas, the maintenance cost estimated for the initial design was predicted to be 5.3 percent lower.

Manufacturing and maintenance cost trends, as the flight propulsion system design has evolved, are quite similar. Several factors are responsible for these cost trends. The design and configuration changes most significantly influencing the increase in costs between the initial design and the May 1979 status were the incorporation of a vortex plate, changing the rear high-pressure compressor seal from a wide channel to a 9 knife edge labyrinth configuration and changing the high pressure rotor bearing and support. Additional cost increases were incurred between May 1979 and October 1979 because of an increase in high-pressure compressor length, several changes in the combustor liner segments, the addition of seals to the highand low-pressure turbines and a revised assessment of requirements for the fabrication of parts from titanium-aluminide material. Substantial manufacturing and maintenance cost improvements were experienced with the current flight propulsion system design relative to the October 1979 definition because of the incorporation of a shrouded fan blade in place of the shroudless blade configuration.

4.14.4 Airplane Performance and Economics

Flight performance and operating economics of future commercial airplanes using the flight propulsion system have been assessed in order to measure the capability of the flight propulsion system to meet the goals established for the program by NASA. These goals consist of a twelve percent reduction in thrust specific fuel consumption, a five percent reduction in direct operating cost, and a fifty percent reduction in performance deterioration relative to the JT9D-7A reference engine. Additional goals include meeting both FAR Part 36 (1978) noise rules and EPA proposed 1981 exhaust emissions standards.

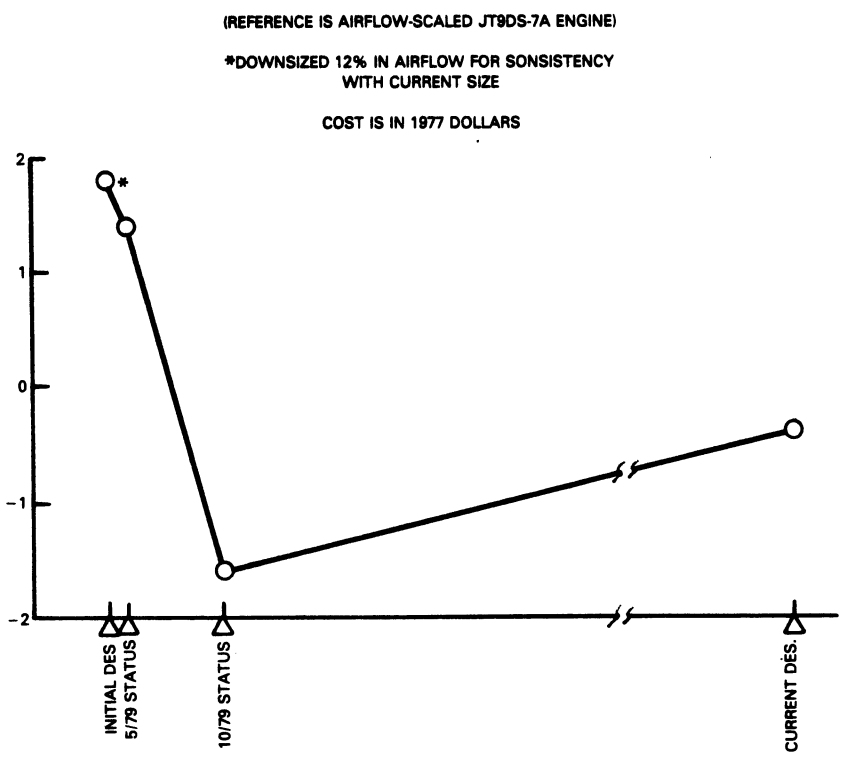

Figure 51 Flight Propulsion System Manufacturing Cost Evolution

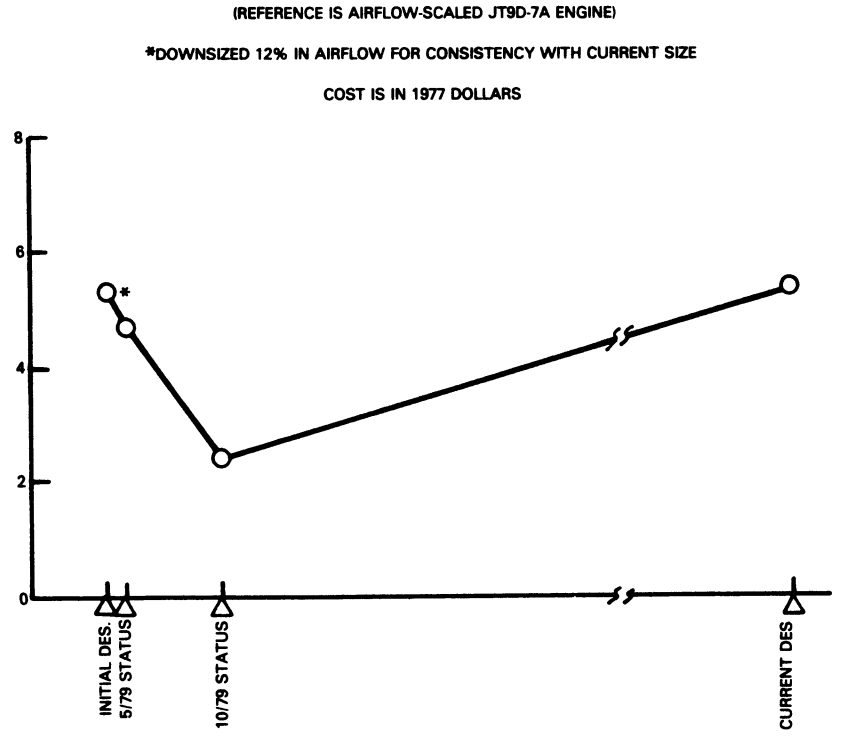

Figure 52 Flight Propulsion System Maintenance Cost Evolution

The original evaluation was conducted during the initial design phase of the flight propulsion system. Boeing, Douglas, and Lockheed assisted in that evaluation, results of which are published in Reference 2. That evaluation consisted of airplane-mission analyses of the flight propulsion system and JT9D-7A reference engine in seven of the eight airplanes shown in Table 47. An eighth airplane, the 150-passenger twin, was added to the current analysis because it has become a market factor since inception of the Energy Efficient Engine program.

The current evaluation was conducted utilizing trade factors which were derived from the initial evaluation and used to determine the effects of changes to the flight propulsion system on the fuel burned and direct operating costs of all the airplanes. This method was deemed accurate enough to accommodate the relatively small changes involved in this update.

TABLE 47

ENERGY EFFICIENT ENGINE AIRPLANE DEFINITIONS

DOMESTIC

	Boeing	Douglas	Lockheed	Pratt & Whitney	(Current Update Only) Pratt & Whitney
Type	Twin	Trijet	Trijet	Trijet	Twin
In Service Date	1990's	1990's	1990's	1990's	1990's
Design Range - km (nm)	3700(2000)	5560(3000)	5560(3000)	5560(3000)	2775(1500)
Passengers	196	458	500	440	150
Cruise Speed - Mn	0.80	0.80	0.80	0.80	0.78

INTERCONTINENTAL

	Douglas	Lockheed	P&WA
Type	Trijet	Quadjet	Quadjet
In Service Date	1990's	1990's	1990's
Design Range - km (nm)	10190(5500)	12040(6500)	10190(5500)
Passengers	438	500	510
Cruise Speed - Mach No.	0.8	0.8	0.8

Weight, price, and maintenance values used for the flight propulsion system in the original airplane performance and economic evaluation (Reference 2) represent interim levels prior to completion of the initial design. They are the levels presented at the Energy Efficient Engine Preliminary Design Review held in September 1978, adjusted for the mounting of airframe and engine accessories on the core. These levels were estimated prior to completion of the initial designs of the fan and combustor. Weight, price (in terms of manufacturing cost), and maintenance cost throughout the rest of this report are for the flight propulsion system as defined at the completion of the initial design efforts for all components.

Manufacturing and maintenance cost economic bases have been updated for the current evaluation. The initial evaluation was in terms of 1977 dollars, whereas the current evaluation reflects 1980 dollars.

A summary of flight propulsion system values used in the original and current airplane performance and economic evaluations is presented in Table 48.

TABLE 48

FLIGHT PROPULSION SYSTEM SUMMARY
(References are Airflow-Scaled JT9D-7A Engine)

	Original Propulsion System/ Aircraft Integration Evaluation	Current Evaluation
Economic Year Dollars	1977	1980
Airflow Size - %	Base	88.0
Thrust Specific Fuel Consumption (ADP)	-14.9	-15.0
Engine Weight - Percent	-7.6	-1.9
Nacelle Weight - Percent	-12.9	-13.4
Engine Price - Percent	-4.7	-4.7
Nacelle Price - Percent	-12.9	-13.4
Maintenance Cost - Percent	-4.6	-4.6

Nacelle price has been assumed to be a function of nacelle weight consistent with the appropriate level of technology. The rapid escalation of cost for advanced materials over the last few years has caused engine price to increase rapidly and has accelerated the flight propulsion system price compared to the JT9D-7A because of the flight engine's use of advanced materials.

4.14.4.1 Fuel Burn

Although it is not a program goal, the original analysis relative to fuel burned has been updated because of the significance this parameter has in indicating direct change in aircraft fuel consumption. Results of the current evaluation are shown in Figures 53 and 54 for the design and typical (average) flight stage lengths and load factors, respectively. Fuel burn advantages relative to the JT9D-7A reference engine were estimated by Pratt & Whitney for each of the airplanes described in Table 45, using the basic flight propulsion system data summarized in Table 46. The results were correlated with the design fuel weight fraction (design fuel weight/takeoff gross weight).

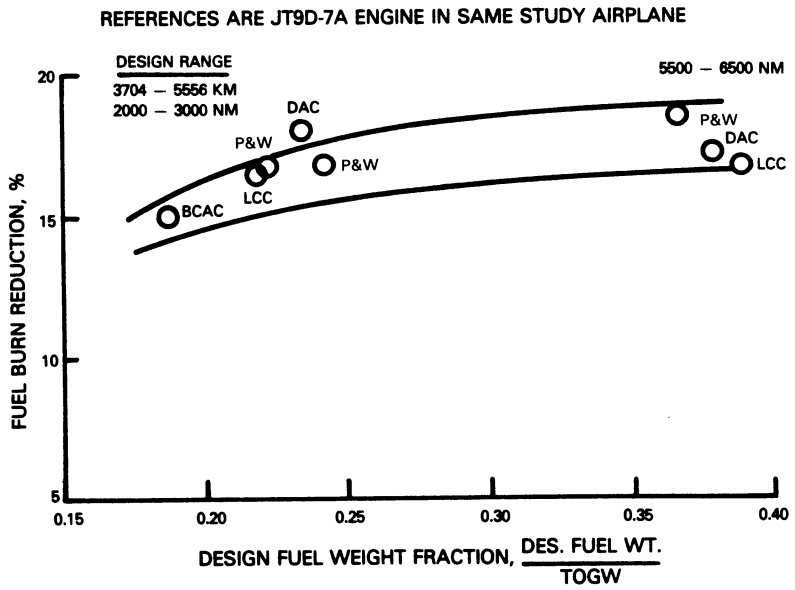

Figure 53 Current Flight Propulsion System Fuel Burn Advantage - Design Missions

Trade factor analysis of the current flight propulsion system compared to the JT9D-7A reference engine showed that the average fuel burn advantage for the flight propulsion system has decreased from 17.4 percent to 17.2 percent for intercontinental airplanes and 16.5 percent to 16.3 percent for domestic airplanes. The loss in fuel burn advantage was minimized because the small gain in thrust specific fuel consumption coupled with the small decrease in relative nacelle weight helped to offset the relative engine weight increase.

4.14.4.2 Direct Operating Cost

For the current evaluation, economic groundrules and equations were updated to 1980 levels from the 1977 levels used in the original evaluation. These new groundrules and equations are presented in Tables 49 and 50, respectively. Since projection of fuel prices for the 1990 time period has an inherent degree of uncertainty, three price levels were evaluated: $1.00, $1.50, and $2.50 per 3.78 liters (1.0 U.S. gallon).

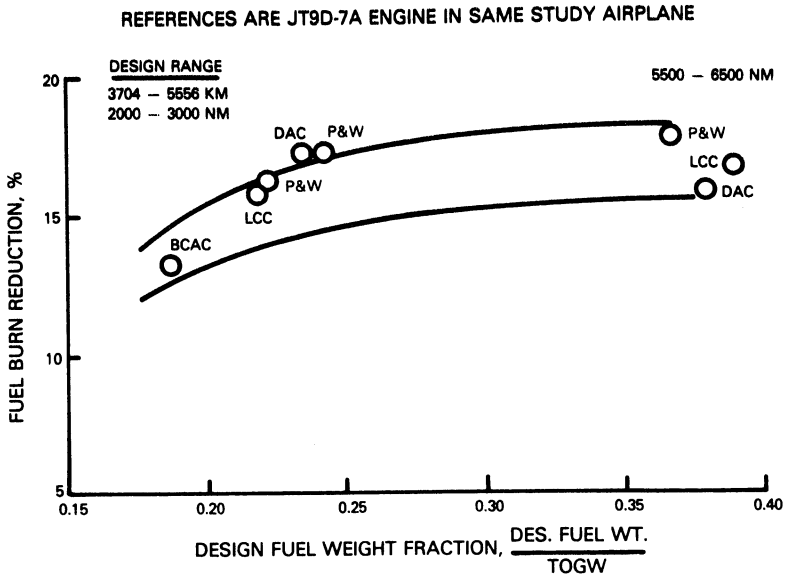

Figure 54 Current Flight Propulsion System Fuel Burn Advantage - Typical Missions

TABLE 49

GROUNDRULES FOR CURRENT FLIGHT PROPULSION SYSTEM ECONOMIC ANALYSIS - DIRECT OPERATING COST (DOC)

Crew Cost*	1980 update of 1977 Boeing
Fuel**	$1.00, $1.50 and $2.50 per 3.78 liters (1.0 U.S. gallon) in 1980 money
Aircraft	
Price*	PWA 1980
Utilization*	1980 update of 1977 Boeing
Block Time*	1980 update of 1977 Boeing
Insurance***	0.5 percent flyaway per year
Airframe Maintenance*	1980 update of 1977 Boeing
Maintenance Burden***	200 percent on labor
Depreciation***	Straight line, 15 years to 10 percent residual
Spares	Airframe 6 percent Engine 30 percent
Engine Maintenance***	Mature engine, no immaturity bump, no derate
Year Dollars**	1980

* - Different from original groundrules (See Table 50 for equations/ explanations

** - Different from original groundrules

*** - No change from original groundrules

TABLE 50

ECONOMIC EQUATIONS FOR CURRENT
FLIGHT PROPULSION SYSTEM ECONOMIC ANALYSIS

Crew Cost[1]	Domestic = (40.0 Fw + 33.98)Fu +53.30 International = (26.5 Fw + 273.1)Fu +89.1 (Fw and Fu are from 1977 Boeing Method)
Aircraft Price	$0.6435 \left(\frac{WAF}{1000}\right)^{0.7} \times 10^6$ (airframe) +1.287 (0.0089 (number seats) - 0.315) $\times 10^6$ (furnishings) +1.287 (0.0022 (number seats) + 1.81) $\times 10^6$ (avionics)
Utilization	Constant trips/year as function of range (3200 @ 463 km (250 nm), 2200 @ 926 km (500 nm), 1400 @ 1852 km (1000 nm), 850 @ 3704 km (2000 nm)
Block Time	Taxi Times - Domestic 14 minutes International 19 minutes
Airframe Maintenance[1][2]	Material = 0.333 (WAF/1000)/Block Time + 0.267 (WAF/1000) Labor = $0.07345\ (WAF/1000)^{0.7908}$/Block Time + $0.2048\ (WAF/1000)^{0.595}$ x Labor Rate

Fu = Utilization factor
Fw = Gross weight/speed factor
WAF = Airframe Weight (which is equal to operating weight (empty) minus engine weight)
(1) Costs in dollars per block hour
(2) Labor Rate (Direct) = 12.50/hr.

Figures 55 through 60 show current direct operating cost advantages for the flight propulsion system at the design and typical missions for the three fuel price levels. Direct operating cost generally follows the trends indicated for fuel burned, as shown in Figures 53 and 54. These figures provide an indication as to the importance fuel consumption has at the high fuel price levels. Comparing the current direct operating cost results to the original estimates amplifies this point further. The original evaluation was conducted in 1977 dollars at fuel prices of $.40/3.78 liters (1.0 U.S. gallon) for domestic airplanes and $.45/3.78 liters (1.0 U.S. gallon) for international airplanes. Expressed in 1980 dollars, these fuel prices would be in the $.55 to $.65/3.78 liters (1.0 U.S. gallon) range, significantly lower than the prices projected in 1980 dollars for the 1990 time period and used in the current evaluation. A comparison of direct operating cost reductions for domestic and international airplanes along with the overall airplane/mission average is shown in Table 51 for the original and current evaluations. The trend, as the design evolved, is shown in Figure 61. The program goal of 5 percent direct operating cost advantage relative to the JT9D-7A reference engine is seen to have been exceeded by a comfortable margin in all airplane-mission combinations with the flight propulsion system installed.

TABLE 51

AVERAGE DIRECT OPERATING COST COMPARISON
(References are JT9D-7A Engine in Same Study Airplane)

	Average Direct Operating Cost Reduction - Percent			
	Original Evaluation 1977 Dollars	Current Evaluation 1980 Dollars		
	$.40-$.45*	$1.00*	$1.50*	$2.50*
Domestic Airplanes				
Design Missions	7.9	9.0	10.5	12.3
Typical Missions	7.2	8.4	9.9	11.6
Combined Missions	7.6	8.7	10.2	12.0
International Airplanes				
Design Missions	10.4	12.1	13.6	15.3
Typical Missions	9.3	11.0	12.5	14.2
Combined Missions	9.8	11.6	13.1	14.7
Overall Airplanes/ Missions	8.5	9.8	11.3	13.0

*per 3.78 liters (1.0 U.S. gallon)

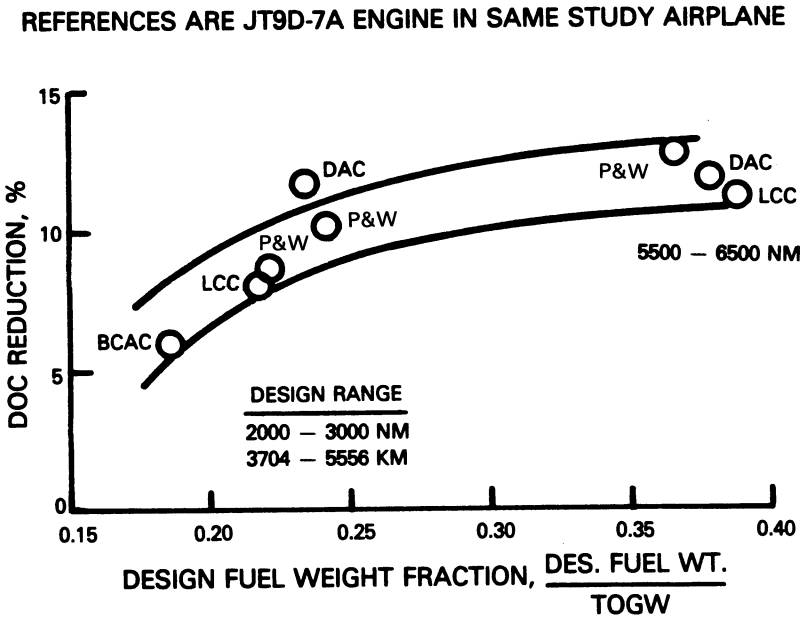

Figure 55 Current Flight Propulsion System Direct Operating Cost Advantage - Design Missions, $1.00/3.78 Liters (1.0 U.S. Gallon) Fuel Price

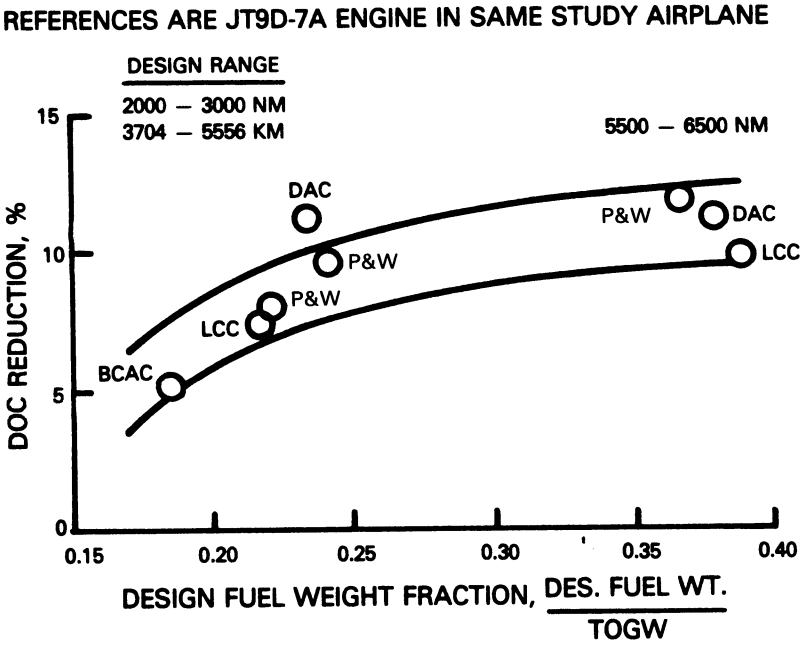

Figure 56 Current Flight Propulsion System Direct Operating Cost Advantage - Typical Missions, $1.00/3.78 Liters (1.0 U.S. Gallon) Fuel Price

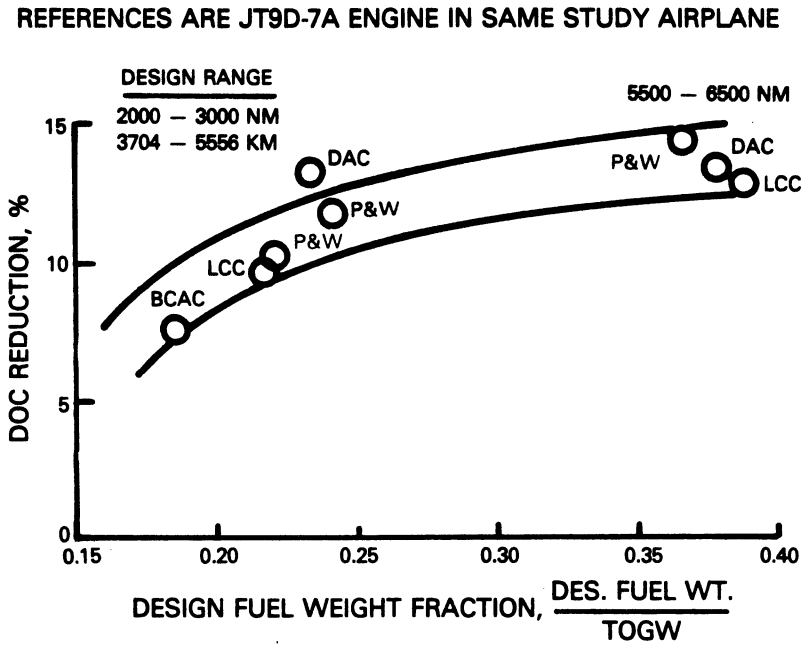

Figure 57 Current Flight Propulsion System Direct Operating Cost Advantage - Design Missions, $1.50/3.78 Liters (1.0 U.S. Gallon) Fuel Price

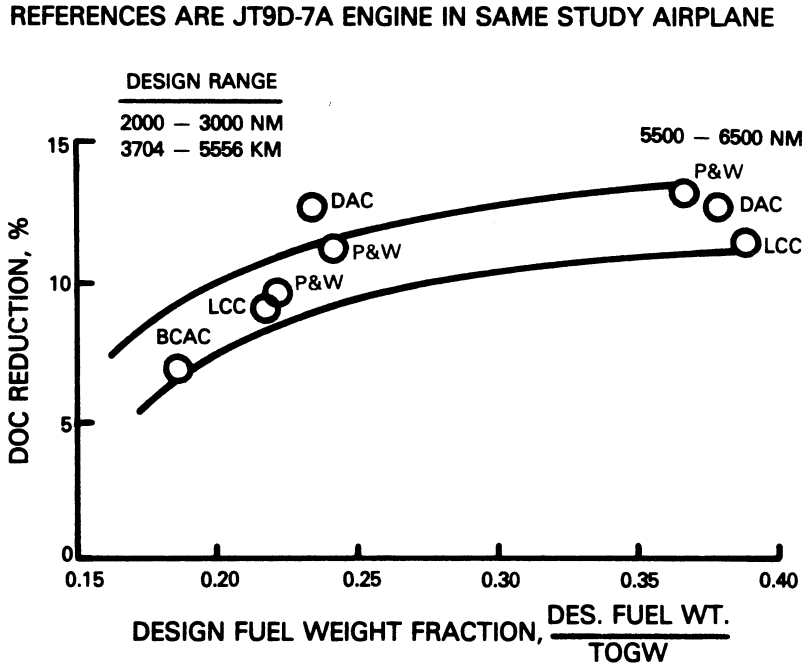

Figure 58 Current Flight Propulsion System Direct Operating Cost Advantage - Typical Missions, $1.50/3.78 Liters (1.0 U.S. Gallon) Fuel Price

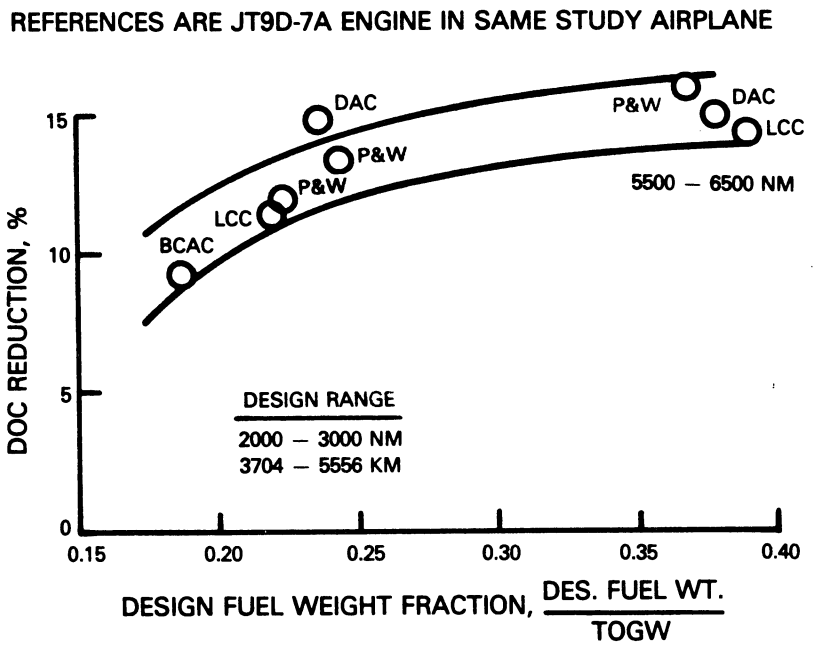

Figure 59 Current Flight Propulsion System Direct Operating Cost Advantage - Design Missions, $2.50/3.78 Liters (1.0 U.S. Gallon) Fuel Price

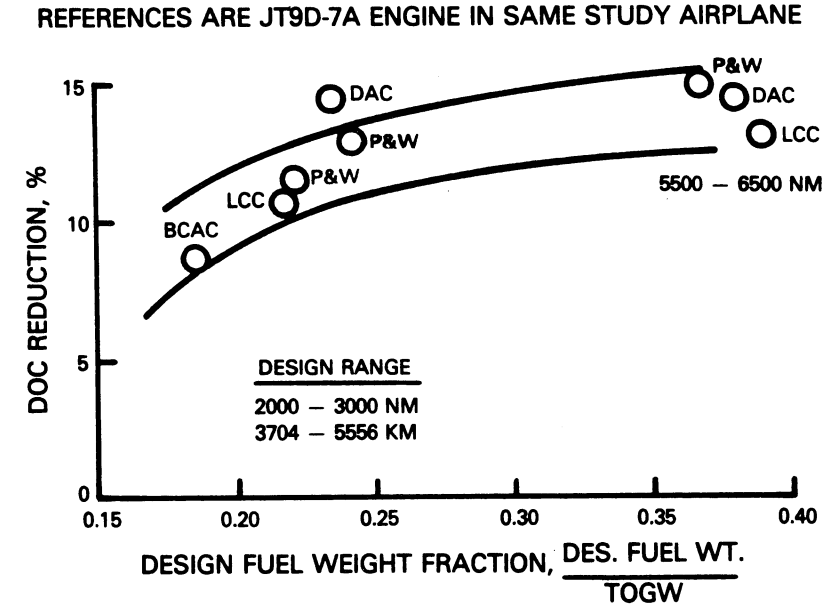

Figure 60 Current Flight Propulsion System Direct Operating Cost Advantage - Typical Missions, $2.50/3.78 Liters (1.0 U.S. Gallon) Fuel Price

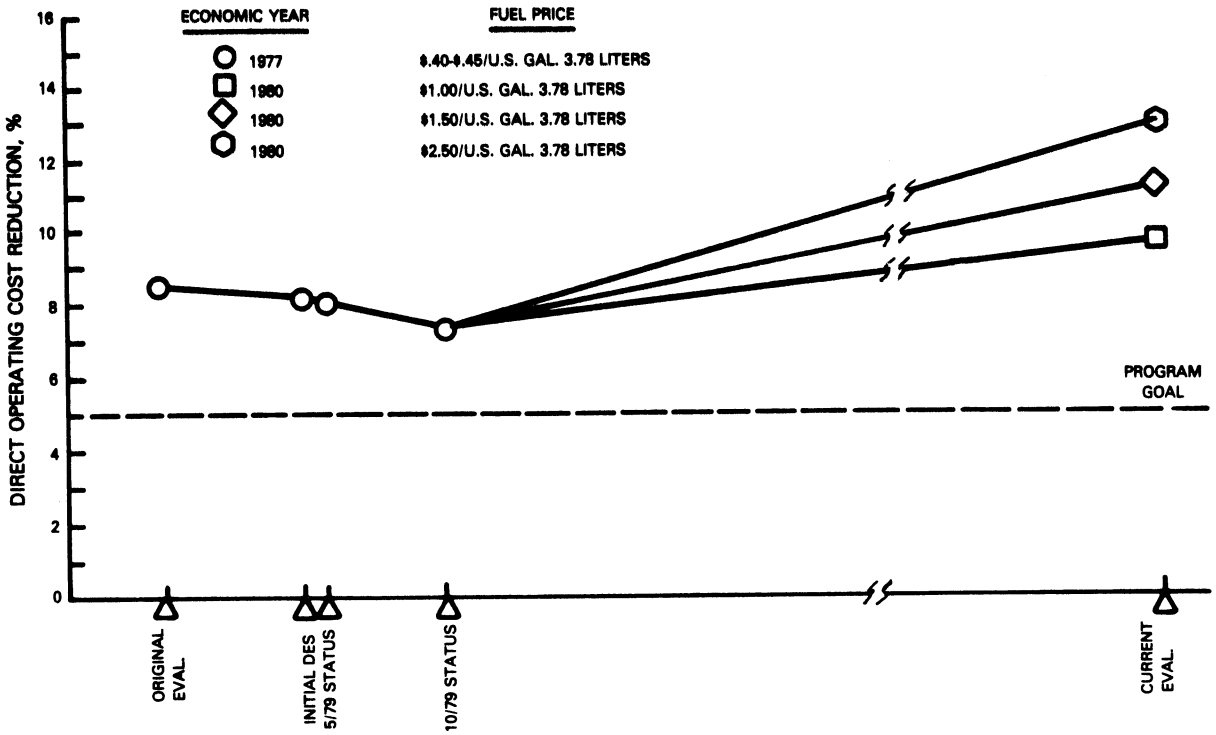

Figure 61 Flight Propulsion System Direct Operating Cost Evolution

4.14.4.3 Performance Deterioration

Initial estimates of performance deterioration were not specifically updated either during or following completion of the detailed component designs. However, performance retention was a primary requisite throughout the detailed design effort, as discussed in Section 4.13.3 of this report. Therefore, the Energy Efficient Engine program goal of 1.5 percent thrust specific fuel consumption deterioration in a 1000 flight cycle (50 percent less than JT9D-7A reference engine deterioration) should be accomplished.

4.14.4.4 Noise

The flight propulsion system noise was reassessed to evaluate the current engine configuration with its status performance using a revised noise prediction procedure. The airplane used was the Pratt & Whitney international quadjet, which was not changed in definition relative to the original evaluation. This reassessment was initiated because a review of the original evaluation indicated that the reference JT9D-7A engine-powered airplane had a relative altitude advantage over the flight propulsion system at the takeoff noise measuring station.

Reassessment results showed that noise was reduced at each of the measuring stations compared to the original evaluation. Table 52 compares the current evaluation results to those of the original, while Table 53 compares the new results to the Energy Efficient Engine program goal (Figure 62 compares to both).

TABLE 52

FLIGHT PROPULSION SYSTEM NOISE ESTIMATE COMPARISON
(P&W International Quadjet)

FAR Part 36 (1978) Condition	Original Goal EPNdB	Current Eval. EPNdB	Improvement EPNdB
Takeoff	102.9	100.9	2.0
Approach	103.9	103.8	0.1
Sideline	95.5	94.9	0.6

TABLE 53

CURRENT FLIGHT PROPULSION SYSTEM NOISE COMPARISON WITH PROGRAM GOAL
(P&W International Quadjet)

FAR Part 36 (1978) Condition	Program Goal EPNdB	Current Eval. EPNdB	Margin EPNdB
Takeoff	105.1	100.9	-4.2
Approach	105.0	103.8	-1.2
Sideline	102.3	94.9	-7.4

These noise improvements resulted from the combination of updated flight propulsion system and airplane performance, and the updated noise prediction system. Of the 2.0 improvement in engine perceived noise decibels (EPNdB) at takeoff, 1.1 EPNdB was caused by an optimization of the quadjet performance. A 45 meter (150 foot) altitude increase over the noise station resulted from higher rated takeoff thrust associated with general component performance improvements compared to the initial evaluation. The remainder of the takeoff improvement, 0.9 EPNdB, resulted from the new noise prediction procedure and a 1.6 percent reduction in exhaust nozzle velocity relative to the original flight propulsion system definition. Hardwall noise at approach was lower because of a combination of factors. However, when the current acoustic treatment data were applied at approach, inlet attenuation was less than predicted in the original evaluation. Consequently, only a minor net improvement in approach noise level was realized.

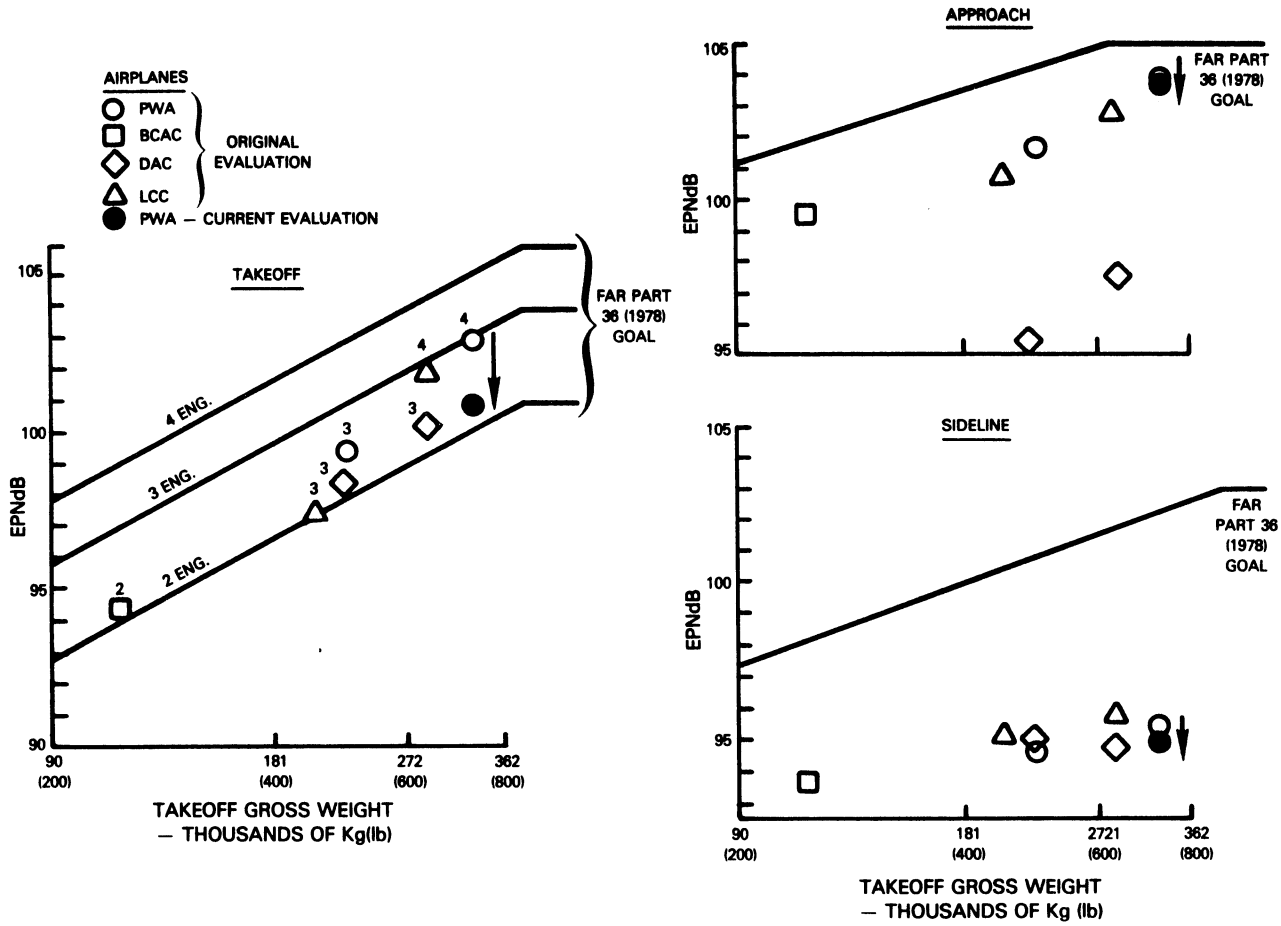

Figure 62 Comparison of Flight Propulsion System Noise Estimates With Program Goals

The incorporation of the shrouded fan blade in place of the shroudless configuration resulted in the current noise evaluation update accounting for 36 fan blades; whereas, the original evaluation was done for the 27 blade configuration that existed at that stage of the initial design effort. The fan tone noise source most likely affected by this increase in blade number is the blade wake-exit vane interaction. The current 36 blade fan would be expected to produce a greater number of propagating modes. This increased potential for interaction is not, however, expected to be a major source of blade passing noise because of the large axial separation between the blades and vanes. The dominant noise source is still projected to be the interaction between the blades and the pylon, which should not be affected by the blade count. A resulting blade passing frequency change was also projected to have a minimal impact on the effective perceived decibel noise level of the flight propulsion system.

The data base formed in a current noise assessment for the integrated core/low spool was used to define updated acoustic treatment requirements. Although these requirements were determined for the integrated core/low spool, the results are considered applicable to the flight propulsion system because of its close similarity. Definitions were obtained by scaling from an extensive array of treatment test results to account for differences in airfoil numbers, speeds, and geometries. The treatment locations considered are shown in Figure 63.

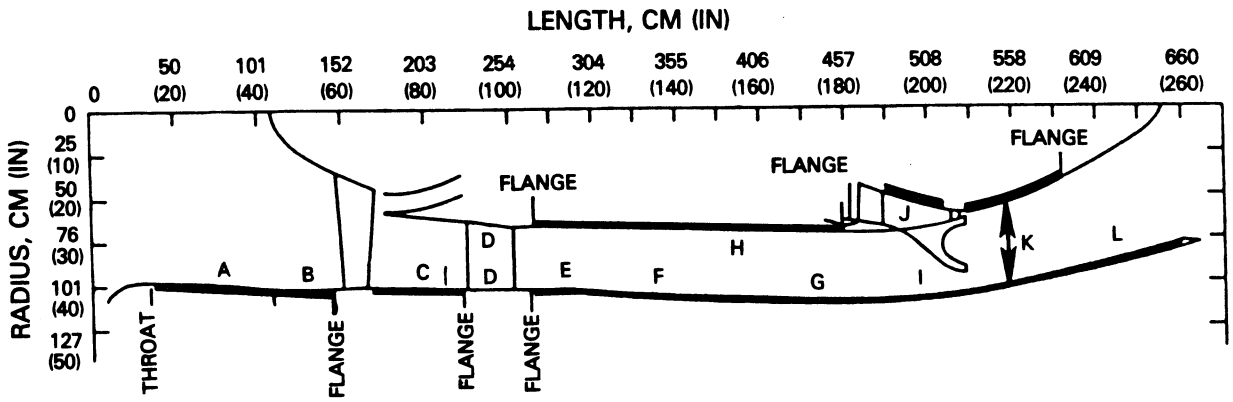

Figure 63 Flight Propulsion System Acoustic Treatment Locations

A brief investigation was conducted to determine the implications of eliminating some sections of the acoustic treatment. Included in this consideration was the treatment on the fan duct walls of the compressor intermediate case (location D), pylon strut and lower bifurcation walls (portion of location H), tailplug (J and portion of K), and tailpipe (I, portion of K, and L). The only relatively insignificant contribution to noise reduction was deemed to be that of the compressor intermediate case duct endwalls. Because its cost was estimated to be 10 percent of the total case cost, the treatment was deleted in this location.

Acoustic treatment definitions resulting from the update analysis are summarized in Table 54. Several changes in treatment requirement occurred relative to the initial design definition. These differences are compared in Table 55. Changes in inlet, fan case, and fan duct treatment thicknesses were caused by revisions in the number of fan blades (27 to 36), a slight reduction in low pressure rotor speed, a 6.2 percent dimensional downsizing, and a refinement in treatment capabilities based on recent test experience. Design changes made during the detailed design effort did not impact acoustic treatment requirements in the remaining portions of the nacelle.

TABLE 54

CURRENT NACELLE ACOUSTICS TREATMENT DEFINITION SUMMARY

General* Location	Construction	Honeycomb Cell-Size (cm)	Honeycomb Depth (cm)	Face Sheet Flow Resistance or Skin Porosity	Face Sheet Hole Diameter (cm)	Face Sheet Thickness (cm)	Effective Treated Area sq.m. (sq.ft.)
A & B	DynaRohr(1)	.952	2.54	82 Rayls	-	-	7.27 (78.2)
C	DynaRohr(1)	.952	2.22	60 Rayls	-	-	3.82 (41.1)
E	DynaRohr(1)	.952	2.22	60 Rayls	-	-	
F	DynaRohr(1)	.952	2.22	60 Rayls	-	-	14.38 (154.6)
G	DynaRohr(1)	.952	2.22	60 Rayls	-	-	
H	DynaRohr(1)	.952	2.22	60 Rayls	-	-	10.37(111.5)(2)
I	PP/Bonded HC**	.952	1.52	8 Percent	0.127	0.063/0.081	2.80 (30.1)
J	PP/Brazed HC**	.952	1.39	13 Percent	0.203	0.063	1.21 (13.0)
K	PP/Brazed HC**	.952	1.11	8 Percent	0.203	0.063	5.77 (62.0)(3)
L	PP/Brazed HC**	.952	2.15	11 Percent	0.238	0.063	3.97 (42.7)

NOTES: (1) All DynaRohr designs have the following parameters:
- o Thickness of perforated plate = 0.063-0.076 cm
- o Hole diameter of perforated plate = 0.127 cm
- o Open area of perforated plate = 34 percent

(2) Includes 2.95 sq. m. in upper and lower bifurcations

(3) Includes 2.01 sq. m. in the I.D. wall and 3.76 sq. m. in the O.D. wall

* - Refer to Figure 63
** - PP = Perforated Plate, HC = Honeycomb

TABLE 55

ACOUSTIC TREATMENT DEFINITION COMPARISON

General Location*	Treatment Depth - cm (in) Initial Design	Current Design
Inlet (A/B)	3.38/5.08 (1.33/2.00)	2.54/2.54 (1.00/1.00)
Fan Case (C)	2.28 (.90)	2.22 (.875)
Fan Duct (E+F+G+H)	2.66 (1.05)	2.22 (.875)
Tailpipe (I/K/L)	1.53/1.12/2.15 (.60/.44/.85)	1.53/1.12/2.15 (.60/.44/.85)
Tailplug (J/K)	1.40/1.12 (.55/.44)	1.40/1.12 (.55/.44)

*Refer to Figure 63

4.14.4.5 Emissions

Flight propulsion system emissions levels were reassessed to evaluate the effects of the currently projected combustor design configuration. This reassessment was based on the results accumulated from multiple builds of the 90 degree sector rig tested under the Energy Efficient Engine Sector Combustor Rig supporting technology program (Reference 16). Results from the testing of the full annular combustor component in the program were included as confirmation of the projected trends.

A comparison of currently projected flight propulsion system emissions and program goal levels is presented in Table 56. Also included in this comparison are emissions levels estimated for the original propulsion system/aircraft integration evaluation and the initial design. Emissions shown include allowances for engine-to-engine variability, deterioration, and development margins.

The comparison shows that, except for smoke number, the current estimates are in reasonably close agreement with previous estimates for flight propulsion system exhaust emissions. Smoke was essentially eliminated with the advanced main zone fuel injection system design. Hydrocarbon and carbon monoxide emissions are projected to be 20 percent and 40 percent, respectively, better than the program goals. The nitrogen oxides estimate misses the goal by over 40 percent but remains substantially below current production engine levels.

TABLE 56

FLIGHT PROPULSION SYSTEM EXHAUST EMISSIONS COMPARISON

	1981 EPA Goal	Original Evaluation	Initial Design	Current Design
Total Hydrocarbons (THC) - EPAP*	0.40	0.20	0.20	0.2
Carbon Monoxide (CO) - EPAP*	3.0	2.0	1.7	1.8
Nitrogen Oxides (NOx) - EPAP*	3.0	4.3	4.6	4.3
Smoke Number	20	20	20	4

*EPAP = Environmental Protection Agency Parameter in kg. of pollutant/ 4,448 N (1000 lb) thrust/hr./flight cycle

4.14.4.6 Design Goal Summary

The definition of the flight propulsion system has been periodically updated as specific program technical objectives have been met. These updates of system characteristics were discussed in the preceding paragraphs in this section of the report where they were compared against the scaled JT9D-7A reference engine and the Energy Efficient Engine program goals. A summary of these comparisons is presented in Table 57. Results from the propulsion system/aircraft integration evaluations are also included. Economic years, fuel prices, and flight propulsion system sizes are indicated for each design update and represent the basis from which each specific analysis was done.

The comparison clearly shows that Energy Efficient Engine program goals have been met throughout the preliminary design effort, with the exception of emissions of nitrogen oxides. Early weight and manufacturing cost advantages relative to the JT9D-7A have disappeared, and the current flight propulsion system is heavier and more costly than the reference. The early maintenance cost advantage for the flight propulsion system has continued throughout.

TABLE 57

SUMMARY OF FPS PRELIMINARY DESIGN EVALUATIONS

	Program Goal	Original Evaluation 10/78	Initial Design 4/79	Status 5/79	Status 10/79	Status 3/80	Status 6/81	Current Des./ Eval 4-82
TSFC Reduction* - %	12.0	14.9	14.9	14.9	14.7	15.1	15.0	15.0
DOC Reduction** - %								
Domestic Average	5.0	7.6	7.2	7.1	6.5	***	***	10.2
International Average	5.0	9.8	9.4	9.3	8.7	***	***	13.1
Noise - EPNdB	FAR 36 (1978)	FAR 36(1978) -2 to -4	***	***	***	FAR 36(1978) -3 to -5	***	FAR 36(1978) -3 to -5
Emissions - EPAP								
Total Hydrocarbons	0.4	0.2	0.2	0.2	0.2	***	***	0.32
Carbon Monoxide	3.0	2.0	1.7	1.7	1.7	***	***	1.8
Nitrogen Oxides	3.0	4.3	4.6	4.6	4.6	***	***	4.3
TSFC Deterioration* -%	50	***	50	***	***	***	***	***
Engine Weight Reduction* -%	-	7.6	2.5	1.3	-3.9	***	***	-1.9
Engine Cost Reduction* -%	-	4.7	1.0	1.4	-1.6	***	***	-4.7
Engine Maintenance Cost Reduction* - %	-	4.6	4.2	4.7	2.4	***	***	4.6
Remarks:	****	Full Size, ****	Full Size, ****	88% Size, ****	88% Size, ****	88% Size, ****	88% Size, ****	88% Size, 1980$, 1.50/ 3.78 Liters (1.0 gallon)

* Relative to JT9D-7A reference engine scaled to FPS airflow size
** Relative to JT9D-7A engine installed in same airplane
*** Not estimated
**** 1977$, $.40-.$45/3.78 Liters (1.0 U.S. gallon)

4.15 CONCLUDING REMARKS

Completion of the final analysis and design update of the flight propulsion system concludes a major effort under the Energy Efficient Engine program. Design updating conducted in conjunction with detailed analysis and design of the integrated core/low spool, component testing, and supporting technology portions of the Energy Efficient Engine program verified the feasibility of the flight propulsion system preliminary design. Listed below are some of the more salient results evolving from the completed evaluation which indicate that the flight propulsion system, as designed, is capable of meeting all design goals except for the oxides of nitrogen emissions standard.

- A 15.0 percent thrust specific fuel consumption relative to that of the JT9D-7A reference engine is currently estimated, which surpasses the program goal of 12 percent for newly installed engines. In addition, a reconfiguration of the flight propulsion system based on trades reflecting the substantial increase in fuel prices since the initiation of the Energy Efficient Engine program resulted in a configuration with a thrust specific fuel consumption reduction of 20 percent relative to the JT9D-7A reference engine (see Section 5.0). Continuing analysis confirmed that performance deterioration can be reduced by 50 percent or more compared to the JT9D-7A.

- An average direct operating cost reduction of 11.3 percent for a $1.50/3.78 liters (1.0 U.S. gallon) fuel price in terms of 1980, relative to the JT9D-7A, is currently projected. This reduction far exceeds the program goal of 5 percent.

- Predicted noise levels for the flight propulsion system installed in the study airplanes are currently estimated to meet FAR Part 36 (1978), the program goal, by margins of up to 3 to 5 EPNdB, sufficient to provide a high probability of compliance with the rule.

- Exhaust emissions of carbon monoxide, total hydrocarbons, and smoke are currently projected to surpass the program goals, which are EPA proposed 1981 regulations. Analysis continues to indicate, however, that nitrogen oxides emissions do not meet the program goal; but they are substantially lower than current production engine levels.

- Weight and manufacturing cost have increased as the preliminary design of the flight propulsion system has evolved. Substantial improvements in materials and structures technologies are required in conjunction with intensive control during detailed analysis and design efforts to achieve a production engine design without these penalties.

Overall, the advanced technology contained in the flight propulsion system will have wide application in future generation gas turbine engines, as well as advanced derivatives of current commercial engines. In addition, a major portion of the technology developed under the current Energy Efficient Engine program is being incorporated into the maximum efficiency engine discussed in the following section of the report.

SECTION 5.0
MAXIMUM EFFICIENCY ENERGY EFFICIENT ENGINE DESIGN UPDATE

5.1 INTRODUCTION

This section of the report provides a general description of an advanced technology baseline reference engine, known as the Maximum Efficiency Energy Efficient Engine (ME^4), by presenting information describing the systems's overall cycle definition, component design status and a brief description of potential benefits as compared to the Energy Efficient Engine flight propulsion system. This baseline engine was defined in conjuction with an ongoing benefit/cost study being conducted under Task I, of more advanced fuel saving technology than that being developed in the current Energy Efficient Engine program. This baseline engine represents a reoptimization of the Energy Efficient Engine developed technology and not an extention of the technology base. It was found necessary to reoptimize the Energy Efficient Engine flight propulsion system in order to establish a baseline engine for the benefit/cost studies which would more properly present the benefits for the advanced technologies being conducted in the benefit/cost study.

5.2 ENGINE DESCRIPTION

5.2.1 General Description

With the dominant influence of fuel costs affecting current airline operating economics, the baseline ME^4 reference engine includes a high bypass ratio cycle and features high-efficiency components designed to substantially improve fuel economy and direct operating costs. Performance improvement changes for the baseline reference engine, as compared to the flight propulsion system, include a higher bypass ratio single-stage fan with a larger diameter (7.6 cm (3.0 in)), a four-stage low-pressure compressor, a ten-stage high-pressure compressor with reduced axial gapping, a simpler one-stage combustor to meet proposed or projected emissions requirements, and two additional turbine stages for a substantial improvement in component efficiencies (see Figure 64). The engine installed in a mixed exhaust nacelle system is shown in Figure 65. Mounting for the engine is the same as for the flight propulsion system with front thrust links situated at the engine centerline horizontally and the rear mount system located at the front of the low-pressure turbine. Flight loads are shared between the engine and nacelle structure. This advanced propulsion system is aimed at providing excellent fuel efficiency and operating economics while meeting EPA-imposed environmental regulations. It is estimated that this engine will provide an improvement of five percent in cruise thrust specific fuel consumption (TSFC) relative to the flight propulsion system.

MAXIMUM PERFORMANCE ENGINE HAS:
(1) 3-INCH LARGER FAN
(2) 3-INCH SHORTER COMPRESSOR
(3) SINGLE STAGE COMBUSTOR
(4) 2-STAGE HIGH-PRESSURE TURBINE
(5) 5-STAGE LOW-PRESSURE TURBINE

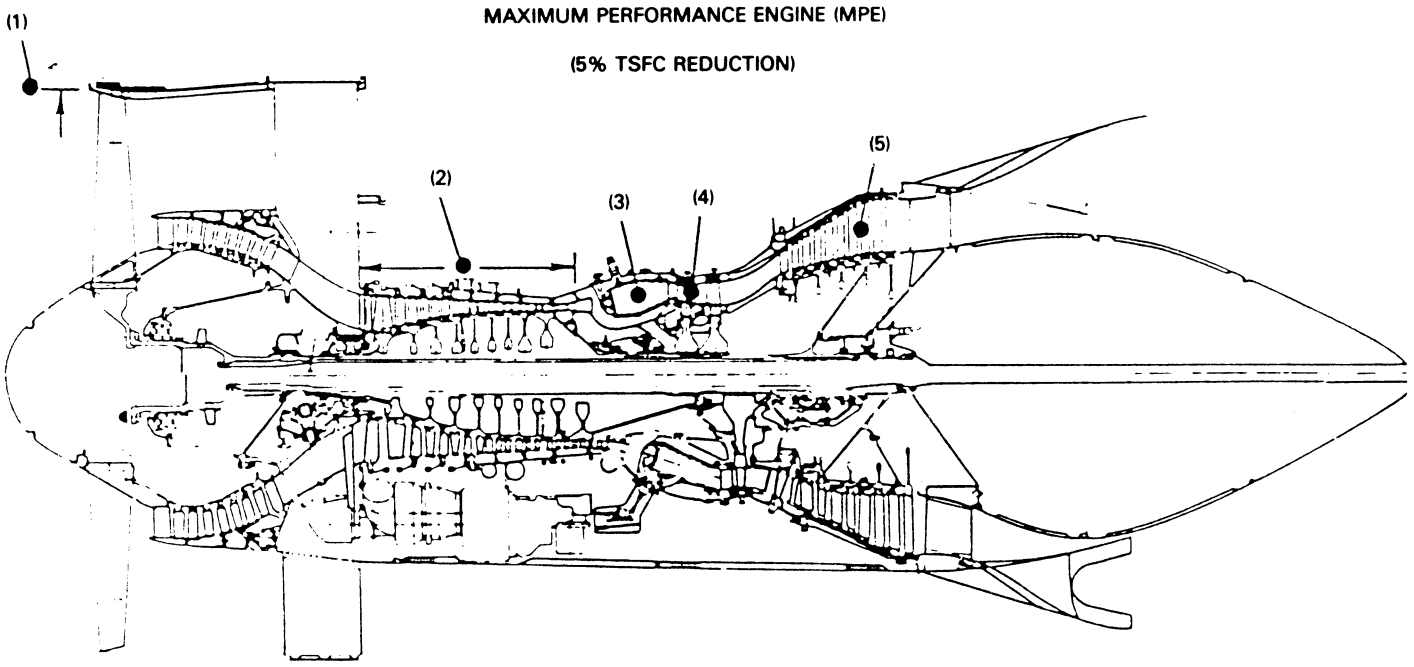

Figure 64 Maximum Efficiency Energy Efficient Engine Changes Compared To The Flight Propulsion System

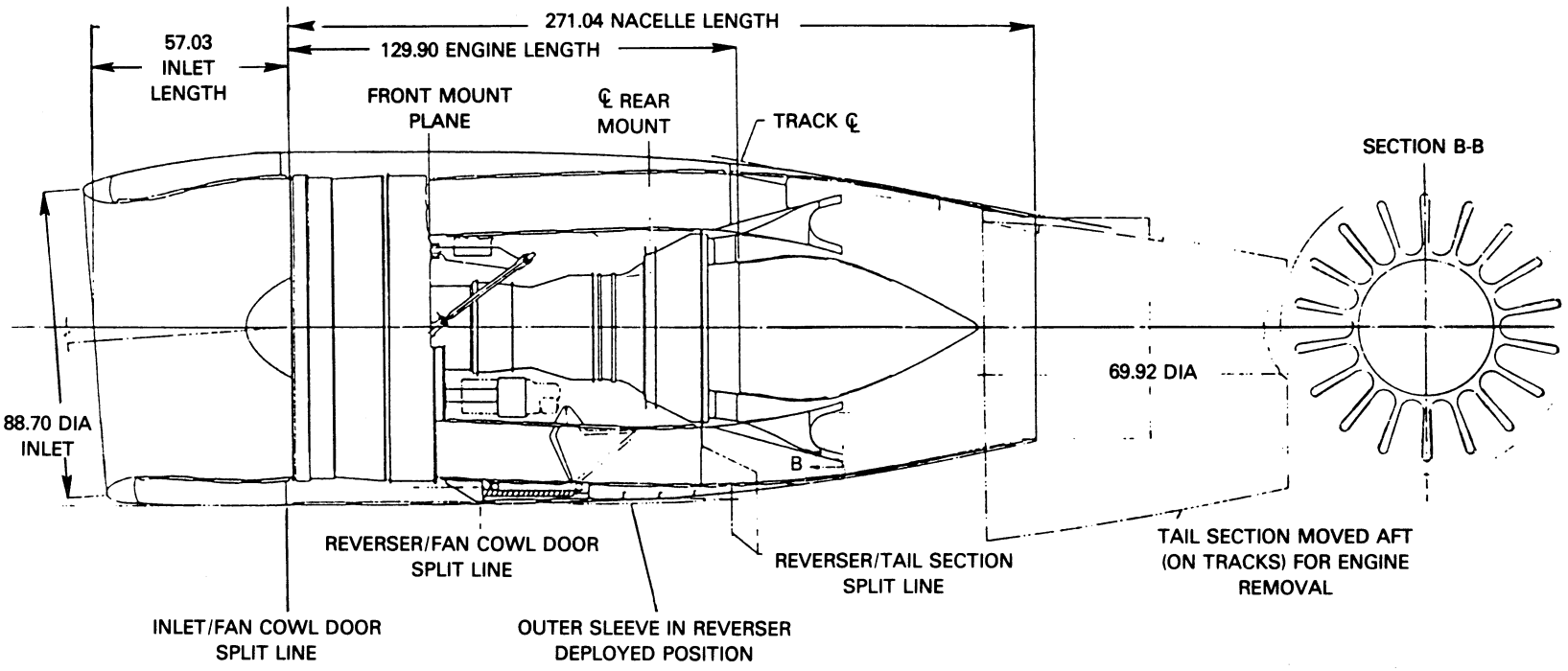

Figure 65 Maximum Efficiency Energy Efficient Engine In Advanced Nacelle System (dimensions are in inches)

5.2.2 Overall Cycle

Engine overall pressure ratio and turbine inlet temperature levels of the flight propulsion system were held fixed to be consistent with Energy Efficient Engine materials and cooling technology. However, bypass ratio was re-examined due to higher 1981 fuel prices compared to the 1977 prices used when the flight propulsion system was configured. Fuel prices ranged from 40-45 cents per 3.78 liters (1.0 U.S. gallon) in 1977, while a more representative level of $1.50/3.78 liters was used in the 1981 study.

Results of both the 1977 and 1981 study are summarized in Figure 66. This summarization is in terms of fuel efficiency and direct operating cost trends as functions of bypass ratio for an advanced 5,556 km (3000 nm) domestic trijet and a 10,186 km (5500 nm) intercontinental quadjet. Fuel burned trends, independent of cost, reflect only the propulsion system performance and weight as the bypass ratio was varied. Therefore, the results are the same for both studies. Study results indicate a bypass ratio of 7.5 would minimize fuel burned. The study results for direct operating cost (DOC) changed dramatically. In the 1977 study, fuel costs accounted for approximately one-third of the direct operating cost with the remaining two-thirds consisting of crew, depreciation, insurance, and maintenance costs. With the $1.50/3.78 liters (1.0 U.S. gallon) fuel price, fuel costs became increasingly important, accounting for over 50 percent of the direct operating costs. The bypass ratio needed to minimize direct operating costs shifted from 6 to 7. This permitted a selection of the bypass ratio to be made without significantly trading fuel efficiency and direct operating cost while compromise was necessary in the 1977 study.

The overall cycles selected in the two studies are summarized in Table 58. As mentioned previously, the overall pressure ratio and combustor exit temperature were held constant to be consistent with Energy Efficient Engine materials and cooling technology. The only difference is a 10 percent higher bypass ratio selected in the 1981 study.

TABLE 58

CYCLE DEFINITION (1977 AND 1981 STUDIES)
(Aerodynamic Design Point: 10675 m (35,000 ft), 0.8 Mn, Maximum Cruise)

	Flight Propulsion System (1977)	Maximum Efficiency Energy Efficient Engine (1981)
Bypass Ratio	6.5	7.2
Overall Pressure Ratio	38.6	38.6
Combustor Exit Temperature (°C)	1268	1268

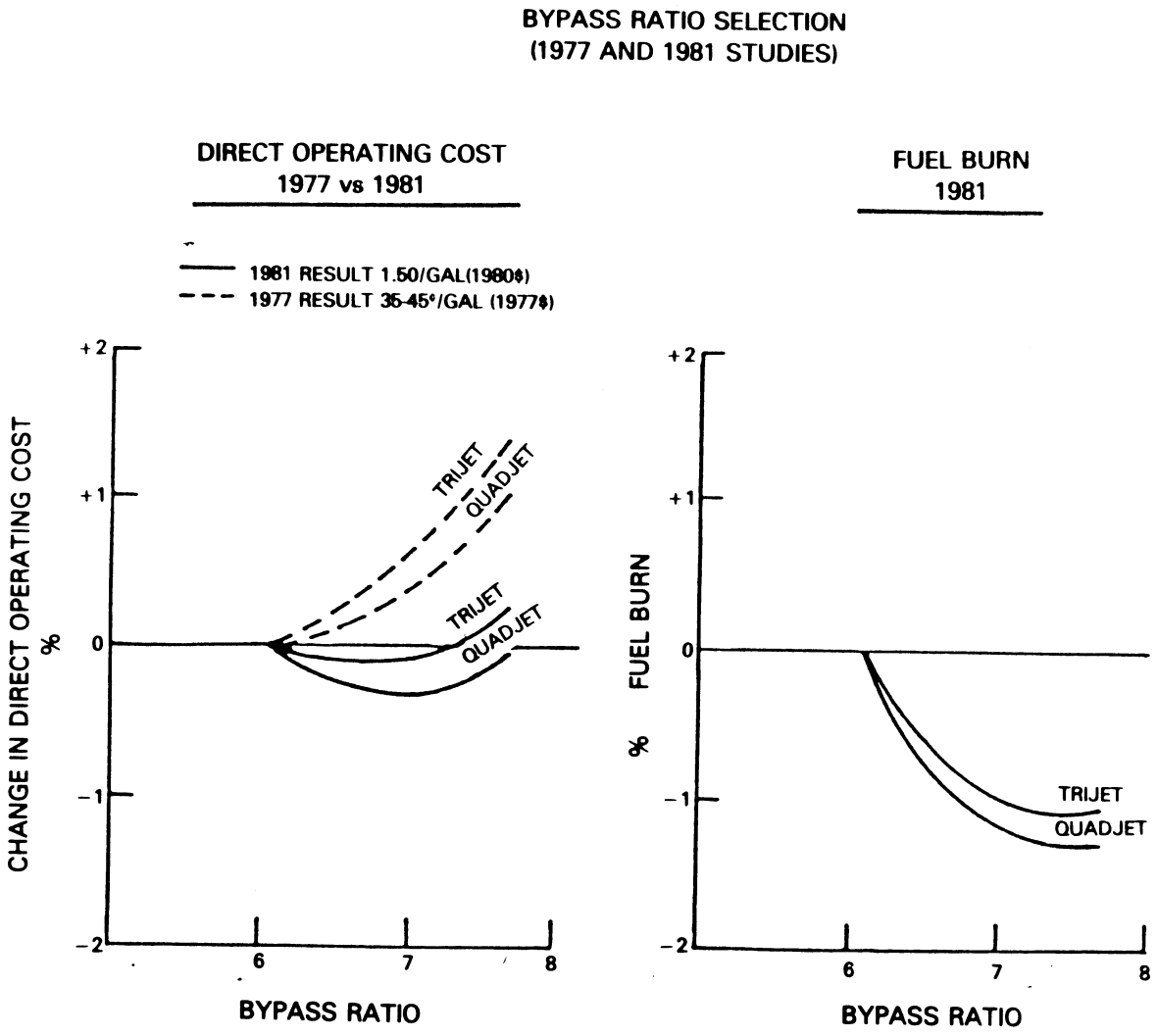

Figure 66 Bypass Ratio Selection For The 1977 and 1981 Studies

5.3 ENGINE COMPONENT AERODYNAMIC DESIGN UPDATE

Engine components were modified relative to the flight propulsion system to accommodate the higher bypass ratio cycle. Individual components were reviewed and updated based on information obtained from the Energy Efficient Engine program, as well as other independent studies at Pratt & Whitney. The following paragraphs present specific information detailing the variations defined for the individual components.

5.3.1 Fan/Low-Pressure Compressor

The higher bypass ratio fan was configured at a lower pressure ratio and lower tip speed design compared to the flight propulsion system. A comparison of flight propulsion system and ME[4] aerodynamic design parameters is shown in Table 59.

TABLE 59

FAN AERODYNAMIC COMPARISON
(Aerodynamic Design Point: 10675 m (35,000 ft), 0.8 Mn, Standard Day)

	Flight Propulsion System	Maximum Efficiency Engine
Corrected Tip Speed - m/sec (ft/sec)	455 (1496)	441 (1450)
Corrected Airflow - kg/sec (lb/sec)	622 (1373)	679 (1498)
Pressure Ratio (Duct Section)	1.74	1.65
(Core Section)	1.56	1.50
Bypass Ratio	6.51	7.20
Tip-to-Tip Diameter - cm (in)	206.7 (81.3)	215 (85)
Specific Flow (kg(lb)/sec/m^2	19.5 (43.0)	19.5 (43.0)
Inlet Hub/Tip Ratio	0.340	0.340
Aspect Ratio (Blade)	4.00	4.00
Duct Exit Guide Vane Area Ratio	1.075	1.095
Efficiency (duct section)	Base	+0.6
(core section)	Base	-0.5
Surge Margin (%)	Base	+3.0

The duct exit guide vane (DEGV) area ratio, i.e., the inlet area divided by the exit area, is increased by two percent on the higher bypass ratio fan to reduce the inlet Mach number and the aerodynamic loadings on the vanes. This approach results in a lower pressure loss through the row. This countered the adverse influence of reducing the pressure ratio on fan efficiency resulting in an equal fan outer diameter efficiency level.

Fan inner diameter pressure ratio was set by holding the root work coefficient of the flight propulsion system. Since the fan is slowed relative to the flight propulsion system fan, the inner diameter pressure ratio is lower resulting in the requirement for a higher low compressor pressure ratio.

The higher pressure ratio in the low-pressure compressor required the axial exit Mach number to be raised in conjunction with exit elevation in order to hold the same surge margin as the flight propulsion system. Table 60 shows the effect of this modification on efficiency; higher Mach number caused an increase in compressibility losses resulting in a 0.80 percent efficiency debit.

TABLE 60

LOW-PRESSURE COMPRESSOR AERODYNAMIC COMPARISON
(Aerodynamic Design Point: 10675 m (35,000 ft), 0.8 Mn, Standard Day)

	Flight Propulsion System	Maximum Efficiency Engine
Pressure Ratio (Sta. 3/2.5)	1.77	1.84
No. of stages	4	4
Average Aspect Ratio	2.24	2.30
Average Gap/Chord Ratio	0.84	0.930
Average Axial Velocity-to-Wheel Speed	0.720	0.860
Inlet Specific Flow - kg(lb)/sec/m^2	16.1 (35.6)	16.3 (36.0)
Axial Exit Mach No.	0.370	0.430
Exit Swirl Angle	0	0
Average Diffusion Factor (D-factor)	0.370	0.370
Average Wall Static Pressure Distribution	0.320	0.290
No. of Airfoils	820	764
Efficiency (%)	Base	-0.8
Surge Margin (%)	Base	Base

The resultant fan and low-pressure compressor flowpath resulting from these aerodynamic choices is shown in Figure 67.

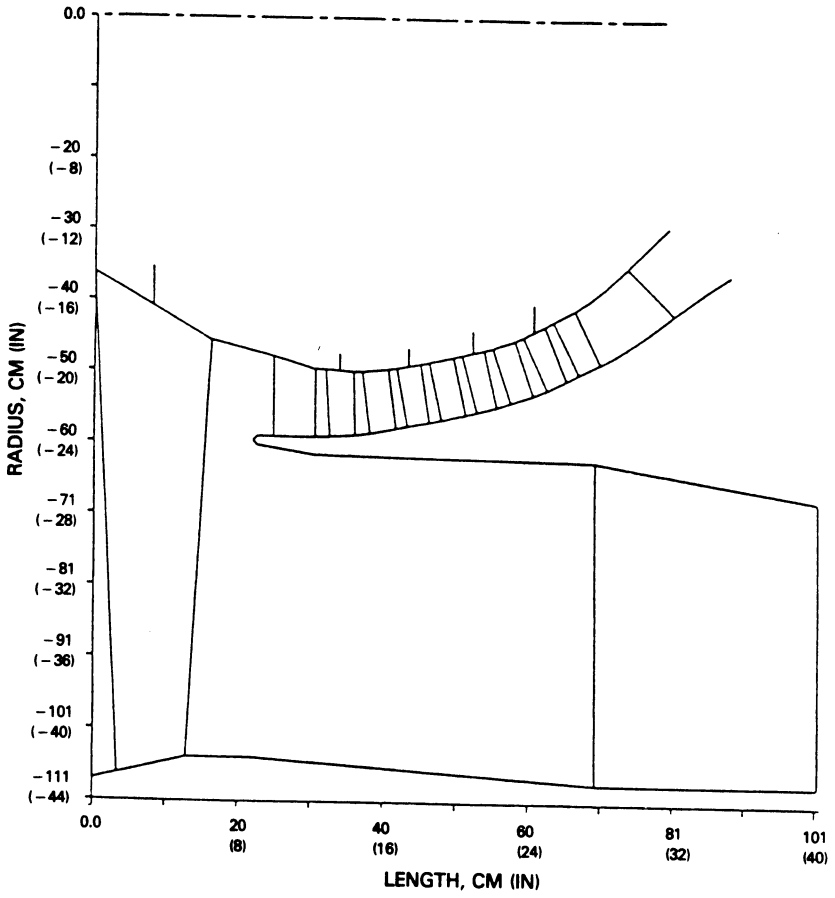

Figure 67 Fan/Low-Pressure Compressor Flowpath

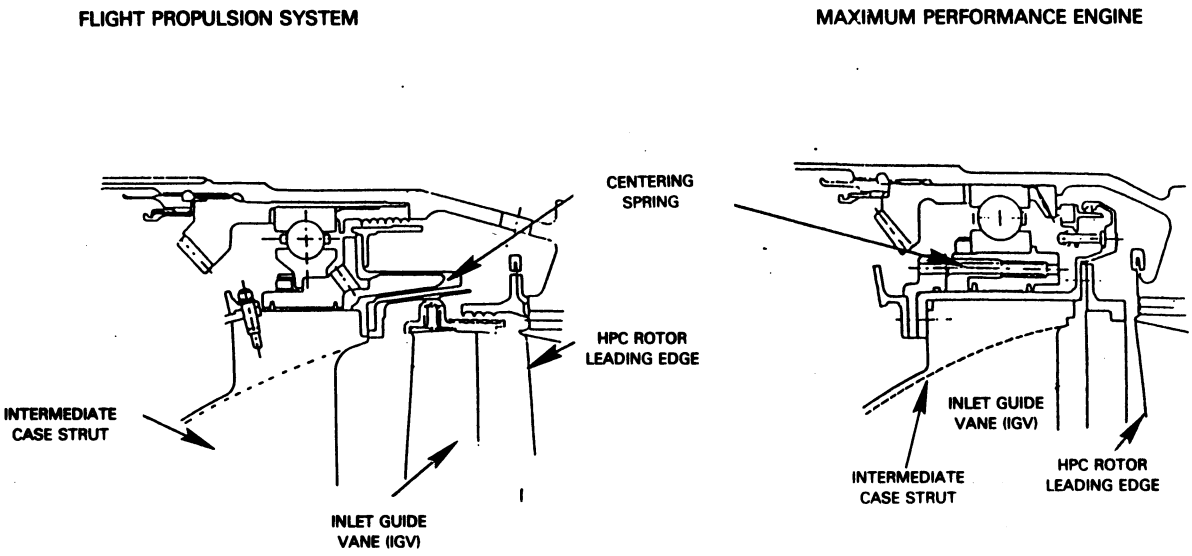

Figure 68 Centerline Spring Rearranged to Shorten Intermediate Case

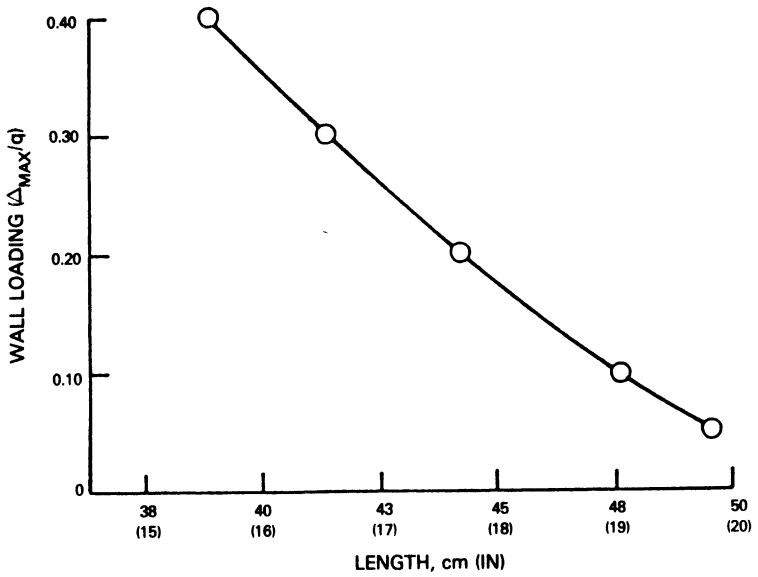

Figure 69 Compressor Intermediate Case Loading Versus Length Trade

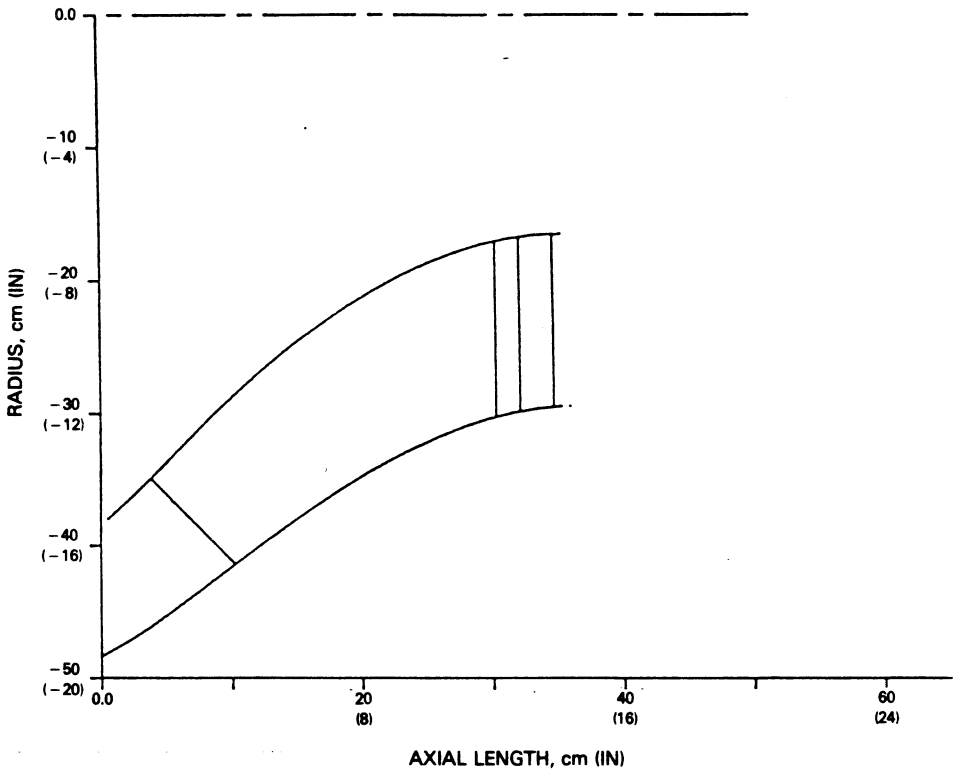

Figure 70 Compressor Intermediate Case Flowpath

5.3.2 Compressor Intermediate Case

The intermediate case length of the flight propulsion system was set by structural consideration (inlet guide vane chord, strut chord, axial gapping, etc.) resulting in an aerodynamically unloaded design. However, in the maximum efficiency engine, the bearing compartment was redesigned by placing the centering spring directly under the bearing. This resulted in an inlet guide vane chord reduction and tighter gapping between the strut and high-pressure compressor rotor leading edge, as shown in Figure 68.

In order to take advantage of this length reduction, the intermediate case aerodynamic loading parameter was increased to 0.40. Table 61 summarizes the aerodynamic comparison between the flight propulsion system and the maximum efficiency engine compressor intermediate cases.

TABLE 61

COMPRESSOR INTERMEDIATE CASE AERODYNAMIC COMPARISON

	Flight Propulsion System	Maximum Efficiency Engine
Loading Parameter	0.05	0.40
Length - cm (in)	42.67 (16.80)	39.49 (15.55)
Strut Axial Chord - cm (in)	25.90 (10.20)	27.43 (10.80)
HPC IGV Axial Chord - cm (in)	4.06 (1.60)	2.54 (1.00)
Inner Diameter Radial Offset - cm (in)	21.33 (8.40)	24.89 (9.80)

Figure 69 correlates wall loading with length. If the loading level was kept equal to that of the flight propulsion system, the length would have been increased by 10.9 cm (4.3 in). The flowpath for the final selected configuration is shown in Figure 70.

5.3.3 High-Pressure Compressor

The high-pressure compressor remains aerodynamically unchanged from the flight propulsion system. A length reduction of 7.3 cm (2.9 in) was achieved as follows:

Removal of flowguides - cm (in)	-1.77 (-0.70)
Incorporation of shorter bleed ports - cm (in)	-0.50 (-0.20)
Elimination of variable vane provisions in stages 9-15 (experimental requirement)-cm(in)	-1.52 (-0.60)
Elimination of excessive gaps - cm (in)	-3.55 (-1.40)
Total Reduction	-7.36 (-2.90)

The flight propulsion system and maximum efficiency energy efficient engine high-pressure compressor aerodynamics are compared in Table 62. The flowpath of the shortened high-pressure compressor is shown in Figure 71.

TABLE 62

HIGH-PRESSURE COMPRESSOR AERODYNAMIC COMPARISON
(Aerodynamic Design Point: 10675 m (35,000 ft), 0.8 Mn, Standard Day)

	Flight Propulsion System	Maximum Efficiency Engine
Pressure Ratio (Sta. 3/2.5)	14.0	14.0
Corrected Flow (kg/sec)	35.2	35.2
Corrected Tip Speed (m(ft)/sec)	379 (1245)	379 (1245)
No. of stages	10	10
Inlet Hub/Tip Ratio	0.56	0.56
Exit Hub/Tip Ratio	0.924	0.923
Average Aspect Ratio	1.52	1.52
Average Gap/Chord Ratio	0.890	0.890
Axial Velocity-to-Wheel Speed (Cx/U)	0.56	0.56
Exit Mach No.	0.28	0.29
Reaction (%)	0.50	0.50
Average Diffusion Factor (D-factor)	0.46	0.46
Average Wall Static Pressure Distribution	0.41	0.41
Length - cm (in)	Base	-7.3 (-2.9)
Efficiency (%)	Base	0

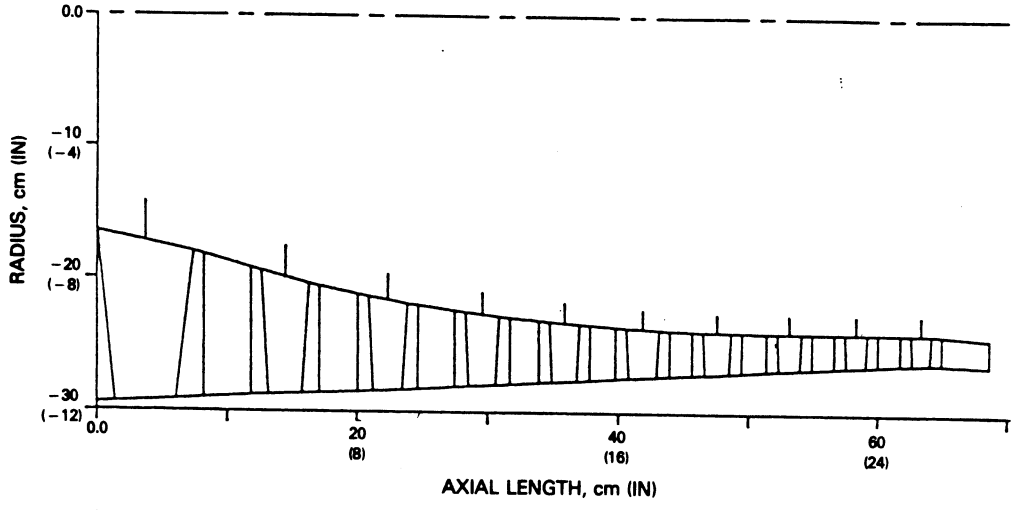

Figure 71 High-Pressure Compressor Flowpath

TABLE 63

EMISSIONS SUMMARY FOR MAXIMUM EFFICIENCY ENGINE

	Regulatory Positions							
	Historical			Current		Estimated Levels(5)		
	EPA 1973 NPRM 1981(1) (EEE Program Goals)	EPA 1978 NPRM(2) 1984(2)	EPA 1973 Equivalent in EPA 1978 Terms(2) (for ref. only)	ICAO Proposed(3) 1986(4)	EPA Projected Action 1984(4)	Maximum Efficiency Engine One-Stage Combustor	FPS Two-Stage Combustor(6)	
THC	0.4(7)	3.3(8)	3.8(8)	19.6(8)	19.6(8)	4.1(8)	3.0(8)	(.32)(7)
CO	3.0(7)	25(8)	28.2(8)	118(8)	None	42(8)	16.9(8)	(1.8)(7)
NOx	3.0(7)	33.0(8)	28.2(8)	100(8)	None	57(8)	40.4(8)	(4.3)(7)
Smoke No.	20	21	21	21	21	12	20 (4)	

(1) Effective date newly certified engines
(2) Change in EPA calculation method and units
(3) Based on 7 percent idle thrust for emissions certification
(4) Effective date for both newly certified and manufactured engines
(5) 2 margin for hardware variability and measurement accurately included
(6) Flight Propulsion System update of April 1982
(7) Lb. pollutant/1000lb FN-hr/cycle
(8) Gm. pollutant/kilo Newton FN

5.3.4 Combustor

The combustor was changed from the two-stage design of the flight propulsion system to a single-stage aerating design in the maximum efficiency engine. This change was made on the basis of a review of proposed or projected emissions requirements determined by the International Civil Aviation Organization (ICAO) and the Environmental Protection Agency (EPA). As shown in Table 63, a single-stage combustor is estimated to meet future emissions levels projected by both organizations.

The maximum efficiency engine combustor component has a 1.1 percent lower pressure loss than the flight propulsion system. This benefit is primarily due to the use of a straight wall diffuser rather than a curved-wall diffuser as used in the flight propulsion system. Also, a 3.3 cm (1.3 in) length reduction was shown as a result of the adoption of a smaller diameter two-stage high-pressure turbine which reduced the combustor cant angle. A comparison of flight propulsion system and maximum efficiency engine combustors is summarized in Table 64. The flowpath for the maximum efficiency engine is shown in Figure 72.

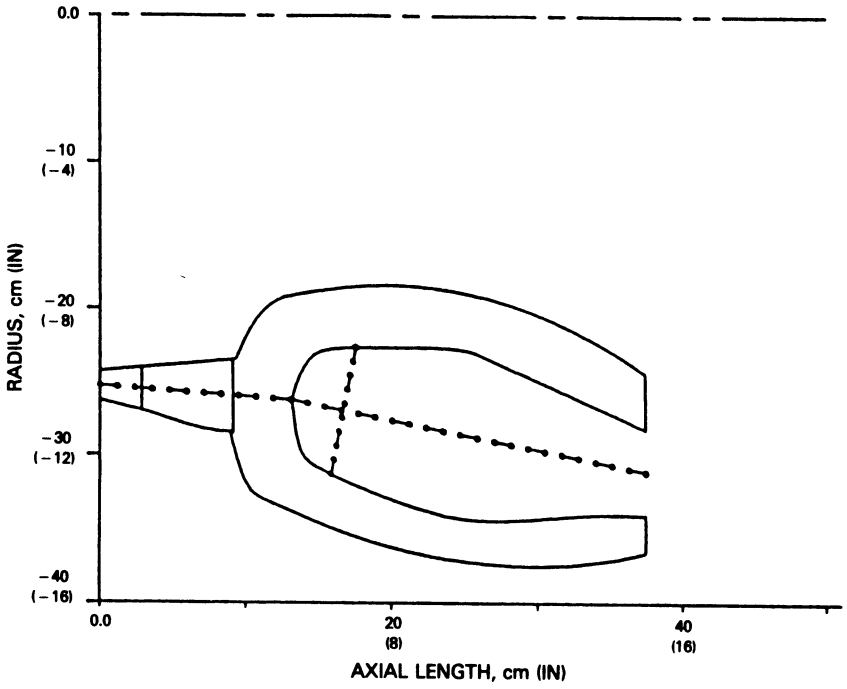

Figure 72 Combustor Flowpath

TABLE 64

COMBUSTOR AERODYNAMIC COMPARISON

	Flight Propulsion System	Maximum Efficiency Engine
Type	Two-stage Vorbix	Single-stage Aerating
Liner Construction	Segmented	Segmented
Overall Length - cm (in)	Base	-3.3 (-1.3)
Δ P/PT (percent)	5.5	4.4

5.3.5 High-Pressure Turbine

A two-stage design was selected to replace the flight propulsion system single-stage high-pressure turbine. The two-stage design incorporated flight propulsion system blade and vane trailing edge thicknesses. However, airfoil loadings were slightly lower along with an increased AN^2 and higher mean velocity ratio (see Table 65). Higher velocity ratio and higher AN^2 along with reduced turning and lower exit swirl are major contributors to the 2.6 percent improvement in efficiency. The flowpath of the turbine is presented in Figure 73.

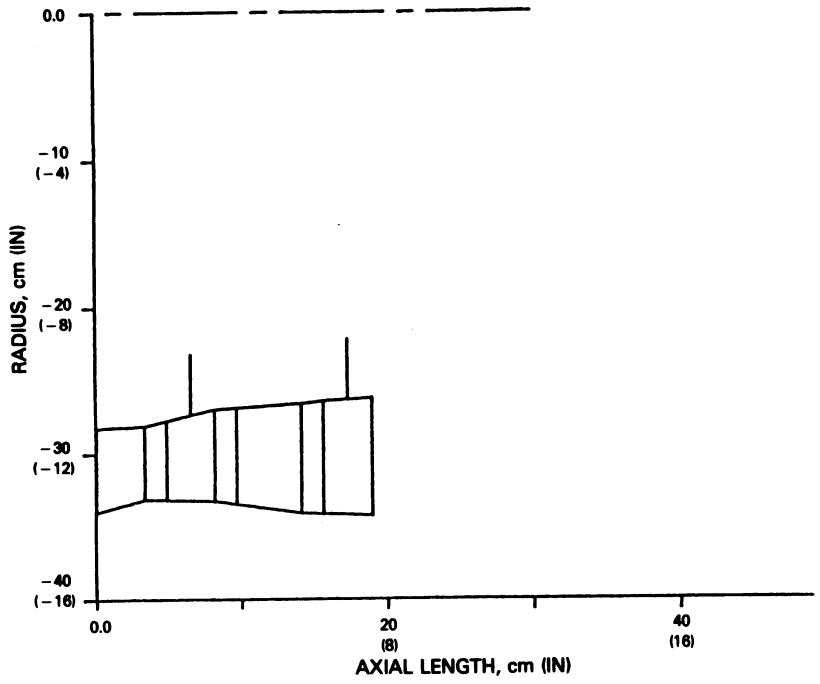

Figure 73 High-Pressure Turbine Flowpath

TABLE 65

HIGH-PRESSURE TURBINE AERODYNAMIC COMPARISON
(Aerodynamic Design Point: 10675 m (35,000 ft), 0.8 Mn, Standard Day)

	Flight Propulsion System	Maximum Efficiency Engine
Number of Stages	1	2
Expansion Ratio	3.99	3.90
Mean Velocity Ratio	0.560	0.640
Maximum AN^2 - $(cm)^2$ $(rpm)^2$	305.8 X 10^9	322.6 X 10^9
Redline Rim Speed (m/sec)	521	397
Maximum Mean Blade Turning (degrees)	117.5	98
Exit Swirl Angle (degrees)	44.0	15.0
Average Axial Velocity/Wheel Speed (Cx/U)	0.330	0.350
Axial Exit Mach Number	0.360	0.310
Number of Airfoils	78	149
Mean Diameter - cm (in)	76 (30)	61.7 (24.3)
Trailing Edge Thickness - cm (in)	0.165 (.065)	0.165 (.065)
Total Cooling Air (%)	13.6	16.2
Efficiency (%)	Base	+2.3 benefit

5.3.6 Turbine Transition Duct/Low-Pressure Turbine

The combination of an added high-pressure turbine stage and higher bypass ratio resulted in a larger radial offset of the turbines in the maximum efficiency engine. Therefore, the transition duct cant angle was increased to 25 degrees. The resultant transition duct is 3.6 cm (1.4 in) longer than that of the flight propulsion system. A comparison of transition duct sections for both engine configurations is provided in Table 66.

TABLE 66

TURBINE TRANSITION SELECTION COMPARISON

	Flight Propulsion System	Maximum Efficiency Energy Efficient Engine
Length - cm (in)	19.81 (7.80)	23.36 (9.20)
Mean Cant Angle	17.0	25.0
Area Ratio	1.53	1.22
Delta Inner Diameter Radius - cm (in)	5.33 (2.10)	11.43 (4.50)

The five-stage low-pressure turbine was configured with the same level of blade turning, exit axial Mach number, and maximum diameter as the flight propulsion system. With the added stage, both the mean velocity ratio was increased and the exit swirl angle was reduced. This provided efficiency improvement and a reduction in the turbine exit guide vane pressure loss, as summarized in Table 67. A flowpath of this turbine section is shown in Figure 74.

TABLE 67

LOW-PRESSURE TURBINE AERODYNAMIC COMPARISON
(Aerodynamic Design Point: 10675 m (35000 ft), 0.8 Mn, Std. Day)

	Flight Propulsion System	Maximum Efficiency Engine
Number of Stages	4	5
Expansion Ratio	5.72	6.1
Mean Velocity Ratio	0.47	0.490
Rotor Speed (rpm)	3900	3620
Maximum Mean Blade Turning (degrees)	114	114
Exit Swirl Angle (degrees)	35	25
Average Axial Velocity/Wheel Speed (Cx/U)	0.73	0.72
Axial Exit Mach Number	0.36	0.36
Number of Airfoils	756	1119
Exit Tip Diameter - cm (in)	132 (52)	132 (52)
Axial Length - cm (in)	62.9 (24.8)	65.2 (25.7)
△Difference Pressure/Pressure TEGV (%)	Base	-0.4 penalty
△Efficiency (%)	Base	+0.9 benefit

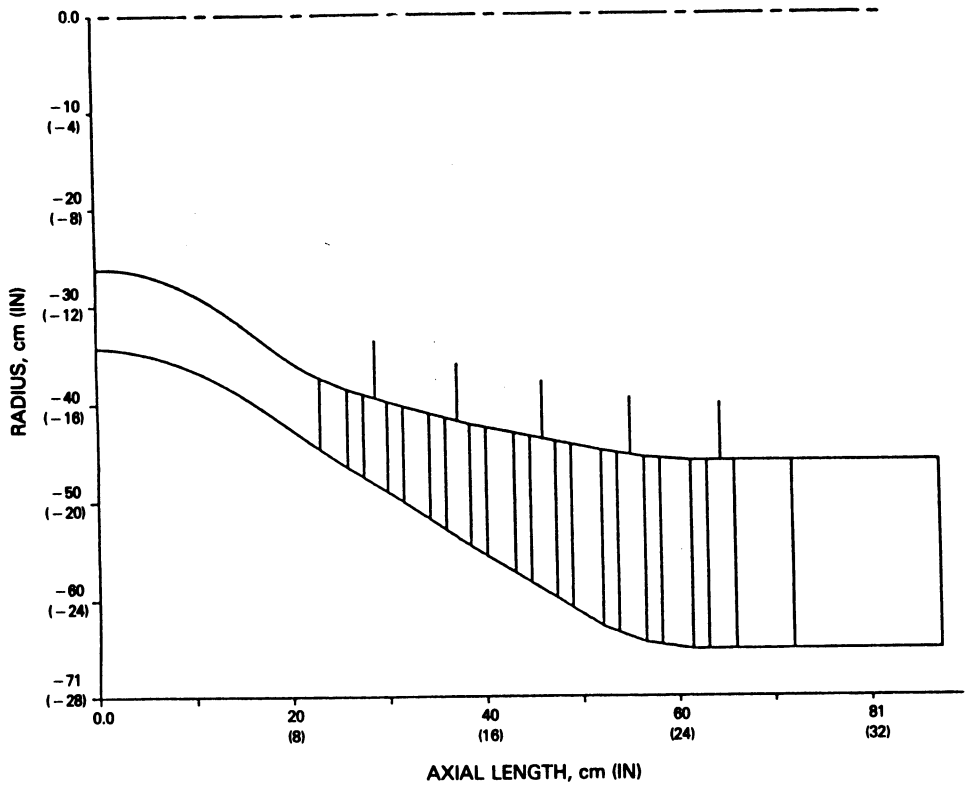

Figure 74 Turbine Transition Duct and Low-Pressure Turbine Flowpath

5.3.7 Trade Analyses

With the selection of the higher (7.2) bypass ratio, a low rotor speed and turbine staging study was undertaken. By varying the rotor speed and the number of turbine stages, trades were identified between fan efficiency, low-pressure compressor efficiency, turbine elevation, and turbine efficiency. Two rotor speeds were studied, based on 417 m/sec (1370 ft/sec) and 441 m/sec (1450 ft/sec) fan corrected tip speeds, along with an investigation concerning five and six stage turbines.

Figure 75 shows that as tip speed was increased by 24 m/sec (80 ft/sec), fan outer diameter performance worsened while fan inner diameter efficiency improved three-tenths of a percentage point and low-pressure compressor efficiency improved seven-tenths of a percentage point. The low-pressure turbine performance, shown in Figure 76, remained nearly constant (assuming constant velocity ratio and constant staging). The net effect, however, was an uninstalled thrust specific fuel consumption (TSFC) penalty. Transition duct length and low-pressure turbine maximum diameter decreased as speed was increased resulting in a nacelle drag reduction benefit. Therefore, on an installed basis, there is only a 0.15 percent thrust specific fuel consumption (TSFC) difference rather than the percent shown in Figure 76. The increased rotor speed with a shorter turbine transition duct and reduced low-pressure turbine maximum diameter would also result in reduced weight and cost, and provide more room to locate the rear mount so as to minimize the impact on mixer performance.

With the higher fan tip speed 441 m/sec (1450 ft/sec), a five-stage low-pressure turbine at same mean velocity ratio, comparable aerodynamic loadings, equal maximum blade and vane turnings and equal transition duct area ratio as a six-stage turbine resulted in a 0.22 percent efficiency penalty. This penalty is attributable to shorter blade and vane spans for the same flow area. This manifests itself into a clearance/span penalty.

Weights and costs were then estimated for the alternative configurations in order to assess fuel burned and direct operating cost trends. Results of these analyses are summarized in Table 68. Relative to the Energy Efficient Engine flight propulsion system, the three alternatives were estimated to provide approximately the same fuel burn reduction. The lower tip-speed fan, six stage turbine option showed a marked weight increase which increased the direct operating cost. The two other options offered the same fuel efficiency and direct operation cost advantage within 0.2 percent. The lower cost five-stage turbine option was selected for the final configuration.

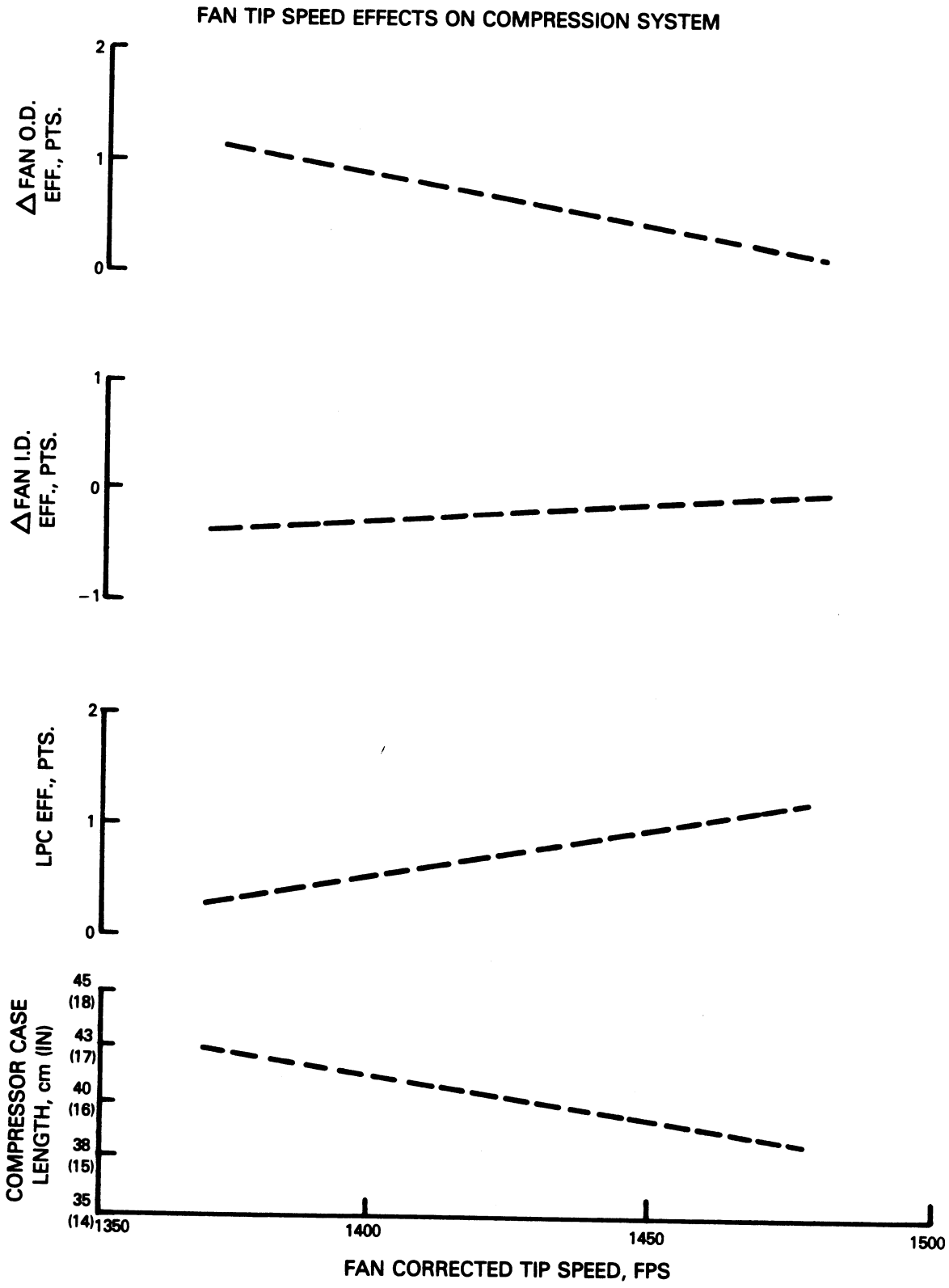

Figure 75 Fan Tip Speed Effects On Compression System

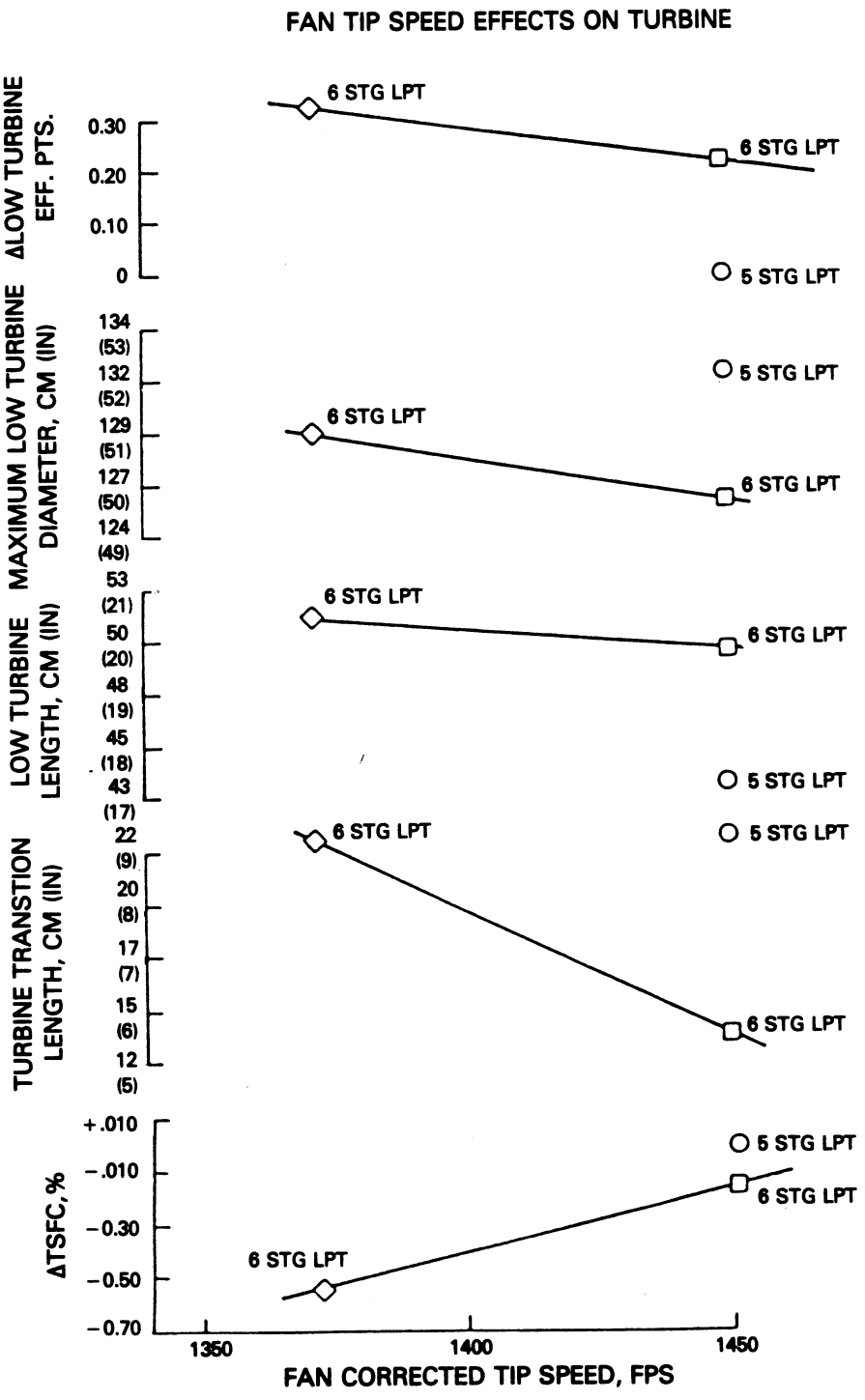

Figure 76 Fan Tip Speed Effects On Turbine

TABLE 68

FAN/LOW-PRESSURE TURBINE CONFIGURATION STUDY
RELATIVE TO FLIGHT PROPULSION SYSTEM

Configurations Considered

Fan Corrected Tip Speed - m/sec	441	441	417
Low-Pressure Turbine Stages	5	6	6
		Benefits Summary	
TSFC Fully Installed (percent)	-4.7	-4.8	-5.0
Weight Installed (kg)*	+104	+104	+145
Acquisition Cost Installed (K$)	+70	+100	+130
Maintenance Cost Installed ($/EOH**)	+13	+14	+14
Fuel Burned			
2,778km (1500nm) Twinjet (percent)	-5.1	-5.2	-5.3
5,556km (3000nm) Trijet (percent)	-5.4	-5.6	-5.7
10,186km (5500nm) Quadjet (percent)	-6.1	-6.3	-6.4
Direct Operating Cost ($1.50/3.78 liters (1.0 U.S. gallon))			
2,778km (1500nm) Twinjet (percent)	-0.9	-0.7	-0.4
5,556km (3000nm) Trijet (percent)	-1.7	-1.6	-1.4
10,186km (5500nm) Quadjet (percent)	-2.5	-2.4	-2.3

* Constant Installed Cruise Thrust
** Engine Operating Hour

5.4 CONCLUDING REMARKS

The maximum efficiency Energy Efficient Engine has been defined with fuel consumption improved almost five percent relative to the flight propulsion system. This improvement is attributed to the revision in bypass ratio, the lower minimum loss combustor, a two stage high-pressure turbine and a five stage low-pressure turbine. The engine configuration that reflects these changes is an optimization rather than an extension of the Energy Efficient Engine technology base.

APPENDIX A
FLIGHT PROPULSION SYSTEM MATERIAL COMPARISON

Some materials differences exist between the initial and current versions of the flight propulsion system. The primary reason for these differences is to improve strength or temperature capability. Materials currently selected for the flight propulsion system are listed below.

	Current (Initial*)
Fan	
Blade	AMS 4928
Disk	PWA 1215
Stubshaft	PWA 733 (AMS 4928)
Containment Case	AMS 4150/Kevlar
Sound Treatment	Al Honeycomb
Low-Pressure Compressor	
Blades	AMS 4928
Disks	AMS 4928
Hub	AMS 4928
Vanes	
S1	AMS 4312 (4135)
S2-S5	AMS 4312 (4135)
Cases	AMS 4150
Intermediate Case	
Structural Struts	AMS 4911
Inner Case	PWA 1262
Non-Structural Struts	AMS 4911
Outer Case	AMS 4150
High-Pressure Compressor	
Blades	
R6 and R7	PWA 1202
R8 - R15	PWA 1010 (1003)
Disks	
R6 and R7	AMS 4928
R8 - R11	PWA 1224 (MERL 130)
R12	PWA 1225 (MERL 130)
R13	PWA 1225 (MERL 80)
R14 and R15	MERL 80

* Shown only where changes have occurred

APPENDIX A (continued)

	Current (Initial*)
Non-Vortex Tubes	AMS 4911
Center Tube	AMS 5613
Vanes	
IGV	AMS 4132
S6 - S8	AMS 5613
S9 - S12	AMS 5508 (5616)
S13 and S14	AMS 5596 (5671)
EGV	PWA 649
Front Case	AMS 4928
Rear Case	PWA 1214
IGV ID Shroud	AMS 4132
Diffuser/Burner	
Diffuser30	
Inner Prediffuser Wall	AMS 5662
Strut Assembly	PWA 649 - HIP
Burner	
Bulkhead	AMS 5754 (PWA 1038)
OD Liner Segments	PWA 1455
OD Bird Cage	AMS 5754
ID Liner Segments	PWA 1455
ID Bird Cage	AMS 5754
High-Pressure Turbine	
Rotor	
Blade	SC 2000
Disk/Hub	MERL 80
Sideplates (Fr-Rr)	MERL 80
Vortex Plate	MERL 80
HPC Discharge Seal	AMS 5895 (MERL 80)
Static	
Vane S1	SC 2000 (MERL 220)
OAS	PWA 655(647)/Ceramic
OAS Supports (Fr-Rr)	PWA 1007
TOBI System	PWA 649/AMS 5596
Outer Case	AMS 5662 (PWA 649)

*Shown only where changes have occurred

APPENDIX A (continued)

	Current (Initial*)
Turbine Intermediate Case	
Hot Strut	
Aero Fairings	SC 2000
Bearing(4-5)Support	AMS 5662 (PWA 649)
Structural Struts	AMS 5662 (PWA 649)
Low-Pressure Turbine	
Rotor	
Blades R2	PWA 1447 (PWA 1442)
R3 and R4	PWA 655
R5	MERL 101
Disks	PWA 1099 (MERL 80)
Spacers/Seals	PWA 1099 (1003)
Hub PWA 1003	
Static	
Vanes S2	SC 2000
S3	PWA 1447 (PWA 655)
S4 and S5	PWA 655
Shrouds & Seals	AMS 5536/5754
Inner Case	AMS 5662
Outer Case (AMS 5662/5596)	AMS 5858/5895
Exhaust Case	
ID/OD Case	MERL 101
Struts	MERL 101
LPT Shaft	PWA 733
Mixer & Exhaust	
Mixer	
Mixer	PWA 1231
Mixer Support	- (MERL 101)
Tailplug	AMS 5599/4910
Center Vent Static	AMS 5504

*Shown only where changes occurred

Table of Material Equivalence

PWA Designation	Material Equivalency
PWA 647	MAR-M-509
PWA 649	Inconel 718
PWA 655	Inconel 713C
PWA 733	17-22-A; Templex (Low Alloy Steel)
PWA 1003	Incoloy 901
PWA 1007	Waspaloy
PWA 1010	Inconel 718
PWA 1038	Hastelloy X
PWA 1099	Modified IN-100 Alloy (Formerly MERL 76)
PWA 1202	Titanium (8AL-1MO-1V)
PWA 1214	Titanium (6AL-2SN-4ZR-2MO) High Creep Strength
PWA 1215	Titanium (6AL-4V) Forged Below Beta Transus
PWA 1224	Titanium (6AL-2SN-4ZR-2MO) Forged Below Beta Transus
PWA 1225	Titanium (6AL-2SN-4ZR-2MO) Forged Above Beta Transus
PWA 1226	Titanium (6AL-2SN-4ZR-2MO) Forged, Beta Annealed, Precipitation Heat Treated
PWA 1231	Titanium (6AL-2SN-4ZR-2MO) Cross Rolled, Beta Annealed, Precipitation Heat Treated
PWA 1262	Titanium (6AL-4V) Cast
PWA 1422	MAR-M-200+HF
PWA 1447	MAR-M-247
PWA 1455	Modified B-1900
PWA 1480	Single Crystal NI Alloy
MERL 80	Modified IN-100 Alloy
MERL 101	Titanium Aluminide Alloy
MERL 130	High Tensile Strength Titanium Alloy
SC 2000	Single Crystal NI Alloy
MERL 220	Single Crystal NI Alloy

APPENDIX B
LIST OF ABBREVIATIONS/SYMBOLS

A	area
A_H	highlight area
A_T	throat area
AA	arithmetical average angstroms (surface roughness)
abs	absolute
ACC	active clearance control
Aerodynamic Design Point	
eval	evaluation
AL	aluminum
AMS	Aerospace Material Specifications
avg	average
BCAC	Boeing Commercial Airplane Co.
brg	bearing
Btu	British Thermal Unit
c	centigrade
cal	calorie
C/A	Cooling Air
cm	centimeter
CO	Carbon Monoxide
comp	Compressor
comp't	compartment
D	diameter
DH	highlight diameter
DM	maximum diameter
DAC	Douglas Aircraft Company
deg	degrees
des	design
det	deterioration
dia	diameter
DOC	direct operating cost
E	excitation
E^3	Energy Efficient Engine
EGV	exit guide vane
eng	engine
EPA	Environmental Protection Agency
EPAP	Environmental Protection Agency Parameter
EPNdB	effective perceived noise, decibels
aerodynamic design point	
F	Fahrenheit
Fu	gross weight/speed factor
Fw	utilization factor
FAR	Federal Aviation Regulations
FEGV	fan exit guide vane
FPS	flight propulsion system
frt	front
ft	foot
gal	gallon
G/I	ground idle
h	enthalpy
HC	Hydrocarbon, honeycomb
HF	hafnium
HIP	hot isostatic press
hp	horsepower
HPC	high pressure compressor
HPT	high pressure turbine
hr	hour
I/C	intermediate case
IC/LS	integrated core/low spool
ID	inner diameter
IGV	inlet guide vane
in	inch

I/C	intermediate case
int	intermediate
K	thousand, Kelvin
KE	knife edge
kg	kilogram
Km	kilometer
l	liter
L	length
lab	labyrinth
lb	pound
LCC	Lockheed California Company
LP	low pressure
LPC	low pressure compressor
LPT	low pressure turbine
m	meter
M	thousand
max	maximum
MERL	Materials Engineering Research Laboratory
min	minimum, minute
mm	millimeter
Mn	Mach number
MO	Molybdenum
N	Newton
N	rotor speed
N/A	not applicable, not available
NASA	National Aeronautics and Space Administration
NI	nickel
nm	nautical mile
no	number
NOx	nitrogen oxides
OAS	outer air seal
OD	outer diameter
OWE	operating weight empty
P	pressure
Pa	Pascal
Pt	total pressure
PP	perforated plate
PR	pressure ratio
PS/AIE	Propulsion System/Aircraft Integration Evaluation
psia	pounds per square inch absolute
pt	point
P&W	Pratt & Whitney
R	radius, Rankine, rotor
RH	highlight radius
rad	radians
rev	revolutions
RPM	revolutions per minute
RR	rear
S	second, stator, structural strut
SAE	Society of Automotive Engineers
sec	seconds
SHP	shaft horsepower
SLS	sea level static
SLTO	sea level take off
SN	tin
Sq	square
st	standard
T	temperature
Tt	total temperature

THC	total hydrocarbons	W	air or gas flow
T/O	takeoff	WAE	core airflow
TOBI	tangential on-board injestion	WF	fuel flow
TOGW	takeoff gross weight	WAF	airframe weight
TSFC	thrust specific fuel consumption	Wgt	weight
		wt	weight
U	rotor tangential velocity	Zr	zirconium
US	United States		
V	vanadium		
Δ	change	"	inches
δ	corrected pressure (P/14.7)	<	less than
θ	corrected temperature (T/459.7)	-	minus
°	degrees	#	number, pounds
$	dollars	%	percent
=	equals	+	plus
>	greater than	Σ	sum

REFERENCES

1. Energy Efficient Engine Project Engineering, et. al.: 'Energy Efficient Engine Flight Propulsion System Preliminary Analysis and Design Report,' NASA CR-159487, April 1979.

2. Owens, R.E.: 'Energy Efficient Engine Propulsion System - Aircraft Integration Evaluation,' NASA CR-159488, March 1979.

3. Halle, J.E. and Michael, C.J.: 'Energy Efficient Engine Fan Component Detailed Design Report,' NASA CR-165466, September 1981.

4. Halle, J.E. and Michael, C.J.: 'Energy Efficient Engine Low-Pressure Compressor Component Test Hardware Detailed Design Report,' NASA CR-165354, June 1981.

5. Zeisser, M.H., Greene W. and Dubiel, D.J.: 'Energy Efficient Engine Combustor Component Detailed Design Report,' NASA CR-167945, March 1982.

6. Thulin, R.D., Howe, D.C., and Singer, I.D.: 'Energy Efficient Engine High-Pressure Turbine Detailed Design Report,' NASA CR-165608, January 1982.

7. Leach, K., Thulin, R.D., and Howe, D.C.: 'Energy Efficient Engine Turbine Intermediate Case and Low-Pressure Turbine Component Test Hardware Detailed Design Report,' NASA CR-167973, 1982.

8. Kozlowski, H. and Larkin, M.: 'Energy Efficient Engine Exhaust Mixer Model Technology Report,' NASA CR-165459, 1981.

9. Howe, D. C. and Bisset, J. W.: 'Energy Efficient Engine Integrated Core/Low Spool Test Hardware Design Report,' NASA CR-168137, 1983.

10. Gardner, W.B.: 'Energy Efficient Engine High-Pressure Turbine Cooling Model Technology Report,' NASA CR-165374, May 1981.

11. Gardner, W.B.: 'Energy Efficient Engine High-Pressure Turbine Leakage Technology Report,' NASA CR-165202, December 1980.

12. Giamei, A.F., Salkeld, R.W., and Hayes, C.W.: 'Energy Efficient Engine High-Pressure Turbine Single Crystal Vane and Blade Fabrication Technology Report,' NASA CR-165400, July 1981.

13. Gardner, W.B.: 'Energy Efficient Engine High-Pressure Turbine Uncooled Rig Technology Report,' NASA CR-165149, October 1979.

REFERENCES (continued)

14. Leach, K. and Thulin, R.: 'Energy Efficient Engine Turbine Transition Duct Model Technology Report,' NASA CR-167996, August 1982.

15. Gardner, W.B.: 'Energy Efficient Engine Low-Pressure Turbine Boundary Layer Technology Report,' NASA CR-165338, April 1981.

16. Dubiel, D.J., Zeisser, M.H., and Greene, W.: 'Energy Efficient Engine Sector Combustor Rig Technology Report,' NASA CR-167913, October 1981.

17. Leach, K.: 'Energy Efficient Engine High Pressure Turbine Component Rig Performance Test Report,' NASA CR-168189, May 1983.

1.REPORT NO. CR- 174701	2. GOVERNMENT AGENCY	3.RECIPIENT'S CATALOG NO.
4.TITLE AND SUBTITLE Energy Efficient Engine Flight Propulsion System Preliminary Analysis and Design Report - Final Update		5. REPORT DATE September 1983 6. PERFORMING ORG. CODE
7.AUTHOR(S) J.W. Bisset and D.C. Howe		8. PERFORMING ORG. REPT. NO. PWA-5594-248
9.PERFORMING ORG. NAME AND ADDRESS UNITED TECHNOLOGIES CORPORATION Pratt & Whitney Engineering Division - Connecticut Operation		10. WORK UNIT NO. 11. CONTRACT OR GRANT NO. NAS3-20646
12. SPONSORING AGENCY NAME AND ADDRESS National Aeronautics and Space Administration Lewis Research Center 21000 Brookpark Road, Cleveland, Ohio 44135		13. TYPE REPT./PERIOD COVERED Contract Report 14. SPONSORING AGENCY CODE

15. SUPPLEMENTARY NOTES
Prepared in cooperation with NASA Project Engineer, Mr. F. D. Berkopec, NASA Lewis Research Center, Cleveland, Ohio.

16. ABSTRACT

The National Aeronautics and Space Administration is sponsoring the Energy Efficient Engine Program to identify and verify the technology required to significantly lower fuel consumption and operating cost for future commercial gas-turbine engines. A major task recently completed under this program is the final design and analysis of the flight propulsion system. This system is the conceptual study engine defined to meet the performance, economic and environmental goals established for the Energy Efficient Engine Program.

This report details results evolving from the final analysis and design of the flight propulsion system. The design effort included a final definition of the engine, major components, internal subsystems, and nacelle. Various analytical representations and results from component technology programs were used to verify aerodynamic and structural design concepts and to predict performance. Specific design goals and specifications, reflecting future commercial aircraft propulsion system requirements for the mid-1980's, were detailed by NASA and used as guidelines during engine definition. This report also presents information detailing salient results from a separate study to define a turbofan propulsion system, known as the maximum efficiency engine, which reoptimized the advanced fuel saving technologies for improved fuel economy and direct operating costs relative to the flight propulsion system.

17. KEY WORDS (SUGGESTED BY AUTHOR(S))	18. DISTRIBUTION STATEMENT
Energy Efficient Engine Flight Propulsion System Maximum Efficiency Engine Advanced Component Technologies	Unclassified - Unlimited

19. SECURITY CLASS THIS (REPT)	20. SECURITY CLASS THIS (PAGE)	21. NO. PGS	22. PRICE *
Unclassified	Unclassified		

* For sale by the National Technical Information Service, Springfield, VA 22161